

THE EMERGENCE OF THE RNA WORLD ON THE  
EARLY EARTH

THE EMERGENCE OF THE RNA WORLD ON THE  
EARLY EARTH

By BEN K. D. PEARCE, B. SC.

A Thesis Submitted to the School of Graduate Studies in Partial Fulfillment of the  
Requirements for the Degree Master of Science

McMaster University MASTER OF SCIENCE (2017) Hamilton, Ontario (Physics & Astronomy - Astrobiology)

TITLE: Thesis Example

AUTHOR: Ben K. D. Pearce, B.Sc. ( $\times 2$ ) (University of British Columbia, University of Calgary)

SUPERVISOR: Professor Ralph E. Pudritz

NUMBER OF PAGES: ix, 146

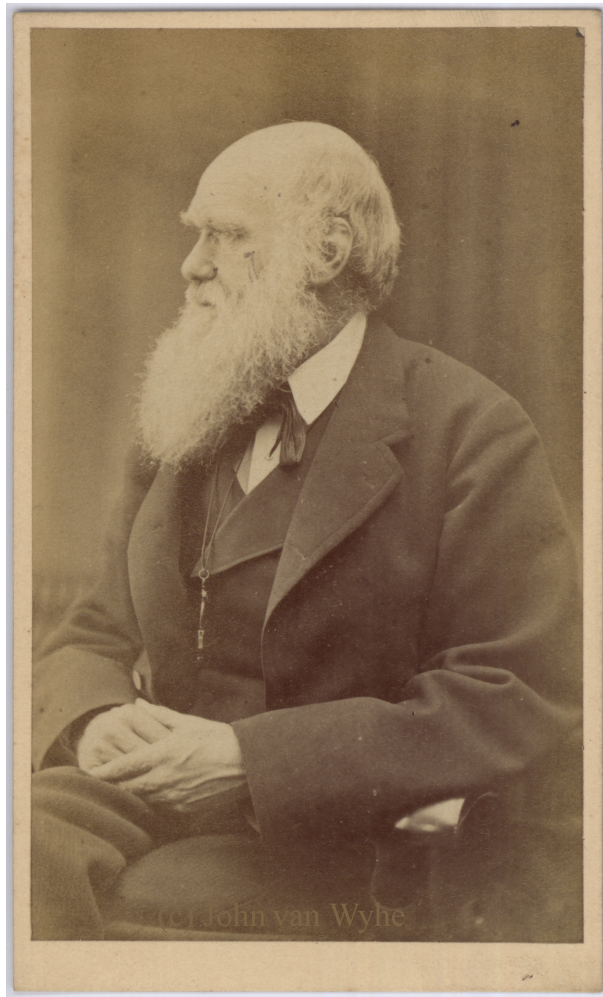


Figure 1: Portrait of Charles Darwin in 1871 by Oscar Gustave Rejlander.

*“But if (& oh what a big if) we could conceive in some warm little pond with all sorts of ammonia & phosphoric salts,—light, heat, electricity &c present, that a protein compound was chemically formed, ready to undergo still more complex changes, at the present day such matter wd be instantly devoured, or absorbed, which would not have been the case before living creatures were formed.”*

Darwin to J. D. Hooker, 1871

## Abstract

Life on Earth likely began as an RNA world, where cell-free or compartmentalized ribonucleic acid (RNA) molecules dominated as the replicating and evolving lifeforms prior to the emergence of DNA- and protein-based life. The focus of this thesis is on when and how this RNA world emerged. We use astrophysical and geophysical studies to constrain when the Earth was habitable, and biosignature studies to constrain when the Earth was inhabited. From this we obtain a time interval for the emergence of life. Considering all these constraints, we find that the Earth was habitable as early as 4.5 Ga, or as late as 3.9 Ga, depending on whether the early influx of asteroids inhibited life from emerging. The time that the Earth was inhabited is more precisely constrained to 3.7 Ga. This suggests life emerged within 800 Myr, and possibly in  $< 200$  Myr. Between 4.5–3.7 Ga, the continental crust was slowly rising up from the global ocean, providing dry land on which warm little ponds could form. We develop the theory for the emergence of RNA polymers in these pond environments, whose wet-dry cycles promote polymerization. RNA is comprised of chains of nucleotides, and the latter is made up of ribose, phosphate, and a characteristic nucleobase. We numerically model the survival and evolution of nucleobases in warm little ponds from meteorite and interplanetary dust sources. The wet-dry cycles of our ponds are controlled by precipitation, evaporation, and seepage. The nucleobase sinks include photodissociation, seepage, and hydrolysis. Nucleobase and nucleotide seepage is efficient, therefore nucleotides and RNA molecules must have emerged rapidly ( $<$  a few years) in order to avoid falling through pores at the base of the pond. We find that meteorites, not interplanetary dust particles, are the dominant source of nucleobases used for RNA synthesis. Finally, under these conditions, we find that first RNA polymers likely emerged before 4.17 Ga.

## Acknowledgments

There are more than a few people who played important roles in the completion of this thesis that I would like to thank. Firstly, Ralph Pudritz, my supervisor, is always encouraging and excited by the science we do. A big reason I chose to stay on for a PhD is because of our mutual excitement towards origins of life research, and our mutual trust and respect. Thank you for your dedication to our research and to furthering my career as a scientist. You always work hard to make our manuscripts as high quality as possible, and you challenge me to leave no stone unturned. I have learned a lot from you, and I look forward to learning much more over the next 4 years.

Thank you to all my collaborators. Thomas Henning and Dima Semenov, your ideas have been essential to the writing of Chapter 3. Thank you for the fruitful discussions, and for your comments and guidance throughout the writing of the manuscript. Paul Higgs, you are extremely encouraging and insightful and your talent for writing is something I hope to emulate some day. Thank you for your dedication to the writing of Chapter 2, and for your encouragement of Andrew and I working together. Andrew Tupper, discussions with you have been invaluable to me. Thank you not only for your work on Chapter 2, but for your persistence in challenging my ideas, and your personal insights. I look forward to years of further discussions and collaborations.

Thank you to my committee members, Thomas Henning and Greg Slater, for providing useful advice and for your comments and questions during my committee meeting. Also, thank you Greg for allowing me to serve on the Canadian Space Agency topical team in astrobiology. I have always been interested in the exploration of space and the search for life beyond Earth, and being on this committee has been extremely meaningful to me.

Thank you to the readers of early drafts of our manuscripts: Maikel Rheinstädter, Allyson Brady, and Radhey Gupta. Your comments were valuable to improving the content and clarity of Chapters 2 and 3.

Thank you to Steve Janzen, for providing high quality illustrations for Chapters 2 and 3. Your artistic talents truly amaze me.

Thank you to all the astrophysics and physics grad students, and particularly my research group members and office mates: Sarah, Alex, Corey, Matt and Sam. Sometimes being a grad student is stressful, but going through it with those who

completely understand your plight makes it a bit easier. Thank you also to the astrobiology grad students, I feel very much at home in the presence of our mutual nerdiness.

Thank you to the collaborators I have ongoing projects with. Anand Patel, thank you for teaching me about theoretical chemistry. I really hope we collaborate on a project in the future. Oliver Trapp, thank you for allowing me work in your lab a couple days each week for the summer, and for all our discussions. Thank you to all Oliver's grad students, who sat with me every lunch (and let me use their student cards to purchase food). Thank you particularly to Saskia Lamour for spending a whole day in the lab with me, teaching me about experimental chemistry, and also to Sebastian Pallmann, Jana Steflava, and Golo Storch for discussions on the project we started.

Finally, thanks to my friends and family for your support throughout this degree. In the end, I am nothing without those who love me. So I want to thank Laura Savoie for being a supportive girlfriend these past few months.



# Contents

<b>1</b>	<b>Introduction</b>	<b>1</b>
1.1	The RNA World . . . . .	2
1.2	The Emergence of Life on Earth . . . . .	5
1.2.1	Nucleobase Sources . . . . .	6
1.2.2	Site for the Emergence of Life . . . . .	13
1.2.3	Nucleobase Sinks . . . . .	14
1.3	The Emergence of Life on Habitable Exoplanets . . . . .	17
1.4	Outline of Thesis Research . . . . .	19
<b>2</b>	<b>Constraining the Time Interval for the Origin of Life on Earth</b>	<b>21</b>
2.1	Introduction . . . . .	22
2.2	Formation of the Solar System . . . . .	26
2.2.1	Formation of the Sun and the Protoplanetary Disk . . . . .	26
2.2.2	Formation of the Earth . . . . .	27
2.2.3	Formation of the Moon . . . . .	28
2.3	Habitability of the Earth . . . . .	29
2.3.1	Radiative Cooling of the Magma Ocean . . . . .	29
2.3.2	Evidence of a Continental Crust . . . . .	31
2.3.3	Snowball Earth? . . . . .	32
2.3.4	Evidence of Surface Water . . . . .	34
2.3.5	The Late Heavy Bombardment . . . . .	35
2.4	The Fossil Record . . . . .	38
2.4.1	Microfossils . . . . .	38
2.4.2	Stromatolites . . . . .	41
2.5	Isotopic Signatures . . . . .	44
2.5.1	Signatures for the Presence of Oxygen . . . . .	44

2.5.2	Carbon Isotope Biosignatures . . . . .	45
2.6	Molecular Evolution and Phylogenetics . . . . .	50
2.7	Discussion - How Quickly Did Life Emerge on Earth? . . . . .	53
2.8	Acknowledgments . . . . .	56
<b>3</b>	<b>Origin of the RNA World: The Fate of Nucleobases in Warm Little Ponds</b>	<b>57</b>
3.1	Introduction . . . . .	58
3.2	Model: Fates of Nucleobases in Evolving WLPs . . . . .	61
3.3	Meteorite Sources and Targets . . . . .	62
3.4	Life Cycles of WLPs . . . . .	63
3.5	Nucleobase Evolution in WLPs . . . . .	64
3.6	Dominant Source of Surviving Nucleobases . . . . .	66
3.7	Nucleotide and RNA Synthesis . . . . .	68
3.8	Discussion and Conclusions . . . . .	69
3.9	Acknowledgments . . . . .	69
3.10	Supporting Information (SI) . . . . .	70
3.10.1	Calculating WLP Surface Area on the Early Earth . . . . .	70
3.10.2	Calculating Carbonaceous Meteorite Depositions in WLPs . . . . .	72
3.10.3	Sources and Sinks Model Overview . . . . .	80
3.10.4	Pond Water Sources and Sinks . . . . .	81
3.10.5	Nucleobase Sinks . . . . .	83
3.10.6	Nucleobase Outflow and Mixing . . . . .	85
3.10.7	Nucleobase Evolution Equation From IDPs . . . . .	88
3.10.8	Nucleobase Evolution Equation From Meteorites . . . . .	90
3.10.9	Additional results . . . . .	92
3.10.10	Appendix A: Advection and Diffusion Model . . . . .	98
<b>4</b>	<b>Conclusions &amp; Future Work</b>	<b>105</b>
<b>A</b>	<b>Nucleobase Synthesis in WLPs</b>	<b>145</b>

# List of Figures

1	Portrait of Charles Darwin in 1871 by Oscar Gustave Rejlander. . . .	iii
1.1	Ribonucleic acid (RNA) molecules in <b>(a)</b> unfolded and <b>(b)</b> folded states. RNA molecules are made up of a sequence of nucleobases (adenine, guanine, uracil, cytosine) attached to a backbone made up of ribose and phosphate. RNA nucleobases can base pair (adenine to uracil and guanine to cytosine) which allows RNA to fold onto itself and become catalytic, or form double-stranded RNA for template replication. Sources: [10, 11] . . . . .	2
1.2	A DNA polymerase (faded yellow) attaching a nucleotide from the environment to the appropriate nucleotide site on the DNA template strand. RNA polymerases would function generally the same on an RNA template. Source: [14]. . . . .	4
1.3	A diagram of a black smoker hydrothermal vent. Hydrothermal fluid is heated by a high temperature magma chamber, and enriched with organic-synthesizing reactants such as magmatic CO <sub>2</sub> , and H <sub>2</sub> from serpentinization. The black smoker plume is composed of CO <sub>2</sub> , H <sub>2</sub> S, CH <sub>4</sub> and other molecules that are released when the enriched hydrothermal fluids mix with seawater. Source: [43]. . . . .	8
1.4	The Miller-Urey spark discharge apparatus. Water boils in the lower spherical compartment sending vapour to collect in the upper spherical compartment with highly reduced gases such as CH <sub>4</sub> , NH <sub>3</sub> , H <sub>2</sub> , and CO. An electrical spark then discharges in the upper spherical compartment producing organics which condense into a cooled trap. (a) A schematic drawing of the apparatus. (b) A Photo of the original apparatus. Source: [45]. . . . .	10

1.5	(a) The Murchison meteorite, which fell to Earth near Murchison, Victoria, Australia in 1969. The Murchison meteorite contains 3 of the 4 nucleobases in RNA (guanine, adenine, and uracil). (b) A typical IDP collected by an airplane at high altitude. Sources: [72, 73]. . . . .	12
1.6	Liquid water favourably destroys cytosine, adenine, and guanine by replacing the NH <sub>2</sub> group in these molecules with an oxygen molecule, and releasing ammonia in the process. The product molecules in these reactions are uracil, hypoxanthine, and xanthine, respectively. Source: [95]. . . . .	15
1.7	A schematic of molecular photoexcitation. Curves S <sub>0</sub> and S <sub>1</sub> represent the potential energy versus bond distance for the ground and first excited states of a molecule. The horizontal lines represent the vibrational levels. When the molecule absorbs a photon, the molecule transitions from S <sub>0</sub> to S <sub>1</sub> . Transition <b>1</b> leads to a vibrational level which breaks the bond, causing dissociation. Transition <b>2</b> leads to vibrational relaxation and either fluorescence ( <b>F</b> ) to the ground state, or transition to state <b>T</b> <sub>1</sub> , leading to more vibrational relaxation and phosphorescence ( <b>P</b> ) to the ground state. Source: [96]. . . . .	17
2.1	Timeline which illustrates the astrophysical constraints constraining the time of the habitability boundary and the biological signatures constraining the time of the biosignature boundary. Uncertainties about whether there was a late heavy bombardment mean that the position of the habitability boundary is still poorly constrained, while the evidence for the biosignature boundary is beginning to converge. . . . .	24
2.2	Four possible scenarios for the late heavy bombardment, calibrated to crater counts and surface ages at the Apollo landing sites. All scenarios except the 50 Myr half-life model are supported by the available data. This figure is taken directly out of Zahnle <i>et al.</i> [114]. . . . .	37
2.3	(a) – (f) Hollow, tubular microfossils from the 3.4 Gyr-old Strelley Pool formation (indicated by arrows, boxes, or numbers). A couple highlights are the tubular microfossil cross-sections in frame (d) and the dense patch of tubular microfossils in frame (e). P stands for pyrite. This figure is taken directly out of Wacey <i>et al.</i> [131]. . . . .	40

2.4	(a) Stromatolites in an exposed outcrop of 3.7-Gyr-old metacarbonate rocks in the Isua supracrustal belt in southwest Greenland. (b) Interpretation of (a), with both an isolated stromatolite (strom) and a conglomerate of stromatolites (stroms). (c) Asymmetrical, peak-shaped stromatolite and (d) linked, dome-shaped stromatolites from the 2-Gyr-old Woolly Dolomite carbonate platform in Western Australia. This figure is taken directly out of Nutman <i>et al.</i> [104]. . . . .	43
2.5	Isotopic carbon composition of various major groups of plants, protists, and bacteria compared with those of $\text{CO}_2$ , $\text{HCO}_3^-$ , and $\text{CO}_3^{2-}$ in the surface environment. Negative $\delta^{13}\text{C}$ values correspond to $^{13}\text{C}$ depletion relative to the Pee Dee Belemnite (PDB) standard. The positive extremes for methanogens were from experiments of cultures that were placed in conditions irrelevant to natural populations. This figure is taken directly out of Schirmer <i>et al.</i> [201]. . . . .	47

3.1 **History of carbonaceous meteorite deposition in warm little ponds:**

**(A)** History of mass delivery rate to the early Earth and of effective warm little pond (WLP) surface area. Three models for mass delivered to the early Earth are compared: a Late Heavy Bombardment model, and a minimum and maximum bombardment model. All mass delivery models are based on analyses of the lunar cratering record [269, 271]. The effective WLP surface area during the Hadean eon is based on a continental crust growth model [272], the number of lakes and ponds per unit crustal area [273], and the lake and pond size distribution [273]. **(B)** Cumulative WLP depositions for the small fragments of carbonaceous meteoroids of diameter 40–80 m landing in any 1–10 m-radius WLP on the early Earth. A deposition is characterized as a meteoroid debris field that overlaps with a WLP. We assume the ponds per area during the Hadean eon is the same as today, and that all continental crust remains above sea-level, however we vary the ponds per area by  $\pm 1$  order of magnitude to obtain error bars. 95% of WLP depositions in each model occur before the corresponding dotted vertical line. 40–80 m is the optimal range of carbonaceous meteoroid diameters to reach terminal velocity, while still landing a substantial fraction of mass within a WLP area. 1–10 m is the optimal range of WLP radii to avoid complete evaporation within a few months, while also allowing non-negligible nucleobase concentrations to be reached upon meteorite deposition. The numbers of carbonaceous meteoroid impactors in the 20–40 m-radius range are based on the mass delivery rate, the main-belt size-frequency distribution, and the fraction of impactors that are of type CM, CR or CI [269, 271, 274] (see SI Text). . . . . 60

3.2	An illustration of the sources and sinks of pond water and nucleobases in our model of isolated warm little ponds on the early Earth. The only water source is precipitation. Water sinks include evaporation and seepage. Nucleobase sources include carbonaceous IDPs and meteorites, which carry up to $\sim 1$ picogram and $\sim 3$ mg of each nucleobase, respectively. Nucleobase sinks include hydrolysis, UV photodissociation, and seepage. Nucleobase hydrolysis and seepage are only activated when the pond is wet, and UV photodissociation is only activated when the pond is dry. . . . .	62
3.3	<b>Histories of pond water and adenine concentration from interplanetary dust particles:</b> <b>(A)</b> The change in water level over time in our fiducial dry, intermediate, and wet environment WLPs due to evaporation, seepage, and precipitation. Precipitation rates from a variety of locations on Earth today are used in the models, and represent 2 classes of matching early Earth analogues: hot (Columbia, Indonesia, Cameroon), and warm (Thailand, Brazil, and Mexico) (for details see Table 3.1). All models begin with an empty pond, and stabilize within 2 years. <b>(B)</b> The red and black-dotted curves represent the adenine concentrations over time from carbonaceous interplanetary dust particles (IDPs) in our fiducial WLPs. The degenerate intermediate WLP environment used in this calculation is for a hot early Earth at $65^\circ\text{C}$ and a warm early Earth at $20^\circ\text{C}$ . The blue curve represents the corresponding water level in the WLP, with initial empty and full states labeled in brown and blue text. Three features are present: 1) The maximum adenine concentration at the onset of the dry phase. 2) A flat-top equilibrium between incoming adenine from IDPs and adenine destruction by UV irradiation. 3) The minimum adenine concentration just before the pond water reaches its highest level. . . . .	65

**3.4 Comparative histories of adenine concentrations from interplanetary dust particles and meteorites:** (A) A comparison of the accumulation of adenine from carbonaceous IDPs and meteorites in our fiducial WLPs. The meteorite fragments are small (1 cm), and originate from a 40 m-radius carbonaceous meteoroid. Adenine concentrations for intermediate (wet-dry cycle) and wet environments (never dry) are compared and correspond to both a hot early Earth at 65 °C and a warm early Earth at 20 °C (for details see Table 3.1). (B) The effect of meteorite fragment sizes on adenine concentration. The degenerate intermediate WLP environment used in these calculations is for a hot early Earth at 65 °C and a warm early Earth at 20 °C. The fragments are either only small in size (1 cm in radius), only medium in size (5 cm in radius), or only large in size (10 cm in radius). Three features are present: 1) Adenine is at its highest concentration at the onset of the pond’s dry phase. 2) Upon drying, adenine ceases to outflow from large fragments, and UV radiation rapidly destroys all previously released adenine. 3) Re-wetting allows the remaining adenine within large fragment pores to continue to outflow. The U-shape is due to the increase and decrease in water level. . . . . 67

3.5	<p>The dotted circle represents the target area for landing the dispersed fragments from a single meteoroid into any WLP on the early Earth. The smaller, light grey circle in the center is the total combined WLP surface area on the early Earth at a given time (WLPs would have been individually scattered, however for a geometric probability calculation they can be visualized as a single pond cross-section). The larger, surrounding circles represent the area of debris when the fragments of the meteoroid hit the ground. Shortly after 4.5 Ga, the area of debris from a single meteoroid would be large compared to the the combined WLP surface area. At any time, the target area for a meteoroid to deposit fragments homogeneously into at least 1 WLP is slightly larger than the combined area of WLPs. The effective target area grows linearly with total WLP surface area. The diagonally striped intersections between the circles represent the largest individual WLP for which the meteoroid fragment deposition probability is being calculated. The logic is that if a meteoroid enters the atmosphere at distance <math>d</math> from the center of the combined pond cross-section, at least 1 pond of any size in the WLP distribution will completely overlap with the area of debris. . . . .</p>	77
3.6	<p>Normalized probability distributions of fragments from CM-, CI-, and CR-type meteoroids with radii 20–40 m landing in WLPs on the early Earth of radii 1–10 m. Three models for mass delivery are compared: the Late Heavy Bombardment model, and minimum and maximum mass models for a sustained, declining bombardment preceding 3.9 Ga. All models are based on analyses of the lunar cratering record [269, 271]. See Figure 3.1 in the main text for display of mass delivery rates. The 95% confidence intervals are shaded, and correspond to the most likely deposition intervals for each model. . . . .</p>	78
3.7	<p>Fraction of the total initial nucleobases remaining in <b>(A)</b> a 100<math>\mu</math>m-radius IDP and <b>(B)</b> 1 cm-, 5 cm-, and 10 cm-radii meteorites over time as a result of diffusion across a rock-pond boundary. The IDP and meteorites are considered to be laying on the bottom of a WLP, and are diffusing nucleobases symmetrically in the radial direction. The times at which 99% of the initial contained nucleobases have diffused into the WLP are labeled on the plots. . . . .</p>	86

3.8	The nucleobase mixing time in a base-to-surface convection cell (length = $2r_p$ ) within 1 m-, 5 m-, and 10 m-deep WLPs, beginning from a local concentration at the base of the pond. Nucleobase mixing is measured using the maximum percent local nucleobase concentration difference from the average. The time at which the maximum local nucleobase concentration difference from the average drops to 10% is labeled on the plot for each pond size. At this time, we consider the nucleobases in the WLP to be well mixed. For WLPs with radii 1 m, 5 m, and 10 m, the convection cell nucleobase mixing times are 35 minutes, 104 minutes, and 150 minutes, respectively. . . . .	87
3.9	The effect of temperature on the change in water mass over time in wet environment cylindrical WLPs with radii and depths of 1 m. Temperatures are varied for a hot early Earth model (50 °C, 65 °C, and 80 °C) and a warm early Earth model (5 °C, 20 °C, and 35 °C). Precipitation rates from Columbia and Thailand on Earth today are used to represent the hot, and warm early Earth analogues, respectively (for details see Table 3.1 in the main text). . . . .	92
3.10	The accumulation of adenine from only carbonaceous IDP sources in cylindrical WLPs with radii and depths of 1 m. The three curves (dry, intermediate, and wet environments) differ by their precipitation rates, which are from a variety of locations on Earth today, and represent 2 classes of matching early Earth analogues: hot (Columbia, Indonesia, Cameroon), and warm (Thailand, Brazil, and Mexico) (for details see Table 3.1 in the main text). <b>(A)</b> The degenerate WLP models used for these calculations correspond to a hot early Earth at 65 °C and a warm early Earth at 20 °C. <b>(B)</b> The degenerate WLP models used for these calculations correspond to a hot early Earth at 50 °C and a warm early Earth at 5 °C. . . . .	93

3.11 The accumulation of guanine, adenine, uracil, and cytosine from only carbonaceous IDP sources in cylindrical WLPs with radii and depths of 1 m. The degenerate dry WLP models used for these calculations correspond to a hot early Earth at 65 °C and a warm early Earth at 20 °C. Precipitation rates from Cameroon and Mexico on Earth today are used to represent the hot, and warm early Earth analogues, respectively (for details see Table 3.1 in the main text). The cytosine abundance in IDPs used to calculate the max cytosine curve, matches the average abundance of guanine in IDPs (see Table 3.3). The curves are obtained by numerically solving Equation 3.34. . . . . 94

3.12 **The no seepage limit:** The accumulation of adenine from only carbonaceous IDP sources in cylindrical WLPs with radii and depths of 1 m. The two curves represent the adenine concentrations in a wet environment pond on a hot (65 °C), and warm (20 °C) early Earth (for details see Table 3.1 in the main text). The thickness of the lines is due to the seasonal oscillations in adenine concentrations. . . . . 95

3.13 The accumulation of adenine from 1 cm fragments of an initially 40 m-radius carbonaceous meteoroid in a cylindrical WLP with a radius and depth of 1 m. The degenerate WLP models used for these calculations correspond to a hot early Earth at 65 °C and a warm early Earth at 20 °C. **(A)** The accumulation of adenine from carbonaceous meteorites in an intermediate environment (for details see Table 3.1 in the main text). The wet-dry cycles of the pond are also shown to illustrate the effect of water level on adenine concentration. **(B)** The three curves (dry, intermediate, and wet environments) differ by their precipitation rates, which are from a variety of locations on Earth today, and represent 2 classes of matching early Earth analogues: hot (Columbia, Indonesia, Cameroon), and warm (Thailand, Brazil, and Mexico) (for details see Table 3.1 in the main text). The curves are obtained by numerically solving Equation 3.38. . . . . 96

- 3.14 The maximum concentration of adenine accumulated from 1 cm fragments of a carbonaceous meteoroid 20–40 m in radius in cylindrical WLPs with radii and depths of 1 m. The degenerate WLP models used for these calculations correspond to a hot early Earth at 65 °C and a warm early Earth at 20 °C. The three curves (dry, intermediate, and wet environments) differ by their precipitation rates, which are from a variety of locations on Earth today, and represent 2 classes of matching early Earth analogues: hot (Columbia, Indonesia, Cameroon), and warm (Thailand, Brazil, and Mexico) (for details see Table 3.1 in the main text). The curves are obtained by numerically solving Equation 3.38. . . . . 97
- 3.15 The accumulation of guanine, adenine, and uracil from 1 cm fragments of an initially 40 m-radius carbonaceous meteoroid in cylindrical WLPs with radii and depths of 1 m. The degenerate WLP models used for these calculations correspond to a hot early Earth at 65 °C and a warm early Earth at 20 °C. The two curves for each nucleobase differ by their precipitation rates, which create intermediate (solid lines), and wet (dotted lines) environments, and are from a variety of locations on Earth today representing 2 classes of matching early Earth analogues: hot (Columbia, Indonesia), and warm (Thailand, Brazil) (for details see Table 3.1 in the main text). The curves are obtained by numerically solving Equation 3.38. . . . . 98
- 3.16 Example simulations, including the initial conditions, for our two part nucleobase transport model. Each line represents a different snapshot in time. **(A)** Initially homogeneous nucleobase diffusion from a 100  $\mu\text{m}$ -radius carbonaceous IDP. **(B)** Initially locally concentrated nucleobase mixing in a convection cell within a 1 m-deep WLP. The convection cell is a  $L = 2r_p$  eccentric loop flowing between the bottom to the top of the WLP. This loop is sliced at  $r' = 1$  m in the convection cell's moving frame and unraveled for display in the above 1D plot. . . . . 104

# List of Tables

2.1	Summary and scientific basis of the events and biosignatures in the Figure 2.1 timeline. . . . .	25
3.1	Precipitation models matching dry, intermediate, and wet environments on a warm (5–35°C) and hot (50–80°C) early Earth. Precipitation data from a variety of locations on Earth today [57, 281] represent 2 classes of matching early Earth analogues: warm (Thailand, Brazil, and Mexico) and hot (Columbia, Indonesia, Cameroon). For example, the conditions in Mexico on a warm early Earth match the conditions in Cameroon on a hot early Earth. $\bar{P}$ is the mean precipitation rate, $\delta_p$ is the seasonal precipitation amplitude, and $s_p$ is the phase shift. . . . .	66
3.2	Sources and sinks of pond water and nucleobases in our model of early Earth WLPs. . . . .	80
3.3	Average guanine, adenine and uracil abundances (in ppb) in the CM, CR, and CI carbonaceous chondrites. Abundances obtained from [36]. Some CM and CR meteorite analyses found no adenine or uracil, these samples were excluded from the average. Weighted nucleobase averages are also displayed based on relative fall frequencies [274]. Uracil has not been measured in CR meteorites. Cytosine has not been measured in any meteorites. . . . .	88

3.4	Different equations for modeling the effective diffusion coefficient of species in porous media. Estimates of the effective diffusion coefficients of single nucleobases through the pores of carbonaceous IDPs and meteorites are also calculated for each model. The free water diffusion coefficient, $D_0$ , represents the unobstructed diffusion of a species, the porosity factor, $\phi$ , represents the void fraction of the medium, the constrictivity factor, $\delta$ , represents the bottleneck effect due to small pore diameters, and the tortuosity factor, $\tau$ , represents the restriction in diffusive flow due to curves in the pores. Estimates of these factors, and the empirical exponent, $m$ , for carbonaceous IDPs and meteorites are, $D_0 = 4 \times 10^{-10} \text{m}^2 \text{s}^{-1}$ , $\phi = 0.25$ , $\delta = 1$ , $\tau = 1.45$ , and $m = 2$ [306–309].	100
3.5	Summary of parts one and two of our 1D nucleobase transport model. Part one is a model of nucleobase outflow from carbonaceous IDPs and meteorites while they lay at the base of a WLP. Part two is the mixing (i.e. homogenization) of a local concentration of nucleobases throughout the WLP.	103

# List of Abbreviations and Symbols

‰ parts-per-thousand

$^{26}\text{Al}$  Aluminum-26

•OH Hydroxyl radical

-NH<sub>2</sub> Amino group

AMP Adenosine monophosphate

ATP Adenosine triphosphate

BRA Brazil

BTCS backward time, centered space

CAM Cameroon

CH<sub>2</sub>O Formaldehyde

CH<sub>3</sub>NO Formamide

CH<sub>4</sub> Methane

CMP Cytidine monophosphate

CO Carbon monoxide

CO<sub>2</sub> Carbon dioxide

COL Columbia

DNA Deoxyribonucleic acid

**FTT** Fischer-Tropsch-type

**Ga** Giga years ago

**GMP** Guanosine monophosphate

**GOE** Great oxidation event

**H<sub>2</sub>** Hydrogen

**H<sub>2</sub>S** Hydrogen sulphide

**HCN** Hydrogen cyanide

**HNO** Nitroxyl

**HST** Hubble Space Telescope

**IDN** Indonesia

**IDP** Interplanetary dust particle

**JWST** James Webb Space Telescope

**LUCA** Last universal common ancestor

**MEX** Mexico

**MIF** mass independent fractionation

**mRNA** Messenger ribonucleic acid

**N<sub>2</sub>** Nitrogen

**NH<sub>3</sub>** Ammonia

**ppb** parts-per-billion

**ppm** parts-per-million

**ppq** parts-per-quadrillion

**pptr** parts-per-trillion

**RNA** Ribonucleic acid

**SO<sub>2</sub>** Sulfur dioxide

**THA** Thailand

**tRNA** Transfer ribonucleic acid

**UMP** Uridine monophosphate

**UV** Ultraviolet

**WFC3** Wide Field Camera 3

**WLP** Warm little pond

## **Declaration of Academic Achievement**

I, Ben K. D. Pearce, declare that this thesis titled, ‘The Emergence of the RNA World on the Early Earth’ and the work presented in it are my own. Where the thesis is based on work done by myself jointly with others, I have made clear exactly what was done by others and what I have contributed myself. The details of such contributions are outlined below.

As my supervisor, Dr. Ralph Pudritz contributed a great deal of writing and ideas to all parts of this thesis.

Chapters 1 and 4 of this thesis were written by Ben K. D. Pearce, and edited by Dr. Ralph Pudritz.

Chapter 2 of this thesis is the result of a marriage between the literature reviews written by Ben K. D. Pearce and Andrew Tupper for the ORIGINS 701 graduate course. The majority of the research for and writing of Chapter 2 was performed by Ben K. D. Pearce. Sections 2.3.2 and 2.3.4 were originally written by Andrew Tupper and reworked by Ben K. D. Pearce, and Section 2.6 was written by Dr. Paul Higgs and lightly edited by Ben K. D. Pearce. Dr. Ralph Pudritz, Dr. Paul Higgs, Andrew Tupper all contributed to the writing and editing of this chapter.

The research for Chapter 3 was designed by Ben K. D. Pearce, Dr. Ralph Pudritz, Dr. Dmitry Semenov, and Dr. Thomas Henning. The majority of the research for and writing of Chapter 3 was performed by Ben K. D. Pearce. Dr. Ralph Pudritz contributed a great amount of writing and editing to this chapter. Dr. Ralph Pudritz, Dr. Dmitry Semenov, and Dr. Thomas Henning all contributed to the writing and editing of this chapter.

*Dedicated to Berlin: your culture, your energy, your people.  
You taught me who I am.*

# Chapter 1

## Introduction

One of the deepest questions intelligent beings can ponder is, where did we come from? Charles Darwin discovered the theory of evolution by natural selection in the 1850's, which explains how simple cellular life progressed into the diverse set of species we observe on Earth today [1]. However it is still unclear how non-living, organic molecules converted into something that can reproduce and evolve. Alexander Oparin and John Haldane independently introduced the primordial soup hypothesis in the 1920's to try to answer this question. They asserted that simple organics were produced in the early atmosphere, and “must have accumulated until the primitive oceans reached the consistency of hot dilute soup [2].” From this rich organic soup, they deduced, biopolymers and ultimately life could form. In other words, given the right ingredients are settled in the right environment, life should arise naturally.

There are still many unknowns with regards to this hypothesis, including the conditions of the “right” environment, the origin of life's building blocks, and how long it took for the first life molecules to emerge and evolve into the incredibly fine-tuned system we call the genetic code.

Although numerous definitions for life exist, the most popular definition is a self-sustaining chemical system capable of Darwinian evolution [3]. For this thesis, we consider something that satisfies this definition, as living.

## 1.1 The RNA World

The RNA world is the leading hypothesis that describes first life on Earth. This idea posits that the first life forms were ribonucleic acid (RNA) molecules, either cell-free, e.g. floating in a pond or pore, or compartmentalized in cell-like structures [4–9]. RNA is a polymer made up of any sequence of 4 ribonucleotide monomers: adenosine monophosphate (AMP), guanosine monophosphate (GMP), uridine monophosphate (UMP), and cytidine monophosphate (CMP). Each ribonucleotide is composed of an identifying nucleobase (adenine, guanine, uracil, or cytosine), a ribose, and a phosphate molecule (see Figure 1.1).

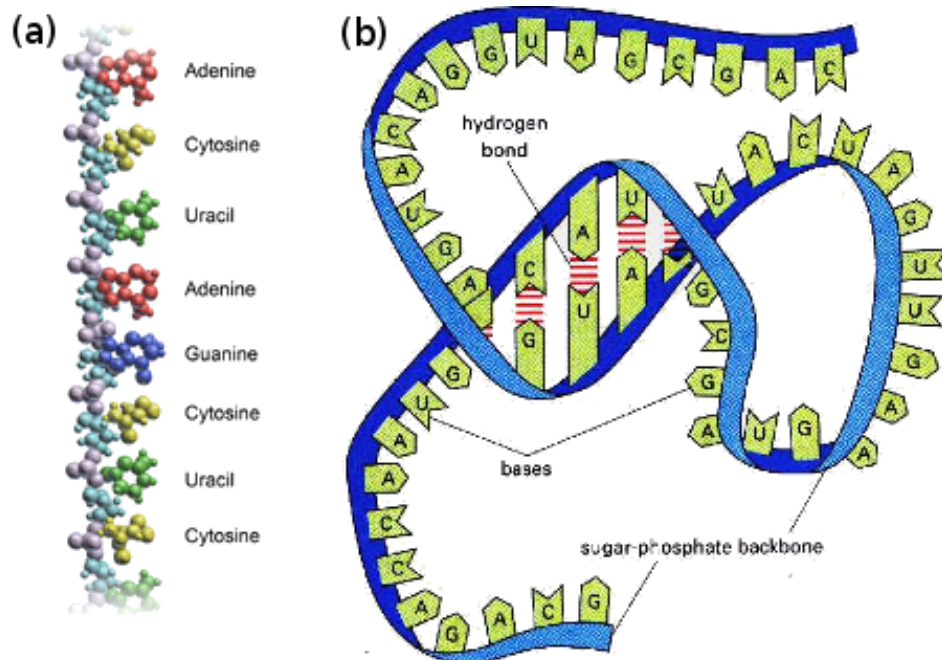


Figure 1.1: Ribonucleic acid (RNA) molecules in (a) unfolded and (b) folded states. RNA molecules are made up of a sequence of nucleobases (adenine, guanine, uracil, cytosine) attached to a backbone made up of ribose and phosphate. RNA nucleobases can base pair (adenine to uracil and guanine to cytosine) which allows RNA to fold onto itself and become catalytic, or form double-stranded RNA for template replication. Sources: [10, 11]

The simplest reason for thinking RNA molecules expressed first life is that DNA-, RNA-, and protein-based life, i.e., life as we know it, is too complex to form spontaneously. For example, consider the process of building proteins. Several proteins bind to a particular site on a DNA double helix, forming a complex to initiate copying.

Using energy in the form of adenosine triphosphate (ATP), the RNA polymerase and a couple other proteins create a small separation of the DNA double helix, and traverse along the molecule, using ribonucleotides from the environment to copy the DNA template as they go. Once the copying of the genetic information is complete, the resultant RNA strand, called messenger RNA (mRNA), travels to the ribosome to initiate translation. The ribosome then translates the information from the 4-letter nucleotide alphabet into the 20-letter amino acid alphabet by linking groups of three mRNA nucleotides (i.e. codons) to a tRNA molecule containing the encoded amino acid. This map comprises the genetic code. As tRNA molecules link up along the mRNA molecule, the amino acids attached to the ends of the tRNA molecules chain together into a functioning protein. This process, which occurs within all living organisms, is impeccably error-prone, with about 1 amino acid misincorporation every 1,000 to 10,000 codons [12].

Such a process requires DNA, RNA, and proteins—all biopolymers composed of different building blocks—to be present simultaneously. This is a proverbial chicken-or-egg problem, as DNA is required to make proteins, and proteins are required to make DNA. One way out of this paradox is to have a different molecule initially play the role of both [3]. In other words, there must have existed a living functional intermediate between non-living organic molecules, and DNA-, RNA-, and protein-based life that was capable of using one to evolve into the other. RNA is a superb candidate for the following reasons:

1. RNA can store genetic information as a particular sequence of ribonucleotides, just like DNA does for all living things today.
2. RNA nucleotides can pair up, and thus a mechanism exists for making copies (AMP pairs with UMP, and GMP pairs with CMP).
3. RNA nucleotide pairs are not exclusive, as GMP infrequently pairs with UMP, allowing for imperfect copying, and thus evolution.
4. RNA can act as a catalyst for replication, i.e., folded RNA molecules can promote the pairing of ribonucleotides to an unfolded RNA template. (Proteins take on this role for DNA replication.)
5. RNA is present in all living organisms, and thus is a logical intermediate (as an

analogy *Homo sapiens* and the primates from which they evolved contain much of the same anatomy.)

6. The ribosome, i.e. the machine responsible for protein synthesis in all living cells, is predominantly composed of RNA, and thus acts as a logical endpoint for RNA evolution.

One complexity of the RNA world hypothesis is that RNA molecules cannot simultaneously be catalysts and genetic carriers. In order for an RNA molecule to be catalytic, it must fold onto itself, i.e. make single-strand base pairs (Figure 1.1(b)). Conversely, in order for an RNA molecule to be a template for replication, it must be unfolded (Figure 1.1(a)) [8]. This idea is partially solved by molecules called RNA polymerases. RNA Polymerases are catalytic (i.e. folded) RNA molecules that bind onto the end of any RNA template, and, while traversing its length, attach the appropriate base pair from the environment to each nucleotide site on the template. At the end of this process, the polymerase reaches the end of the template, and leaves behind a double-stranded RNA molecule. The mechanism of splitting the double-stranded RNA apart is still uncertain, however experiments suggest temperature cycling may be necessary [13]. This replication process is illustrated for a DNA polymerase in Figure 1.2.

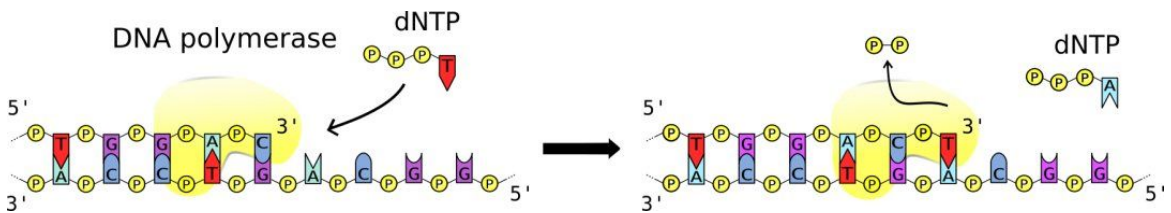


Figure 1.2: A DNA polymerase (faded yellow) attaching a nucleotide from the environment to the appropriate nucleotide site on the DNA template strand. RNA polymerases would function generally the same on an RNA template. Source: [14].

This mechanism for RNA replication explains how genetic information is carried forward in an RNA world setting, however given the first polymerase formed naturally, such a system cannot grow unless the polymerase can also be replicated. Therefore the holy grail in RNA polymerase research would be to find a polymerase that spends a portion of its time folded, and a portion of its time unfolded, i.e., can replicate all RNA templates including itself. RNA polymerases have been synthesized in the lab by *in vitro* evolution [15, 16], i.e. mimicking the process of natural selection in a test tube.

However as of yet, no polymerase has been synthesized which can act as a template for self-replication.

Perhaps the closest thing that resembles a self-replicating system is an RNA ligase synthesized by Lincoln & Joyce [17]. An RNA ligase is similar to an RNA polymerase, however instead of using nucleotides in the environment to replicate an RNA template, an RNA ligase takes two RNA strands in the environment and ligates (connects) them together on an RNA template. The RNA ligase synthesized by Lincoln & Joyce [17] can act as a template and a ligase, making it the first self-replicating ribozyme to be formed in the lab. However, in order for this ligase to replicate itself, the exact complementary RNA strands must be available in the environment to ligate, and the two strands are of non-trivial lengths (53 and 13 nucleotides long).

Simulations of various RNA molecules on a surface (e.g. self-replicating polymerases, templates, parasites) show that as long as the error rates of replication are below a critical threshold, an RNA world can grow and reach stability [18, 19]. And, because the RNA world qualifies as a self-sustaining chemical system capable of Darwinian evolution, the questions of when and how life emerged on Earth are therefore actually questions of when and how the RNA world emerged.

## 1.2 The Emergence of Life on Earth

Constraining *when* life emerged on the Earth relies on two types of evidence. Astrophysical evidence constrains the time at which the Earth became habitable, and therefore the earliest time life could theoretically exist on the planet. For example, isotopic analyses and theoretical models have been used to constrain the age of the Solar System, the time scale for the formation of the Earth and Moon, and the time scale for the cooling of the magma mantle into a solid crust. The second type of evidence is biosignatures. Biosignatures reveal the times at which life already existed on the surface of the Earth. For example, potential remnants of ancient single-celled organisms in the form of microfossils, stromatolites, and biologically reduced carbon isotopes have been discovered in rocks with ages between 4.3–1.9 Ga (giga years ago). (For detailed descriptions of each of these biosignatures, see Sections 2.4.1, 2.4.2, and 2.5.2). However a consensus does not exist as to whether all such samples have a biological origin, as there also exists abiotic processes that may create structures resembling microfossils and stromatolites, and may lighten rocks in their carbon isotopes.

To begin to answer *how* the RNA world emerged, we need to understand where the building blocks of RNA came from. Ribonucleotides—composed of a nucleobase (adenine, guanine, uracil, or cytosine), ribose, and phosphate—are not easily synthesized in the lab, however two distinct reaction pathways have been met with some success. These pathways are the Lego block approach [20], and the sequential addition approach [21]. The Lego block approach to forming ribonucleotides involves putting the three components (i.e. Lego blocks) of a ribonucleotide together in a reaction vessel, and giving them sufficient time to react. This has only been demonstrated once in the lab, where AMP was synthesized from adenine, ribose and ethyl metaphosphate in 1 hour in a single step [22]. However, there has been more success in forming AMP in two steps by reacting adenine with ribose to form adenosine [23, 24], and reacting adenosine with different phosphorous sources to form AMP [25, 26]. The other three nucleosides (guanosine, uridine, and cytidine) have not been synthesized in the lab by reacting the corresponding nucleobase with ribose, however there has been success in phosphorylating guanosine, uridine, and cytidine to form GMP, UMP, and CMP [27–32]. The sequential addition approach to forming ribonucleotides involves reacting cyanamide, cyanoacetylene, glycolaldehyde, glyceraldehyde and inorganic phosphate in a particular sequence of 4 steps to form CMP, and upon UV degradation, UMP [21]. At each reaction step, a new reactant is added to the reaction vessel for a selected temperature ranging from 40–60°C, and is left for a time ranging from hours to days.

Nature however, is not an experimental chemist, and does not add one reactant at a time into a pond or a hydrothermal pore—as would be required to consider the sequential addition approach for prebiotic chemistry. When experimental chemists add cyanamide, cyanoacetylene, glycolaldehyde, glyceraldehyde and inorganic phosphate to a single reaction vessel simultaneously, only tar forms (Sebastien Pallmann, personal communication). For this reason, the more likely pathway to forming ribonucleotides prebiotically may be the Lego block approach. In which case understanding the source of prebiotic nucleobases, i.e. the characteristic molecules of ribonucleotides, becomes an important first step in discovering the origin of the RNA world.

### 1.2.1 Nucleobase Sources

In general, organics can either be produced endogenously, i.e. on the surface, or in the atmosphere of the early planet, or they can be exogenously delivered to the planet from an outside source. Chyba & Sagan [33] performed a benchmark study on the origin

of prebiotic organics by comparing organic carbon yields and influxes from various sources. The endogenous sources they considered were synthesis by lightning, coronal discharges (i.e. electric discharges from pointed objects on the Earth that concentrate the local electric field), ultraviolet (UV) light, and shocks due to cometary or asteroidal bodies entering the atmosphere and impacting the surface. The exogenous sources they considered were interplanetary dust particles (IDPs), meteorites (cometary or asteroidal), and interstellar dust. They discovered that the dominant source of organic carbon to the early Earth depends strongly on the composition of the atmosphere at that time. In the case that the early Earth atmosphere was strongly reducing, UV photochemistry, impact shock synthesis, and Miller-Urey type reactions driven by lightning would dominate [33]. However, based on the oxidation state of  $\sim 4.4$ -Gyr-old zircons, the Earth's early atmosphere is thought to be mainly composed of  $\text{CO}_2$ ,  $\text{N}_2$ ,  $\text{SO}_2$ , and  $\text{H}_2\text{O}$  [34], rather than strongly reducing gases such as  $\text{H}_2$ ,  $\text{CH}_4$ ,  $\text{NH}_3$ , and  $\text{CO}$  [35]. In this case, they concluded UV photochemistry and IDPs dominate as a prebiotic source of organic carbon [33].

Not all organic carbon sources considered by Chyba & Sagan [33] are a source of nucleobases. For example, there is no known reaction which produces nucleobases by exposing reducing or neutral atmospheric gases to UV light [36]. UV photochemistry is however capable of producing hydrocarbons, HCN, and amino acids [33]. Furthermore, nucleobases have not yet been detected in the interstellar medium; although nucleobase precursors have been detected [37, 38]. Regardless, Chyba & Sagan [33] estimate that interstellar dust delivered 1–2 orders of magnitude less organic carbon than local dust (IDPs) delivered to the early Earth.

We review the potential sources of nucleobases to the early Earth below. Endogenous sources of nucleobases could include Fischer-Tropsch-Type (FTT) synthesis in hydrothermal vents, Miller-Urey synthesis in the primeval atmosphere, various reactions in warm little ponds (WLPs), and meteorite impact shock synthesis. Potential exogenous sources include IDPs, and meteorites (cometary or asteroidal).

### 1.2.1.1 Synthesis in Hydrothermal Vents

Hydrothermal vents are cracks on the ocean floor out of which geothermally heated water spews (see Figure 1.3). These environments are either formed by sustained fault activity (e.g. the Lost City hydrothermal field), or by magma chambers that discharge lavas onto the ocean floor (e.g. black smokers). The fluids vented from such

environments first circulate through the crust where they are heated to temperatures of 40–405°C [39]. This is also where hydrothermal fluids are enriched in magmatic CO<sub>2</sub>, and H<sub>2</sub> produced from interactions between the sea water and igneous rocks at high temperatures (a process known as serpentinization) [40]. The constant source of H<sub>2</sub> and CO<sub>2</sub> in hydrothermal systems is favourable for producing simple organics. For example, H<sub>2</sub> and CO<sub>2</sub> have a thermodynamically favourable reaction pathway to CH<sub>4</sub> and acetate [39]. Moreover, CO<sub>2</sub> can react with H<sub>2</sub> to produce CO and H<sub>2</sub>O, from which subsequent FTT reactions can produce hydrocarbons [41]. Finally, given a source of nitrogen in the form of NH<sub>3</sub> is available in these environments, as well as metal catalysts like alumina, nickel-iron or silica, FTT reactions could produce nucleobases via reaction Equation 1.1 below [36]. Using thermodynamic simulations in the past we have shown that FTT reactions dominate the production of nucleobases in meteorite parent bodies [42].

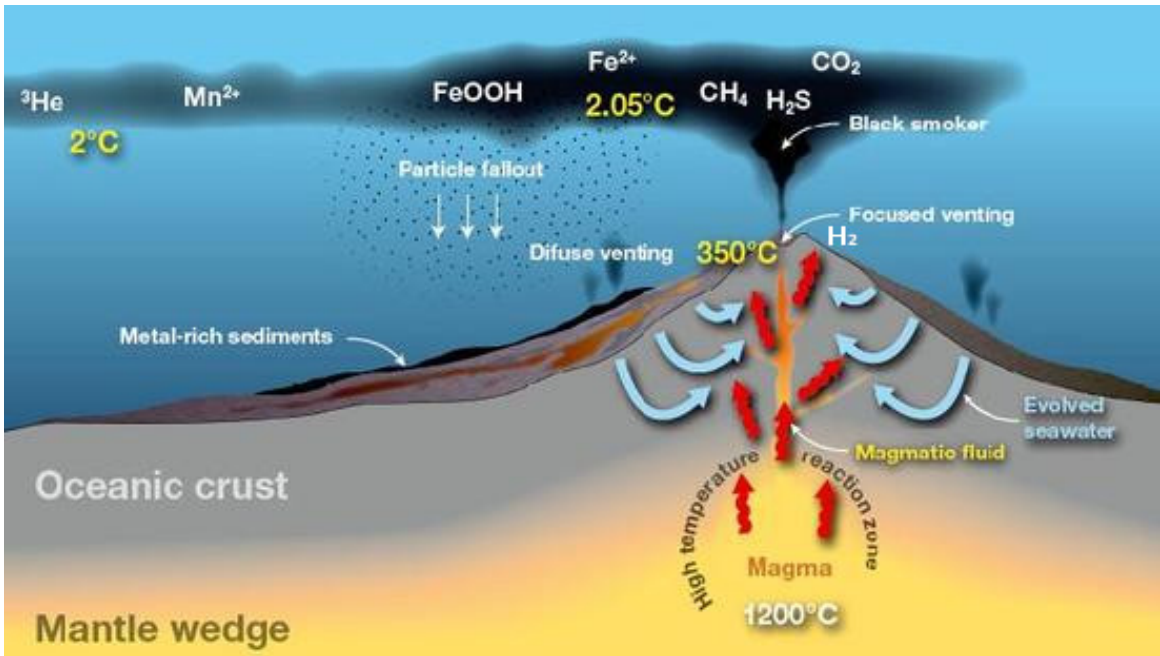
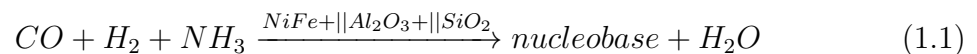


Figure 1.3: A diagram of a black smoker hydrothermal vent. Hydrothermal fluid is heated by a high temperature magma chamber, and enriched with organic-synthesizing reactants such as magmatic CO<sub>2</sub>, and H<sub>2</sub> from serpentinization. The black smoker plume is composed of CO<sub>2</sub>, H<sub>2</sub>S, CH<sub>4</sub> and other molecules that are released when the enriched hydrothermal fluids mix with seawater. Source: [43].



Catalysts are shown above the reaction arrow, with ‘+||’ symbolizing ‘and/or.’

As to the sources of  $\text{NH}_3$ , reduction of  $\text{N}_2$  by  $\text{H}_2\text{S}$  in hydrothermal vents likely only produced dissolved  $\text{NH}_3$  concentrations in the nanomolar range ( $\sim 20$  parts-per-trillion (pptr)) [44]. Moreover, any external  $\text{NH}_3$  sources would have faced difficulties concentrating in the voluminous ocean. Therefore FTT synthesis in hydrothermal settings is probably unlikely as a dominant source of prebiotic nucleobases.

### 1.2.1.2 Miller-Urey Synthesis

In the early 1950’s a PhD student named Stanley Miller and his advisor Harold Urey performed prebiotic chemistry experiments which would usher in the modern era of this field [45]. Their approach stood out from that of previous prebiotic chemistry experiments because they set out to test a specific hypothesis for the origin of life. Their hypothesis was that the organics which led to the emergence of life were produced in the early atmosphere by lightning. Their experimental setup involved capturing early Earth atmospheric gases into a glass flask, within which they discharged a spark, and condensed the products into a cold trap for sampling (see Figure 1.4).

At the time, it was thought that the early Earth’s atmosphere was composed of highly reduced gases, i.e. gases that would be oxidized in the presence of oxygen, such as  $\text{CH}_4$ ,  $\text{NH}_3$ ,  $\text{H}_2$ , and  $\text{CO}$  [45]. For example, two  $\text{O}_2$  molecules react readily with  $\text{CH}_4$  to produce  $\text{CO}_2$  and two  $\text{H}_2\text{O}$  molecules. Using a highly reducing atmospheric composition, their experimental design has successfully produced 13 of the 20 amino acids in proteins [46], and all 4 nucleobases in RNA [47–50]. However, recent models of the early Earth atmosphere and evidence from the oxidation state of  $\sim 4.4$ -Gyr-old zircons suggest the early Earth had a weakly reducing atmosphere, i.e. dominated by inert or highly oxidized gases like  $\text{N}_2$  and  $\text{CO}_2$  [34, 51, 52]. When Miller-Urey experiments are performed with  $\text{CO}_2$ ,  $\text{N}_2$ , and  $\text{H}_2\text{O}$  atmospheres, amino acid yields drop to below 0.001%, based on initial carbon. This is  $\sim 3$  orders of magnitude lower than the yield of amino acids obtained using strongly reducing atmospheres [46]. Furthermore, nucleobases have not been produced in Miller-Urey experiments performed with weakly reducing atmospheres. It is therefore unlikely that the atmosphere was a dominant source of prebiotic nucleobases.

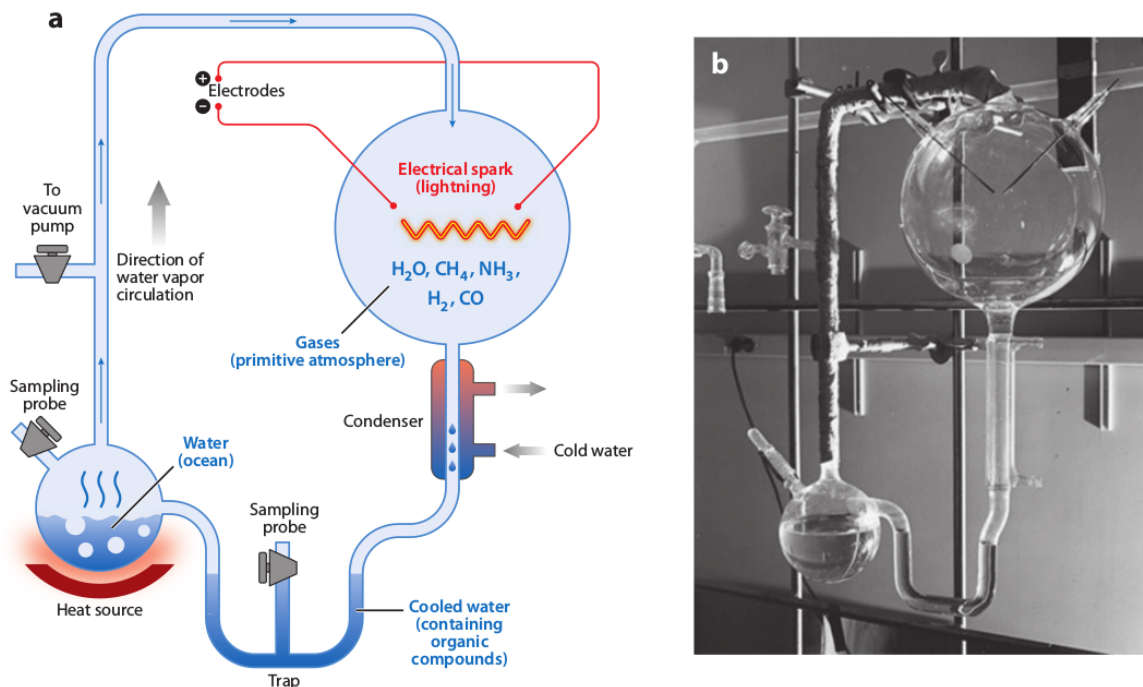


Figure 1.4: The Miller-Urey spark discharge apparatus. Water boils in the lower spherical compartment sending vapour to collect in the upper spherical compartment with highly reduced gases such as  $CH_4$ ,  $NH_3$ ,  $H_2$ , and  $CO$ . An electrical spark then discharges in the upper spherical compartment producing organics which condense into a cooled trap. (a) A schematic drawing of the apparatus. (b) A Photo of the original apparatus. Source: [45].

### 1.2.1.3 Synthesis in Warm Little Ponds

WLPs are typically filled by rainwater, and are emptied by evaporation and seepage through pores at their bases [53, 54] (see Figure 3.2). The greater abundances of radiogenic sources within the early Earth [55] may have caused some WLPs to have temperatures of  $50\text{--}80^\circ\text{C}$  [56]. Annual precipitation rates on Earth follow sinusoidal curves, with rainfall peaks in the summers and drier periods in the winters [57]. This counter-play between sources and sinks provides natural wet-dry cycles which have been shown to promote the polymerization of nucleotides into RNA [58–60].

There are three nucleobase reactions that could potentially occur within WLPs: FTT reactions, HCN-based reactions, and formamide reactions [36]. However, these reactions have not yet been modeled for these environments, and thus it is unknown whether they are plausible nucleobase sources. For a discussion on each of these reactions, see Appendix A.

In future work we intend to calculate the maximum concentrations of nucleobases possible in early Earth WLP environments from these *in situ* reactions.

#### 1.2.1.4 Meteorite Shock Synthesis

The early Earth was bombarded by meteorites at a rate of  $\sim 1\text{--}1000 \times 10^{12}$  kg/yr, which is approximately 8–11 orders of magnitude greater than today [61]. Some of these meteorites impacted water reservoirs at high speeds, causing high-energy shockwaves to propagate through the water solutions. Recent experiments have formed cytosine and uracil by impacting iron, stony and carbonaceous meteorite analogs in a reaction container containing a prebiotically plausible solution representing early Earth bodies of water [62]. The solution contained bicarbonate and ammonium, which would be the main carbon and nitrogen molecules in ponds resulting from the dissolution of atmospheric  $\text{CO}_2$  and  $\text{HNO}$  [63]. This experiment was unable to produce detectable abundances of adenine or guanine, however other experiments simulating impact shocks in solutions of formamide containing clay have successfully produced all nucleobases [64]. Dilute formamide solutions could be possible in early Earth bodies of water (see Section 1.2.1.3 above), however, if ponds containing formamide existed on the early Earth, nucleobases would form in them without the need of impact shocks [36, 42]. Therefore, although meteorite impact shocks may have been a prebiotic source of cytosine and uracil, it seems unlikely at this point to have been a dominant prebiotic source of all 4 RNA nucleobases.

#### 1.2.1.5 Meteorites and IDPs

Meteorites and IDPs (e.g. see Figure 1.5) originated from the protoplanetary disk surrounding our protosun. Early after the formation of the disk, micron-sized dust coalesced into larger grains, which agglomerated and eventually lead to kilometer-sized planetesimals [65]. Some of these planetesimals collided to form planetary embryos, and others remained scattered throughout the disk. Collisions of the remaining planetesimals followed by gravitational perturbations eventually sent some fragments on trajectories towards the early Earth. Some of the carbon-rich planetesimal fragments entering Earth's atmosphere were small ( $< 80$  m in diameter) and as they further fragmented in the atmosphere and spread out, their total surface area to drag increased, allowing them to reach terminal velocity [66]. At such speeds, these smaller fragments

survived impact, becoming meteorites [67]. On the early planet, meteorites delivered intact carbon at a rate of  $\sim 2 \times 10^3$  kg/yr [33]. A carbon-rich class of meteorites known as carbonaceous chondrites are known to contain abiotically produced amino acids, 3 of the 4 nucleobases in RNA, and carboxylic acids [36, 68–71]. Cytosine isn't detected in meteorites today, and likely wasn't delivered to the early Earth by these sources, as it hydrolyzes efficiently into uracil within the aqueous interiors of planetesimals [42]. However the abundances of guanine, adenine, and uracil in carbonaceous chondrites range from 0.25–515 parts-per-billion (ppb), and thus such meteorites are a prebiotically plausible source of these nucleobases [36, 70].

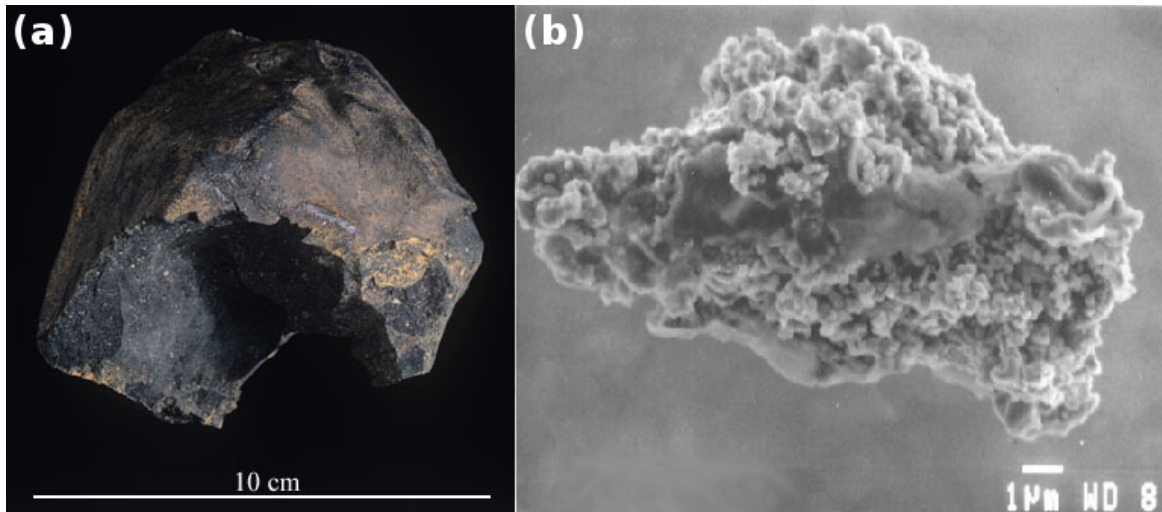


Figure 1.5: (a) The Murchison meteorite, which fell to Earth near Murchison, Victoria, Australia in 1969. The Murchison meteorite contains 3 of the 4 nucleobases in RNA (guanine, adenine, and uracil). (b) A typical IDP collected by an airplane at high altitude. Sources: [72, 73].

Some of the dust produced in planetesimal collisions, and some of the dust that never coalesced in the disk, decayed in orbit due to Poynting-Robertson drag and eventually collided with the early planet [74]. The dust that entered the Earth's atmosphere would have been subjected to pulse heating (temperatures  $> 500^\circ\text{C}$  for a few seconds), however experiments show a modest amount ( $\sim 1\text{--}6\%$ ) of organic molecules can survive these events [75]. IDPs delivered approximately 5 orders of magnitude more intact carbon to the early Earth than did meteorites ( $\sim 6 \times 10^8$  kg/yr) [33]. Amino acids and nucleobases have not been measured in IDPs, however several amino acids, and three of the five nucleobases (uracil, cytosine, and thymine) have been formed on the surfaces of icy IDP analogues in the lab through exposure to UV

radiation [76, 77]. Moreover, given that IDPs are thought to mostly originate from asteroids and comets [33], any dust originating from carbonaceous chondrite parent bodies could contain the same organics as carbonaceous chondrites. Upon deposition of carbonaceous chondrites and IDPs into WLPs, their organic contents would diffuse into the pond water and could concentrate as the ponds cycle from wet to dry.

Nucleobases were able to form within planetesimals because of the incorporation of reactive nitrogen species to these bodies. Simple nucleotide precursors such as  $\text{NH}_3$  and HCN originated from the solar nebula that collapsed to form the protosun and surrounding disk [78–80], and from the chemical processing that occurred during the early disk stages [81–83]. Planetesimals also incorporated  $^{26}\text{Al}$ , which upon decay, releases gamma radiation and heated up their interiors [84]. Planetesimals that formed too early (within  $\sim 1.4$  Myr) incorporated a high initial abundance of  $^{26}\text{Al}$ , which melted their rocky interiors, and made them unsuitable for organic synthesis [85]. However, later-forming planetesimals contained lower abundances of  $^{26}\text{Al}$ , and released just enough heat to maintain aqueous conditions suitable for organic chemistry for millions of years [85, 86]. These  $\text{NH}_3$ - and HCN-rich interiors allowed for the favourable synthesis of nucleobases, primarily via FTT reactions (see Equation 1.1), but also via HCN-based aqueous reactions (see Equations A.2–A.5) [42].

In this thesis, we only consider carbonaceous meteorites and IDPs as sources of prebiotic nucleobases, but we intend to expand our calculations in future work to include nucleobase synthesis in WLPs.

### 1.2.2 Site for the Emergence of Life

A consensus has still not been reached for the site of the origin of the RNA world, however only two different environments are actively being considered: hydrothermal vents and WLPs. Both potential sites for the origin of life have merits. However, perpetual aqueous environments like those surrounding hydrothermal vents are not conducive for forming long RNA polymers, as RNA chains break apart rapidly in water [87]. And RNA molecules need to be at least  $\sim 40$  monomers long in order to exhibit catalytic activities [88]. In fact, experiments simulating the conditions of hydrothermal vents have only succeeded in producing RNA molecules 2 ribonucleotides long [89]. Experiments that cycle through wet and dry phases on the other hand have synthesized RNA polymers greater than 300 monomers long [60].

For this reason, in this thesis, we only consider WLPs as the site for the origin of the RNA world.

Chyba & Sagan [33] concluded that IDPs would be a dominant prebiotic source of organics including nucleobases considering our planet's early atmospheric composition, but what happens to nucleobases once they diffuse from the pores of IDPs into WLPs? Each 100  $\mu\text{m}$ -sized IDP only contains at most  $\sim 1$  picogram of nucleobases, therefore in order for IDP-sourced nucleobases to accumulate within these environments, they must survive for extended periods. This could be difficult in the face of nucleobase sinks, such as seepage (through pores at the base of the pond), which drains ponds on Earth today at  $\sim 1\text{--}5$  mm/day [54], hydrolysis, which destroys nucleobases at temperatures of  $60^\circ\text{C}$  with a half-life of dozens of years [90], and UV photodissociation, which efficiently destroys nucleobases in absence of shielding at a rate of  $1 \times 10^{-4}$  molecules per incident photon [91]. Nucleobases delivered by carbon-rich meteorites may be more likely to reach high concentrations within WLPs, as meteorite falls are a single event, and thus nucleobases delivered by these bodies can concentrate in ponds on the timescale of diffusion. However in any case, the interplay between nucleobase sources and sinks will limit the nucleobase concentrations in WLPs.

### 1.2.3 Nucleobase Sinks

#### 1.2.3.1 Seepage

Unless a pond is sitting on a crystal lattice, water and dissolved molecules will always seep through pores at the base of a pond. Basalt, the most common volcanic rock on Earth, the Moon and Mars, was likely common on the early Earth [55]. Basalt has pores ranging in diameters from  $0.001\text{--}400$   $\mu\text{m}$ , with more weathered samples having a greater fraction of small pores [92]. Basalt porosities range from  $\sim 1\text{--}35\%$ , with the more weathered samples tending towards higher porosities [92]. Soils at the bases of many ponds on Earth today have higher average porosities than basalt, typically ranging from  $30\text{--}70\%$ , but have similar pore sizes [93].

#### 1.2.3.2 Hydrolysis

Liquid water attacks the amino group ( $-\text{NH}_2$ ) of adenine, guanine, and cytosine, replacing it with an oxygen molecule, and releasing an ammonia molecule in the process (see Figure 1.6 below). Upon this so-called “deamination” reaction, adenine

becomes hypoxanthine, guanine becomes xanthine, and cytosine becomes uracil [36, 70]. Uracil does not have an amino group for water to attack, however one possible mechanism for uracil hydrolysis is an attack of the double-bonded carbons and to a lesser extent, the adjacent nitrogen atom, by hydroxyl ( $\bullet\text{OH}$ ) radicals in the solution [94].

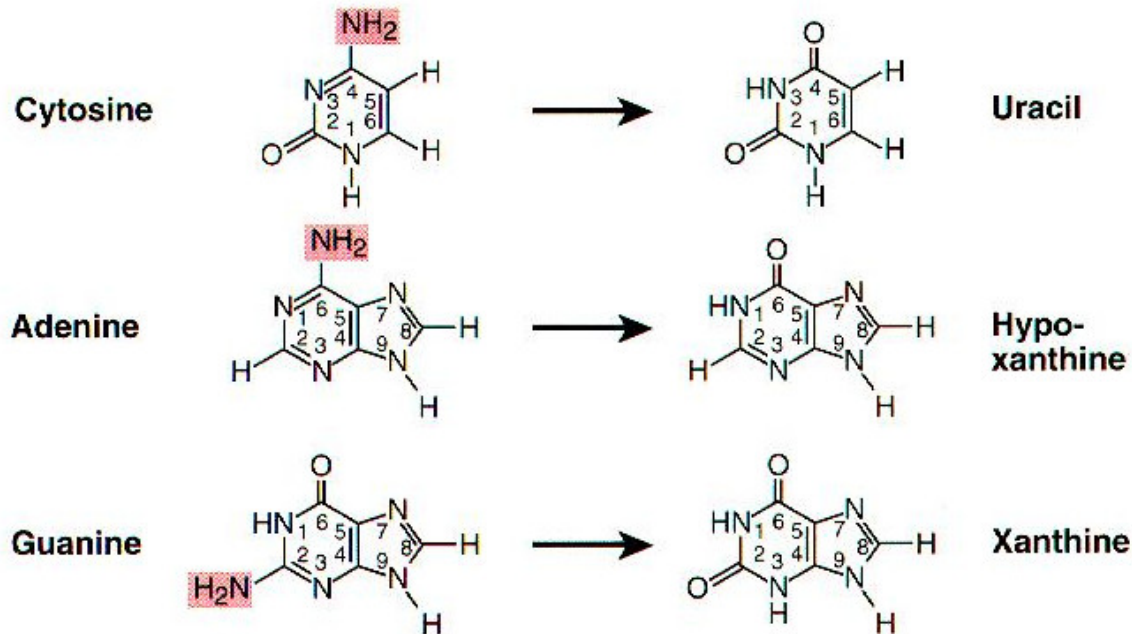


Figure 1.6: Liquid water favourably destroys cytosine, adenine, and guanine by replacing the  $\text{NH}_2$  group in these molecules with an oxygen molecule, and releasing ammonia in the process. The product molecules in these reactions are uracil, hypoxanthine, and xanthine, respectively. Source: [95].

### 1.2.3.3 UV Photodissociation

UV photodissociation breaks the bonds in molecules through the absorption of UV light. When a molecule absorbs a UV photon, it is promoted from (typically) the ground electronic state into an excited electronic state. Absorption occurs when a photon carrying the energy that matches the difference between these two energy states interacts with the molecule. The Franck-Condon principle states that these processes occur much more rapidly than the vibration of atoms in the bonds [96]. Because of this, although the excited molecule has a very different electronic configuration from the ground-state molecule, it is the same as the ground-state molecule in the positions

and kinetic energies of its atoms [96]. However, because the bonds are weaker in excited molecules, the average bond distance between nuclei is greater. Therefore a molecule promoted to an excited state is typically forced to occupy one of several higher vibrational levels.

One way to visualize this is to imagine a diatomic molecule with two nuclei oscillating together and apart in the ground vibrational level. In other words, the bond distance between nuclei oscillates about the average ground-state bond distance. If this molecule absorbs a photon exactly when the bond distance is at a minimum, since the excited molecule has a new, greater average bond distance, the new oscillation will necessarily have a greater amplitude. In other words, the nuclei obtained an increase in potential energy, while maintaining the same kinetic energy.

At this point, one of three outcomes will occur: 1) The molecule will vibrationally relax back to the ground state, either losing all its energy to heat, or just some of its energy and emitting a photon to lose the rest (i.e. phosphoresce) 2) the molecule will emit a photon and return to the ground state (i.e. fluoresce), or 3) the vibration will be strong enough to break the bond and dissociate the molecule. Whether 1, 2, or 3 occurs depends strongly on which vibrational level the molecule in the excited state entered [96], i.e. where the molecule was in its vibrational oscillation when it absorbed the photon. This process is illustrated in Figure 1.7 below.

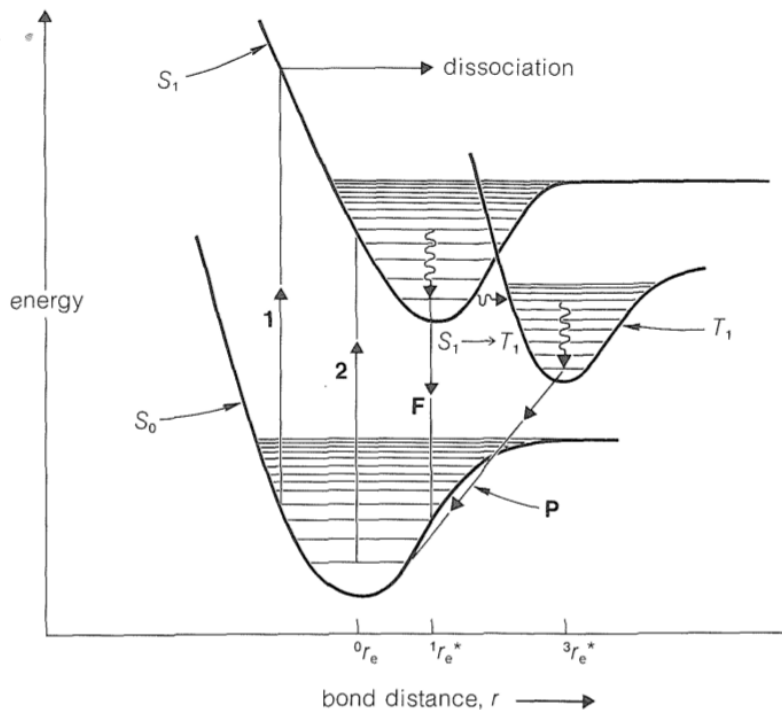


Figure 1.7: A schematic of molecular photoexcitation. Curves  $S_0$  and  $S_1$  represent the potential energy versus bond distance for the ground and first excited states of a molecule. The horizontal lines represent the vibrational levels. When the molecule absorbs a photon, the molecule transitions from  $S_0$  to  $S_1$ . Transition **1** leads to a vibrational level which breaks the bond, causing dissociation. Transition **2** leads to vibrational relaxation and either fluorescence (**F**) to the ground state, or transition to state  $T_1$ , leading to more vibrational relaxation and phosphorescence (**P**) to the ground state. Source: [96].

### 1.3 The Emergence of Life on Habitable Exoplanets

At the time of this writing, we know of 52 potentially habitable exoplanets [97]. All of these planets orbit within an annulus surrounding their parent stars which could provide surface temperatures capable of maintaining liquid water. All but three of these exoplanets have masses of between  $1\text{--}10 M_{\oplus}$  and therefore fit the basic definition of a super-Earth [98], and the others are subterran in mass. However, many of these exoplanets may be more akin to Neptune in composition, with large H/He primary atmospheres surrounding rocky cores of various sizes. Indeed, exoplanet density-radius

relationships show that anything above  $\sim 1.6 R_{\oplus}$  (corresponding to  $\sim 5 M_{\oplus}$ ) is unlikely to be rocky [99, 100]. Such “mini-Neptunes” are far from Earth-like, and are thus unlikely to harbour life as we know it. However 22 of the 52 potentially habitable exoplanets are below  $5 M_{\oplus}$ , and are therefore probably terrestrial [97]. Based on the mass and density of these 22 planets, they are more likely to host secondary atmospheres composed of volatiles mostly degassed from impacts of solid bodies [101].

Nothing is currently known about the atmospheres of these 22 potentially habitable worlds. Therefore we don’t know if these exoplanets resemble Venus, whose water was long boiled away due to the  $>450^{\circ}\text{C}$  surface temperatures driven predominantly by an atmosphere dense in greenhouse gas, Mars, whose tenuous atmosphere and distance from the Sun make sustained liquid water on its surface nearly impossible, or Earth, where liquid water has existed and sustained life on the surface for the majority of its lifetime [102–104]. The world’s best transit spectroscopic capabilities are currently provided by the Wide Field Camera 3 (WFC3) onboard the Hubble Space Telescope (HST) [105]. WFC3 transit spectroscopy is most sensitive to a single band of water vapor in a thin wavelength range ( $1.1\text{--}1.7\mu\text{m}$ ) [105]. As of today, this instrument has made two potential atmospheric detections of super-Earths outside the habitable zone (55 Cancri e, and GJ 1132 b) [106, 107]. Modeling of their observed spectra suggests 55 Cancri e and GJ 1132 b have atmospheres possibly containing HCN, and  $\text{H}_2\text{O}/\text{CH}_4$ , respectively [106, 107]. However, such detections should be considered as “best matches” to weak spectral features. In fact, others have mentioned that no convincing atmospheric detections yet exist for exoplanets below the size of Neptune [105].

With the upcoming launch of the James Webb Space Telescope (JWST), currently slated for 2018, the potential for super-Earth atmospheric detections greatly increases [105]. Unlike HST, JWST is sensitive to strong infrared vibration-rotation bands including  $\text{CH}_4$ , CO, and  $\text{CO}_2$  [105]. Furthermore, JWST’s 6-metre light-collecting diameter will increase signal-to-noise by a factor of 2.5 over HST [105]. However, to get even basic characterizations of habitable super-Earth atmospheres, approximately 100 days of observation will be required [108]. Regardless, progress will soon be made in constraining the Earth-likeness of these 22 potentially habitable worlds.

Can planet formation theory tell us anything about the emergence of life on other worlds? We know that terrestrial exoplanets formed in three stages: collisional growth of submicron-sized dust grains into kilometer-sized planetesimals, then collisional growth

of planetesimals into lunar- to Mars-sized planetary embryos, and finally collisional growth of embryos and remnant planetesimals into planets [65]. We also know that the planetesimals in these exosolar systems would have formed from grains containing the the same basic molecules in all protoplanetary disks (e.g.  $\text{H}_2$ ,  $\text{CO}$ ,  $\text{HCO}^+$ ,  $\text{H}_2\text{O}$ ,  $\text{H}_2\text{CO}$ ,  $\text{CS}$ ,  $\text{CN}$ ,  $\text{HCN}$ ,  $\text{HNC}$ ,  $\text{NH}_3$ ) [109]. Finally, because we observe craters on every solid celestial body in our solar system, we know that left-over planetesimals constantly enter into planet-crossing orbits. For these reasons, we should expect exoplanetesimals and exodust to deliver their organic contents to terrestrial exoplanets in a similar fashion as was done for the early Earth. If we detect atmospheric water and biosignatures (e.g.  $\text{O}_2$ ,  $\text{O}_3$ ,  $\text{N}_2\text{O}$ ,  $\text{CH}_4$ ,  $\text{CH}_3\text{Cl}$ ,  $\text{NH}_3$ ,  $\text{C}_2\text{H}_6$  [110]) on some of these 22 potentially habitable exoplanets suggesting they maintain liquid surface water and inhabit life, and their exoplanetary radii are large enough to suggest they have plate tectonics [111] allowing for rising continental crusts, then the delivery of organics to WLPs on emerging islands and continents may describe a broader picture for the emergence of life.

## 1.4 Outline of Thesis Research

This thesis focuses on specific problems related to when and how life originated on Earth.

In Chapter 2, we focus on the question of when life emerged. We review the literature to collect astrophysical evidence which constrains the *habitability boundary*, i.e. the earliest point at which the RNA world could have emerged on the Earth, and biological evidence which constrains the *biosignature boundary*, i.e. the earliest point at which there is compelling evidence for life's existence. From this we constrain the time interval within which the RNA world emerged, and discuss the implications of its duration for the expectancy of life elsewhere.

In Chapter 3, we follow the time interval obtained in the previous chapter and address the question of how RNA first appeared in WLPs. We do this by building a complete model for the survival and evolution of nucleobases in WLPs on the early Earth, leading to the RNA world. Our model is based on sources and sinks of both pond water and nucleobases. We consider both carbon-rich IDPs and meteorites as sources for nucleobases to WLPs, and seepage, hydrolysis and UV photodissociation as sinks. For pond water we consider precipitation as the sole source, and seepage and

evaporation as sinks. To get an idea as to how frequent nucleobases were delivered into WLPs by meteorites, we use mass delivery models based on the lunar cratering record and the number of emerging WLPs based on a continental crust growth model to calculate the number of deposition events on the early Earth. From all these models we are able to constrain the source of nucleobases to WLPs on the early Earth, the environmental conditions of such WLPs, the timescales of reaction to form first nucleotides and RNA, and the time interval for the emergence of the first RNA polymer.

Finally, in Chapter 4 we summarize the main conclusions from the two previous chapters.

# Chapter 2

## Constraining the Time Interval for the Origin of Life on Earth

**Ben K. D. Pearce, Andrew S. Tupper, Ralph E. Pudritz, & Paul G. Higgs**

*N.B. This chapter was revised in accord with the favourable reviews of 2 referees and resubmitted to Astrobiology on July 4<sup>th</sup>, 2017. This chapter constitutes part I of this thesis.*

### Abstract

Estimates of the time at which life arose on Earth make use of two types of evidence. Firstly, astrophysical and geophysical studies provide a time scale for the formation of the Earth and Moon, for large impact events on the early Earth, and for the cooling of the early magma ocean. From this evidence we can deduce a *habitability boundary*, which is the earliest point at which the Earth became habitable. Secondly, biosignatures in geological samples, including microfossils, stromatolites, and chemical isotope ratios, provide evidence for when life was actually present. From these observations we can deduce a *biosignature boundary*, which is the earliest point at which there is clear evidence that life existed. Studies with molecular phylogenetics and records of the changing level of oxygen in the atmosphere give additional information that helps to determine the biosignature boundary. Here we review the data from a wide range

of disciplines in order to summarize current information on the timings of these two boundaries. The habitability boundary could be as early as 4.5 Ga, the earliest possible estimate of the time at which Earth had a stable crust and hydrosphere, or as late as 3.9 Ga, the end of the period of heavy meteorite bombardment. The lack of consensus on whether there was a late heavy meteorite bombardment that was significant enough to prevent life is the largest uncertainty in estimating the time of the habitability boundary. The biosignature boundary is more closely constrained. Evidence from carbon isotope ratios and stromatolite fossils both point to a time close to 3.7 Ga. Life must have emerged in the interval between these two boundaries. The time taken for life to appear could therefore be within 200 Myr or as long as 800 Myr.

## 2.1 Introduction

When did life on Earth emerge? Not only is this a key question in understanding the origin of life on our planet, but the estimated time interval may eventually lend us insight into the frequency of life's emergence elsewhere in the Universe. Soon after the Earth formed, the collision with a Mars-sized body probably gave rise to the Moon. This cataclysm melted and reshaped the Earth's mantle. Further smaller impacts may have occurred over the ensuing 0.6 Gyr or so, each of which would have been accompanied by partial melts of the Earth's crust, perhaps culminating in a last crescendo: the Late Heavy Bombardment (LHB). The atmosphere was not the "reducing" atmosphere that figures into the early Miller-Urey experiments, but one that is composed mainly of CO<sub>2</sub> (outgassed from volcanoes) and N<sub>2</sub>. The UV irradiation of the planet would be highly significant as there was no oxygen or ozone layer at the time to screen the surface. This radiation can be both highly destructive for the survival of complex organics, but could also have stimulated them. It is in this violent, highly changing environment that the steps that led to life took place.

The window during which the origin of life must have occurred is demarcated by inner and outer time boundaries. We call the outer boundary the *habitability boundary*. This is our estimate of the time at which the Earth first became habitable for life. We call the inner boundary the *biosignature boundary*. This is the time of the earliest convincing evidence of life in the form of fossil and/or chemical biosignatures. In this review we aim to bring together the many different lines of evidence that allow us to estimate the times of the two boundaries. The biosignature boundary has been

reviewed by Schopf [112] and Buick [113]. The habitability boundary has been reviewed by Zahnle *et al.* [114]. More recently, information pertaining to both boundaries were reviewed in a textbook by Gargaud *et al.* [115]. They concluded that life emerged on Earth at an uncertain date between 4.3–2.7 Ga. Here, we bring the latest astrophysical constraints and biological signatures together to more precisely constrain this time interval for the origin of life. This review considers more recent data that reframes the entire argument for when life emerged since the previous reviews on this topic. Much of the relevant information on the timing of the origin comes from astrophysics, planetary science, geology and palaeontology. Here we aim to present these results in a way that is accessible to the broad scientific community.

In his review of the RNA World hypothesis for the origin of life, Joyce [116] illustrated the timeline of events pertaining to the origin of life on Earth, and this has been widely used by various scientific communities. In an attempt to produce a similarly useful summary, we have illustrated the evidence reviewed in this paper in a similar way in Figure 2.1, emphasizing the astrophysical evidence that leads to positioning the habitability boundary and the biological evidence that leads to positioning the biosignature boundary. Table 2.1 gives further information and citations of the events included in Figure 2.1.

We begin with the astrophysical constraints on the habitability boundary, and gather the data on the age of the Solar System, Earth, and Moon, and the radiative cooling time of the Earth’s liquid magma-covered surface. The habitability boundary is mainly constrained by the time at which liquid water could exist on the planet’s surface. Liquid water would have been a requirement for the emergence of the kind of life that exists on Earth today. Water is often considered as a requirement for habitability because of its unique role as a universal solvent, which is why NASA has invoked a “follow the water” strategy towards searching for extraterrestrial life. We will therefore discuss the theories of cooling of the Earth’s surface and atmosphere after major impact events, as these make predictions about the time at which a liquid ocean could have formed. One catastrophic impact is the collision that created the Moon, but other large impacts may have continued for a much longer period, and may have also ‘reset the clock’ as far as habitability is concerned. The rate at which major impacts died away during the early history of the solar system and the debate about whether there was a LHB phase with a high incidence of impacts are therefore very relevant to the timing of the outer boundary. Independent evidence for the outer

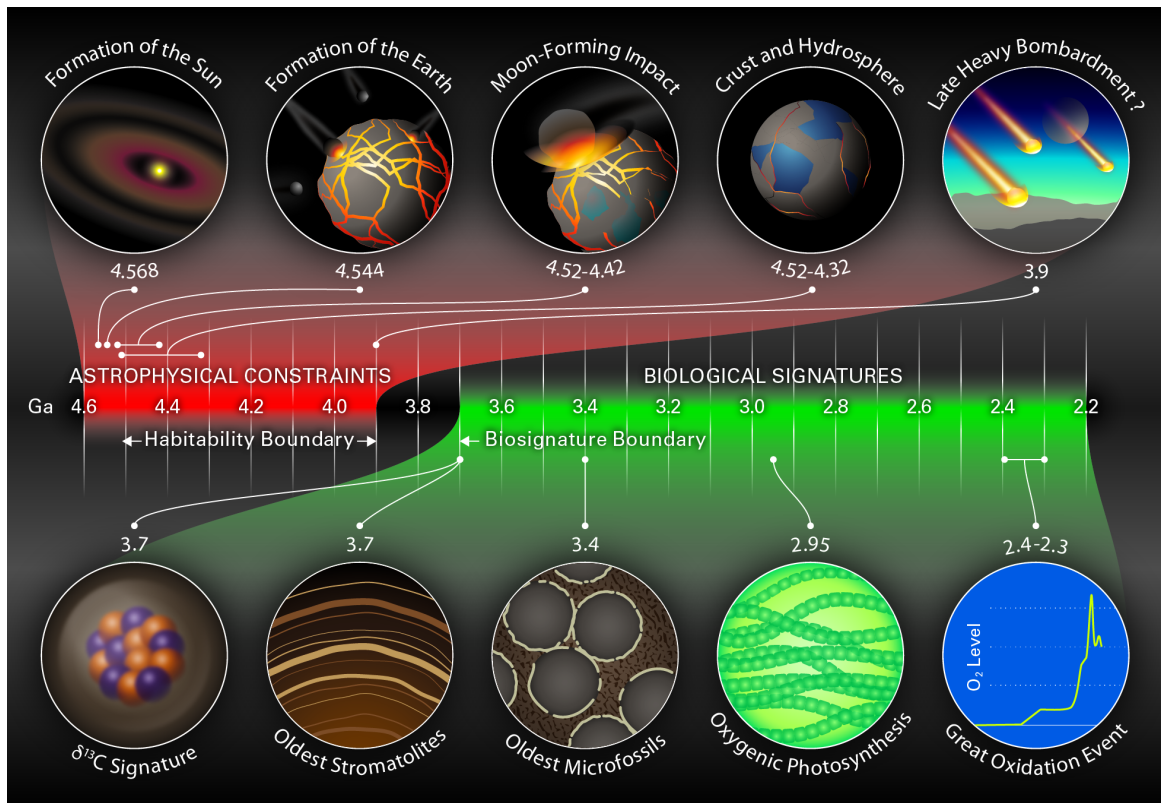


Figure 2.1: Timeline which illustrates the astrophysical constraints constraining the time of the habitability boundary and the biological signatures constraining the time of the biosignature boundary. Uncertainties about whether there was a late heavy bombardment mean that the position of the habitability boundary is still poorly constrained, while the evidence for the biosignature boundary is beginning to converge.

Table 2.1: Summary and scientific basis of the events and biosignatures in the Figure 2.1 timeline.

	Event/Biosignature	Timeline Location (Ga)	Scientific Basis	Reference(s)
Astrophysical Constraints	Formation of the Sun	4.568	CAIs in chondritic meteorites	Bouvier & Wadhwa [117]
	Formation of the Earth	4.544	Hf-W dating	Yin <i>et al.</i> [118]
	Moon-forming impact	4.52–4.42	Hf-W dating, Rb-Sr dating, U-Pb dating, dynamic simulations	Touboul <i>et al.</i> [119], Halliday [120], Barboni <i>et al.</i> [121], Jacobson <i>et al.</i> [122]
	Formation of crust and hydrosphere	4.52–4.32	Numerical simulations, zircon record	Monteux <i>et al.</i> [123], Lebrun <i>et al.</i> [124], Zahnle <i>et al.</i> [114], Harrison <i>et al.</i> [125], Cavosie <i>et al.</i> [126]
	Late Heavy Bombardment?	3.9	Lunar crater record, lunar meteorites, dynamic simulations, physical modeling	Ryder <i>et al.</i> [127], Cohen <i>et al.</i> [128], Gomes <i>et al.</i> [129], Boehnke & Harrison [130]
Biological Signatures	$\delta^{13}\text{C}$ signature	3.7	Light carbon signature in rocks of sedimentary origin	Rosing <i>et al.</i> [102], Ohtomo <i>et al.</i> [103]
	Oldest stromatolites	3.7	Layered structures interpreted as stromatolites	Nutman <i>et al.</i> [104]
	Oldest microfossils	3.4	Cell lumina and carbonaceous cell walls	Wacey <i>et al.</i> [131]
	Oxygenic photosynthesis	2.95	Molybdenum signature	Planavsky <i>et al.</i> [132]
	Great Oxidation Event	2.4–2.3	MIF disappears from geologic record	Sessions <i>et al.</i> [133]

boundary comes from the geological record. The existence of certain minerals that form in the presence of water also gives constraints on the time by which a liquid ocean must have formed.

When we consider the biosignature boundary, the most direct evidence for the existence of life on Earth comes from the presence of fossils. These may be in

the form of microfossils (i.e. remnants of life at the level of individual cells) or macrofossils, in particular stromatolites, which are layered structures thought to be created by photosynthetic micro-organisms. The interpretation of microfossils has been controversial, and we will discuss whether some of the earliest samples claimed to be microfossils are in fact of non-biological origin. However, the timing of the biosignature boundary does not depend too much on the uncertainty around microfossils, because indirect evidence for the presence of life in the form of carbon isotopic signatures precedes most potential microfossil ages. Furthermore, stromatolite samples are known with fairly similar dates to the earliest microfossils, and the most recently proposed stromatolite samples also go as far back as the isotopic signatures.

Another form of evidence for the existence of life comes from the increase in the level of atmospheric oxygen due to the presence of photosynthetic organisms. Atmospheric oxygen is measured through geologic time using sulfur and molybdenum isotopes and transition metals in sedimentary rocks. Although a major increase in oxygen at the time of the great oxidation event (around 2.4–2.3 Ga) is well documented, it is considerably later than the likely time for the origin of life. Evidence for traces of oxygen at 2.95 Ga suggests oxygenic photosynthesis was operating quite early. This provides constraints on the time of the inner boundary that are compatible with evidence from stromatolites.

From this consolidated research, given the uncertainty in the way the LHB unfolded, we present two possible windows for the emergence of life, confined by the two boundaries discussed in this paper. To our knowledge this is the first time such a consolidation of literature has been attempted with this goal in mind.

## 2.2 Formation of the Solar System

### 2.2.1 Formation of the Sun and the Protoplanetary Disk

Observations done with a variety of telescopes (e.g. the Hubble Space telescope, the Atacama Large Millimeter Array, the Submillimeter Array) show that dusty, gaseous “protoplanetary” disks exist around all young stars [109, 134, 135]. The gas phase in such disks lasts 1–10 million years so Jupiter-mass planets must have formed within that time (e.g. review by Dutrey *et al.* [109]). It was during this time that the central stars assembled by accreting material from these surrounding disks. Rocky planets

were assembled somewhat later from collisions between the left-over planetesimals and sub-Mars-sized objects in the now gas-free disk [65]. Our solar system likely formed in this way. It all begins within dense molecular clouds in space, where even denser regions called “cores” about 0.3 light-years across form [136]. These cores cool and eventually collapse under their own gravity to form stars. And because they started with some non-zero angular momentum, the system collapses into a disk out of which forming stars accrete their gas [136, 137].

The age of the Solar System can be defined as the time in which the first solid grains formed in the nebular disk around our protosun [117]. The oldest material in the Solar System is found within chondritic meteorites, which is the most common type of meteorite found on Earth. These meteorites are rocky and undifferentiated, which is to say, their meteorite parent bodies (i.e. 100 km-sized, rocky bodies known as planetesimals) never reached high enough temperatures to melt internally. Most of the meteorites that end up on the surface of the Earth are just fragments of planetesimals that were left over from the process of planet formation. The estimate of our Solar System’s age is 4.568 billion years old [117], and comes from the  $^{207}\text{Pb}$ - $^{206}\text{Pb}$  isotopic dating of the oldest material within these meteorites, the so-called calcium-aluminum-rich inclusions (CAIs).  $^{207}\text{Pb}$  and  $^{206}\text{Pb}$  are the final decay products of decay chains that begin with  $^{235}\text{U}$  and  $^{238}\text{U}$ , whose half-lives are  $\sim 0.7$  Gyr and  $\sim 4.47$  Gyr, respectively. CAIs are submillimetre-to-centimetre-sized grains that are thought to be among the earliest solids to have formed in the protoplanetary disk. This is due to the fact that they form mostly from oxides and silicates of calcium, aluminum, magnesium, and titanium, which condense at high temperatures, and therefore would be among the first solids to form everywhere in the warm early disk [138].

### 2.2.2 Formation of the Earth

The earliest that life could have appeared was soon after Earth’s formation. Therefore, we can slide the outer boundary for the emergence of life inwards from 4.568 Ga, to the age that the Earth formed out of planetesimals in the protoplanetary disk.

Planetary differentiation is a fundamental concept when it comes to dating the formation of the Earth. The internal composition of the Earth varies at different depths due the tendency of higher density fluids to sink under gravity (and similarly, the tendency of lower density fluids to float). During planetary accretion, the kinetic energies deposited by impacts, and the gravitational energies released from the settling

of metals to the core, cause significant melting [139]. The compositions of Earth's layers are therefore influenced by the cooling rate. This is what makes hafnium-tungsten ( $^{182}\text{Hf}$ - $^{182}\text{W}$ ) isotopic dating a useful tool for estimating the formation age of rocky planets in our Solar System. Tungsten is a moderate siderophile (i.e. tends to bond with metallic iron and sink to the core), whereas hafnium is a lithophile (i.e. tends to bond with oxygen, forming compounds that don't sink to the core) [114].  $^{182}\text{Hf}$  also decays to  $^{182}\text{W}$  with a half-life of 9 Myr [114]. Now, if planetary accretion and differentiation ceased before all the planet's  $^{182}\text{Hf}$  decayed into  $^{182}\text{W}$ , one would find positive  $^{182}\text{W}$  abundances in the primitive silicate mantle. This means one can estimate how long the planet was accreting, melting, and differentiating materials by measuring the abundance of  $^{182}\text{W}$  in samples of the primitive mantle. Based on models comparing the tungsten isotopic data measured in meteorites against those of the bulk silicate Earth (i.e. the primitive mantle), the time for the Earth to reach 63% completion is  $11 \pm 1$  Myr, and to reach 90% completion is 24 Myr [118]. These estimates push the outer boundary of the emergence of life on Earth to 4.544 Ga (when the Earth had formed 90% of its mass), but several other factors shift the boundary further than this.

### 2.2.3 Formation of the Moon

It is hypothesized that the Moon formed from a giant collision between a planetary embryo (named Theia) and the proto-Earth [119–122, 140–144]. This is made evident by the nearly identical isotopic compositions of the Moon and Earth, suggesting a vigorous mixing of materials occurred between the two bodies [140]. Computer simulations show how this might have occurred [141–143]. The nearly identical isotopic signatures also suggest that the Moon was the last giant impact experienced by the Earth. The formation of the Moon therefore sets the initial conditions for the early Earth environment.

Similar to the bulk silicate Earth samples, tungsten isotopic abundances were measured for lunar mantle material that was collected as part of the Apollo program, and compared to meteoritic values. Models based on these comparisons estimate a date of Moon formation to be  $62^{+90}_{-10}$  Myr after the formation of the Solar System [119, 144]. Halliday [120] used Sr isotopes of lunar rocks to constrain the Rb-Sr age of the Moon to  $87 \pm 13$  Myr after the Solar System formed. Rb-Sr dating is based on the isotopic decay of  $^{87}\text{Rb}$  to  $^{87}\text{Sr}$ , which has a half-life of 48.8 Gyr. Most recently, Barboni *et al.* [121] coupled U-Pb and Hf isotopes from lunar zircons to develop a

two-stage model age for the Moon, constraining its formation to  $58 \pm 10$  Myr after the formation of the Solar System. Lunar zircons are robust against isotopic disturbances from post-Moon formation impacts, making this model one of the most precise to date [121].

Another line of evidence from astrophysical simulations confirms the results from isotopic dating. Jacobson *et al.* [122] used dynamic simulations involving many small particles interacting under their own gravity to estimate the Moon formation age. By running several simulations beginning from a disk of planetesimals and planetary embryos, Jacobson *et al.* [122] found a clear statistical correlation between the time of the last giant impact (i.e. embryo-embryo collision) and the subsequent accreted mass for Earth-like planets. They then compared the best estimate of Earth's late-accreted mass inferred from highly siderophile element abundances in Earth's mantle (e.g. Rhenium, Osmium, Iridium, Ruthenium) relative to those in chondritic meteorites to estimate the time of the last giant impact on Earth. Based on this analysis, Jacobson *et al.* [122] estimate the time of the Moon-forming impact to be  $95 \pm 32$  Myr after the formation of the Solar System. This result agrees with the results from isotopic data by Touboul *et al.* [119, 144], Halliday [120], and Barboni *et al.* [121]. By making no preference between the three isotopic analyses or the dynamic simulations as methods to estimate the Moon formation age, we can slide the outer boundary for the emergence of life farther inwards, to 4.416–4.52 Ga.

## 2.3 Habitability of the Earth

### 2.3.1 Radiative Cooling of the Magma Ocean

The energy deposited by the Moon-forming impact melted the proto-Earth's mantle and caused a global magma ocean [119, 122]. Hydrodynamic (i.e. fluid flow) simulations of Moon-forming impacts on the nearly fully-formed Earth show post-impact mantle temperatures in excess of 7000 K [145]. Any solid mantle that survived the impact would have likely sunk down to the hot core and then melted [114]. At this stage, the Earth had accreted the majority of its material and began to cool. The atmosphere of the newly-melted Earth, composed of mostly rock vapour and silicate clouds, would have lasted through cooling for  $\sim 1000$  years [114]. During this time, silicates would condense and rain down onto the Hadean Earth's surface at a rate of a meter per

day [114]. As Earth's surface continued to cool, large temperature differences were created between both the surface and the interior, and the atmosphere and the surface, which initiated convection cycles [114, 123, 124]. Convection would promote cooling by continually bringing mantle gases to the surface where they can then rise to the top of the silicate clouds and radiate [114]. This means the magma mantle was likely devoid of gases after cooling. Once the early Earth had cooled enough for the silicate clouds to rain out, the early atmosphere would have been composed of the remaining volatiles that were outgassed during convection cooling. For  $\sim 0.02$ –100 Myr this hot atmosphere would have lived above a deep magma ocean [114, 123, 124]. Thermal blanketing by the hot atmosphere and the surface temperature of the magma ocean would have determined the rate at which the Earth radiatively cooled. The cooler the surface and thicker the atmosphere, the more effective the thermal blanket. To understand this, imagine a hot surface heating up the atmosphere, causing it to puff out. By increasing the volume of the atmosphere, the atmospheric density decreases. Only the top of the atmosphere—where pressures are less than a few tenths of a bar—radiates into space [146], thus by expanding the volume of the top of the atmosphere, more radiation can escape. As the surface cools, the atmosphere cools and contracts, decreasing the volume of the top of the atmosphere, allowing the thermal blanket to trap in more radiation. When the surface of the Earth dropped to some temperature below  $\sim 1800$  K, a constant, inefficient rate of cooling began [114, 124].

Tidal heating by the Moon would have also played a role in maintaining the magma ocean [114, 124]. Tidal heating is the result of the different strengths of the Moon's gravitational force on the near vs. far sides of the Earth. These forces are large for two bodies orbiting close to one another. For example, the Moon orbits the Earth at a distance of approximately 100 Moon diameters, and the highest tides on Earth reach up to about 12.2 meters. Tidal forces can cause a spherical body to stretch into an oblate spheroid, which compresses and re-stretches to adjust for rotation and orbit. This stretching and compressing causes friction between solids in the body, which generates heat and allows the solids to melt. The strongest source of friction would be in materials that are solid, but nearly melting [114]. Since the Moon formed, the Earth's tides have been transferring angular momentum from the Earth's spin to the Moon's orbit [147]. Over time this has slowed the Earth's rotation, and expanded of the Moon's orbit [147], which means during the Hadean, tidal forces were stronger and Earth's tides fluctuated more rapidly [148]. For about the first 1.4 million years

after Moon formation, tidal forces were strong enough to aid in prolonging the Earth's magma ocean [114]. During this time, tidal heating would have generated about the same to 1 order of magnitude less heat than absorbed sunlight, and 2–3 orders of magnitude more heat than radioisotopes [114].

Calculations by Monteux *et al.* [123], Lebrun *et al.* [124], and Zahnle *et al.* [114] have shown that the Hadean Earth would have maintained a magma ocean, and remained above the boiling point of water for  $\sim 0.02$ –100 Myr. These calculations consider a variety of effects, including convective heat transport, radiative cooling, absorbed sunlight, water's solubility in liquid basalt, and tidal heating. Once the magma ocean solidified, water condensed and rained down to the solid surface at  $\sim 1$  m/year [114] forming Earth's oceans in just a few thousand years. The outer boundary for the emergence of life can therefore be moved inwards, to when the Earth was cool enough to maintain liquid water on a solid crust. This would be between 4.316 and 4.52 Ga if we consider the range in Moon formation ages and take no preference to whether cooling was efficient (20 kyr) or inefficient (100 Myr).

### 2.3.2 Evidence of a Continental Crust

Zircons ( $\text{ZrSiO}_4$ ) are minerals which crystallize from melts, and, due to their durability, represent the oldest preserved terrestrial material. Because zircons have U-Pb ages as old as  $4.404 \pm 0.008$  Ga [149], they can be used to glean insight about the Hadean environment. Samples of 4.01- to 4.37-Gyr-old zircons, representing pieces of the Hadean crust, have been isotopically compared with the bulk silicate Earth (BSE) in attempts to estimate the time at which the Earth's crust solidified [125]. The main idea behind this technique is that the formation of a continental crust temporarily halts elemental differentiation, freezing in the ratio of hafnium (Hf) isotopes in the solid crust (and zircons) at that time [125, 150]. However, since the continental crust is continuously remelted and recycled into the mantle, elemental differentiation continues at a slower rate even after crust has formed, leading to an increasingly depleted mantle. For this reason, we would expect that more recent zircons, formed in the upper mantle, would be more depleted in  $^{176}\text{Hf}/^{177}\text{Hf}$  than zircons that formed from an older, less depleted mantle.

One difficulty with this approach is that the Hf isotope composition varies due to the radioactive decay of  $^{176}\text{Lu}$  to  $^{176}\text{Hf}$ . Zircons are useful in this matter since they incorporate a relatively minute amount of Lu, therefore the effect of radiogenic decay

on zircon Hf abundances can be considered negligible [150]. By characterizing the deviation of  $^{176}\text{Hf}/^{177}\text{Hf}$  in zircons of various ages to that of the BSE, it is possible to determine whether the  $^{176}\text{Hf}/^{177}\text{Hf}$  values follow a trend that is consistent with zircon formation from a slowly depleting mantle reservoir. Large negative  $^{176}\text{Hf}/^{177}\text{Hf}$  deviations increasing in time are consistent with the formation of a continental crust. Large positive  $^{176}\text{Hf}/^{177}\text{Hf}$  deviations on the other hand, suggest the zircons were derived from reservoirs with high Lu/Hf ratios, which upon  $^{176}\text{Lu}$  decay to  $^{176}\text{Hf}$ , enrich any forming zircons in Hf. Harrison *et al.* [125] measured large positive and negative  $^{176}\text{Hf}/^{177}\text{Hf}$  deviations from the BSE in zircons with ages as old as 4.37 Ga. However, temporal extrapolations of these results that align with today's rock record suggests that a major differentiation event took place between 4.4 and 4.5 Ga followed by continental crust growth and recycling. Since the Moon-forming impact that melted the Earth's surface likely occurred between 4.416–4.52 Ga, the zircon isotopic analysis performed by Harrison *et al.* [125] is consistent with the  $\sim 0.02$ –100 Myr magma ocean solidification times calculated by Monteux *et al.* [123], Lebrun *et al.* [124], and Zahnle *et al.* [114].

### 2.3.3 Snowball Earth?

As the Earth's mantle solidified and subduction of crustal plates began to occur,  $\text{CO}_2$  would have been removed from the atmosphere due to its high reactivity with silicates [151], and subducted into the Earth's crust. If  $\text{CO}_2$  subduction occurred early, it could have continued to remove  $\text{CO}_2$  from the atmosphere until the partial pressure was well below 1 bar, which is about the pressure required to maintain a clement climate on Earth. However, there is still no consensus as to when these plate-tectonic processes began [152–154]. Ernst *et al.* [153] argue, that the Earth's surface was covered by crustal platelets by 4.4 Ga, and that episodic deep mantle- and plume-driven subduction began as early as 4.4–4.0 Ga. They reason that the terrestrial heat budget requires overturn of platelets during that time, since conduction is much less efficient than convection-advection at transferring heat. Maruyama *et al.* [152] argue that an intense period of meteoritic bombardment at 4.37–4.20 Ga initiated plate tectonics on Earth by delivering water (a lubricant) and thickening the crust with lower viscosity material. Finally, Shirey *et al.* [154] argue that the drastic change in trace element compositions in rocks starting at  $\sim 3.9$  Ga suggests the initiation of subduction occurred around this time. Consequently, because there is no guarantee

that tectonic processes existed during the Hadean, the following discussion about a “Snowball Earth” is purely speculative.

Given that CO<sub>2</sub> subduction led to a Hadean atmosphere much less than 1 bar, the Earth would not benefit from solar radiative heat retention due to the greenhouse effect. Moreover, proceeding the solidification of the magma ocean, geothermal heat was likely insignificant to the Earth’s climate [114]. Finally, the Sun would have been only  $\sim 70\text{--}75\%$  as luminous as it is today, leading to an effective Earth surface temperature of  $< 230\text{ K}$  [114, 155, 156]. As a result, the Earth’s oceans would have frozen over and the Earth would be in a perpetual winter until degassing of CO<sub>2</sub> from the crust built up pressure in the atmosphere. If CO<sub>2</sub> subduction was a quick process, the vastly changing surface conditions may have disrupted the processes of initiating life. If life began via some kind of RNA World, as seems likely [8, 157], such a frozen environment may have been advantageous. In fact, Attwater *et al.* [15] experimentally formed RNA polymerase ribozymes in ice, which were capable of catalyzing templated RNA synthesis at temperatures as low as  $-19^\circ\text{C}$ . However, if the temperature of the snowball Earth was much colder than  $-19^\circ\text{C}$ , large molecules embedded in the ice would cease to move, and the RNA world would be halted or slowed.

The snowball Earth could have undergone periodic, or permanent melting due to large impactors. Sleep [55] estimates that it takes an impactor larger than  $\sim 300\text{ km}$  to boil part of the ocean, and that a few objects of this size probably impacted the Hadean Earth after the Moon-forming impact. However, this prediction is based on the statistics of small numbers, and it’s also possible there were zero impactors of this size [55]. Slightly smaller impactors, similar to the largest lunar impactor ( $\sim 200\text{ km}$ ), would have been more likely to impact the early Earth, and would have also warmed its surface.

Large impactors can also contribute to the loss of an atmosphere through atmospheric stripping [158]. However, N-body simulations show that it takes energies comparable to the Moon-forming impact to strip half an Earth atmosphere [158]. Nothing bigger than  $\sim 1/12$  the size of Theia impacted the Earth after the Moon-forming impact [55], therefore subduction may have been a more important driver of atmospheric loss leading to a potential snowball Earth.

The main evidence against the occurrence of a snowball Earth is in the zircon record. 4.0- to 4.35-Gyr-old zircon formation temperatures ( $\sim 644\text{--}801^\circ\text{C}$ ) suggest at least a portion of the Earth maintained above freezing temperatures during this time

[159]. Moreover, 3.91–4.40 Gyr-old zircons enriched in  $^{18}\text{O}$  would likely require a high level of water-rock interaction, possibly resulting from the presence of Earth oceans at 4.4–3.9 Ga [126, 149, 160–162]. However, the possibility remains that these zircons formed in a sub-surface ocean below an icy crust. Evidence of surface water on the Hadean Earth will be discussed further in the following section.

### 2.3.4 Evidence of Surface Water

There are three stable isotopes of oxygen:  $^{16}\text{O}$  is the most common, followed by  $^{18}\text{O}$  and then  $^{17}\text{O}$ . Zircons crystals preserve the  $^{18}\text{O}/^{16}\text{O}$  ratio inherited from its magmatic source.  $\delta^{18}\text{O}$  is a measure of the  $^{18}\text{O}/^{16}\text{O}$  ratio with respect to the standard (see Equation 2.1 below for a mathematical description). If a zircon formed from magma that was in equilibrium with the primitive mantle, it will have a very narrow range of  $^{18}\text{O}/^{16}\text{O}$  ratios. Specifically, this range is  $\delta^{18}\text{O} = 5.3 \pm 0.3 \text{ ‰}$  [126, 163]. Low temperature liquid water- rock interactions lead to the preferential partitioning of  $^{18}\text{O}$  into minerals, because the bonds formed by  $^{18}\text{O}$  in minerals are stronger than those formed by  $^{16}\text{O}$  [164]. Therefore, if a zircon formed from magma whose parent rock had prolonged contact with low temperature  $\text{H}_2\text{O}$ , the water-rock interactions will have enriched the parent rock in heavy oxygen [126, 160, 163]. It is possible that closed-system crystallization processes can enrich the  $\delta^{18}\text{O}$  of melts by a maximum of  $\sim 1 \text{ ‰}$ , therefore only  $\delta^{18}\text{O}$  zircon values higher than  $6.5 \text{ ‰}$  are interpreted as evidence of liquid water interacting with a solid crust [163].

$$\delta^{18}\text{O} = \left( \frac{\left(\frac{^{18}\text{O}}{^{16}\text{O}}\right)_{\text{sample}}}{\left(\frac{^{18}\text{O}}{^{16}\text{O}}\right)_{\text{standard}}} - 1 \right) \times 1000 \text{ ‰} \quad (2.1)$$

$\delta^{18}\text{O}$  values greater than  $6.5 \text{ ‰}$  have been measured in 3.91–4.40 Ga zircons, and have been interpreted as evidence for surface water on the Hadean Earth as early as 4.4 Ga [126, 149, 160–162]. Liquid water was therefore likely present consistently throughout the Hadean eon.

Evidence of liquid surface water from the zircon record is consistent with the habitability boundary constrained thus far (4.316–4.52 Ga). Because there are no discovered zircons with ages older than 4.4 Ga, this technique cannot determine whether surface water was present on the Earth before that time.

### 2.3.5 The Late Heavy Bombardment

A short and intense bombardment of asteroids and comets may have occurred on the early Earth at around 3.9 Ga. This hypothesis is termed the late heavy bombardment (LHB), or the late lunar cataclysm. The occurrence of the LHB, and therefore its role in the origin of life, remains contentious. The strongest evidence for the LHB came from data taken by the Apollo program.  $^{40}\text{Ar}$ - $^{39}\text{Ar}$  isotopes have been used to date the lunar basins, which were formed by large asteroid impacts at 3.85 Ga (Imbrium), 3.89 Ga (Serenitatis), 3.91 Ga (Crisium), and 3.92 Ga (Nectaris) [127]. These basin dates are supportive of a cluster of 100 km-sized asteroid impacts around 3.9 Ga. Furthermore, because the probability of asteroid impacts decreases with increasing impactor size, the Moon was likely also struck by hundreds of 10 km-sized asteroids at that time [165]. Given that the Earth has a gravitational cross-section 20 times the size of the Moon, it was likely bombarded by 20 times as many asteroids, some which would have been much bigger than the biggest to have impacted the Moon.

However, this interpretation is controversial, as these basins could have also formed from asteroid impacts that made up the tail end of a more sustained, declining bombardment [114]. In fact, results from the Lunar Reconnaissance Orbiter suggest the impact melts collected from the Serenitatis basin may be ejecta from the Imbrium basin-forming impact [166], meaning Serenitatis could be much older than traditionally thought. Furthermore, Boehnke & Harrison [130] developed a physical model of  $^{40}\text{Ar}$  diffusion in Apollo samples, and found that  $^{40}\text{Ar}/^{39}\text{Ar}$  basin age histograms tend to show illusory LHB-type episodes under monotonically declining impacts. Therefore, lunar magmatism and Ar overprinting from subsequent impacts may cause us to misinterpret the cluster of lunar basin ages as a single lunar cataclysm.

Evidence for a sustained, declining bombardment dating back to the accretion of the Moon is however lacking. For example, the lack of impact-melted lunar samples dating prior to  $\sim 3.92$  Ga doesn't support a sustained bombardment [127]. This may however be due to the fact that impact glasses would shatter into smaller pieces gradually with time given a sustained lunar bombardment [167]. Lunar meteorites recovered from Antarctica also have ages no older than 3.92 Ga, which supports the concept of a short intense bombardment period [128]. There is however another possible explanation, that a bias is introduced in sampling Antarctic meteorites; strong rocks near the surface of the Moon that can survive an impact, be ejected towards the Earth, and survive

atmospheric entry, are rare, and only become rarer with age [114].

Astrophysical simulations also support the occurrence of a LHB. In the Nice model of the formation of the Solar System [129, 168, 169], as a result of gravitational interactions with the planetesimal disk, the giant planets begin to migrate inwards or outwards. This planetary migration leads to a 1:2 mean motion resonance between Jupiter and Saturn (i.e. Saturn's period becomes twice that of Jupiter's), which forces the orbits of Neptune and Uranus to destabilize into eccentric ellipses, allowing these planets to cross through the planetesimal disk sitting at least 1–1.5 AU beyond Neptune's orbit. The crossing of the ice giants into the planetesimal disk gravitationally disperses the planetesimals, causing many of them to be sent on Earth- and Moon-impacting trajectories. Following this LHB, which occurs approximately 450–850 million years after the formation of the Solar System [169, 170], the giant planets settle into separations, eccentricities, and inclinations similar to their observational values [168, 171]. The Nice model also correctly explains the orbital distribution and total mass of the Trojan asteroids [129].

All things considered, there is insufficient evidence to reject the occurrence of a LHB, however more lunar research is required before a consensus in the field can be reached. Four possible models for the late lunar bombardment are illustrated in Figure 2.2 which are calibrated to the crater counts and surface ages at the Apollo landing sites (figure reproduced from Zahnle *et al.* [114]).

The bombardment of the early Earth with asteroids and comets could have had both positive and negative effects with respect to the emergence of life. If CO<sub>2</sub> subduction was efficient during the Hadean eon, asteroidal and cometary impacts on the early Earth could have helped maintain the atmospheric pressure necessary for a clement temperature by releasing CO<sub>2</sub> into the atmosphere. However, weathering of the ejecta from such impacts also removes CO<sub>2</sub> from the atmosphere [151], possibly much more efficiently than CO<sub>2</sub> is released by impacts [172]. Impacts could have also delivered or even produced the essential organics required for the emergence of life, e.g. nucleobases, amino acids, and carboxylic acids [33, 36, 68, 70, 71, 173, 174]. On the other hand, asteroidal and cometary impacts could have also hindered the progress of evolving pre-life molecules or destroyed existing life [175].

Abramov *et al.* [176] developed a thermal model for global bombardments to study how significant Earth's crustal melting would have been due to the occurrence of the LHB. Their model, which considered shock heating, impact melt generation, uplift,

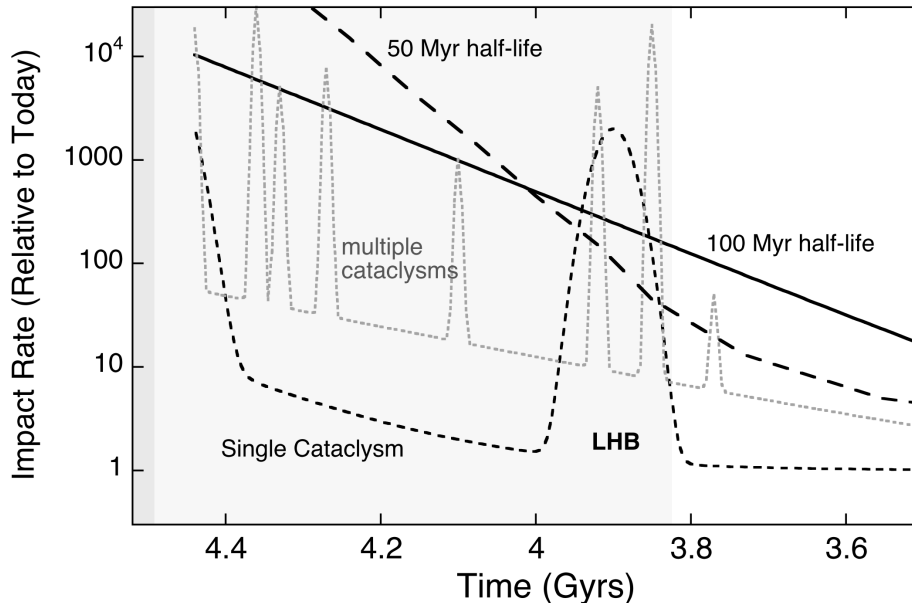


Figure 2.2: Four possible scenarios for the late heavy bombardment, calibrated to crater counts and surface ages at the Apollo landing sites. All scenarios except the 50 Myr half-life model are supported by the available data. This figure is taken directly out of Zahnle *et al.* [114].

and ejecta heating, predicted that about 5–10 % of the Earth’s surface area would have been covered by  $> 1$  km deep impact melt sheets after the LHB. This suggests that living organisms could have potentially survived the event if they inhabited a portion of the surface that remained relatively unscathed. But what if the LHB was just the tail-end of a sustained, declining bombardment? Given this scenario, a higher proportion of the crust would have melted from 4.5–3.9 Ga than would have during a LHB, however it is unclear how much greater this proportion would be. The existence of zircons that formed from melts with ages from 3.91–4.40 Ga confirms that the Earth’s crust experienced periodic melting throughout this period, but more importantly, since re-melting of the crust would have likely age-reset the zircons at that location [176], at least some crust likely didn’t re-melt from 4.4–3.9 Ga.

If there was a LHB and it completely sterilized the planet of any evolving life and pre-life molecules (e.g. nucleotide monomers, dimers, trimers, etc.), the habitability boundary of the emergence of life is 3.9 Ga. Otherwise, if asteroid impacts at or before 3.9 Ga had no negative bearing on the emergence of life, the outer boundary remains at 4.316–4.52 Ga, corresponding to the uncertainty in the date by which the Earth’s magma ocean cooled and a hydrosphere formed.

## 2.4 The Fossil Record

### 2.4.1 Microfossils

It has been said that the only true consensus for a date by which life definitely existed on Earth is in the bacterial fossils found within the Gunflint Formation of Ontario, dated at 1.9 Ga [131, 177]. Brasier *et al.* [178], a prominent challenger of the oldest microfossils reaffirmed this, calling the Gunflint chert a benchmark for the analysis of early fossil preservation. Two key components of the Gunflint microfossil consensus are that (a) these microfossils have 3-dimensional round-walled compartments, a.k.a., cell lumina, and (b) the walls are composed of carbonaceous (kerogenous) matter [179, 180]. These two traits above others, have become critical evidence in establishing the authenticity of microfossils [181]. However, authentic microfossils are also backed by other more common indicators such as the presence of a variety of specimens ranging from relatively well-preserved to partially or completely degraded [182]. For a complete list of microfossil indicators, see Wacey [183].

It has been argued by many that microfossils have been discovered within carbonaceous cherts (i.e. the fine-grained silica-rich sedimentary rocks) and sandstones in Western Australia [131, 184–192], within ferruginous sedimentary rocks in Northern Quebec [193], and within pillow lavas, siliciclastic deposits (noncarbonate, almost exclusively silica-bearing sedimentary rocks), and cherts in South Africa [194–200] that range in diameter from  $\sim 0.1$ – $289 \mu\text{m}$ . The rocks in the formations hosting these possible microfossils have U-Pb dates of approximately 3.20–3.77 Ga. (For a more complete review of potential microfossils, including those younger than 3.2 Ga, see Schirmer *et al.* [201].) These potential microfossils come in many morphologies: spiral, branched, thread-like, disc, spheroidal, cylindrical, tubular, and filamentary.

The difficulty in determining the authenticity of microfossils, is that there are abiotic processes that can lead to similar structures [178, 183, 202–205]. Brasier *et al.* [205] reinterpret the potential microfossils discovered in the Apex Basalt of Western Australia [184, 185] as being secondary artefacts formed by amorphous graphite reorganized in the form of filaments within multiple generations of hydrothermal chert breccia veins and volcanic glass. These potential microfossils showed similar morphologies to structures within rocks that were hydrothermally altered or completely melted, which questions a biological origin of the possible microfossil morphologies

[205]. To show this, Brasier *et al.* [205] compared these potential microfossils with several similar structures produced in both the clasts (fragments) and matrix of hydrothermally altered chert beds, within glass rims of volcanic shards, and in the associated chalcedony (i.e. milky quartz) matrix of the felsic tuffs (i.e. igneous rocks, rich in elements producing feldspar, fused from smaller grains by heat). These potential microfossil structures [184, 185] are also generally isolated, irregularly distributed, and randomly oriented in several generations of hydrothermally altered formations. This is unlike typical cyanobacteria, in which the trichomes (hair-like outgrowths) of such organisms commonly cluster together in layers, often with a specific orientation relative to rock bedding [205].

Furthermore, García-Ruiz *et al.* [204] demonstrated the abiotic formation of noncrystallographic, curved, helical morphologies, similar to these same potential microfossils [184, 185]. García-Ruiz *et al.* [204] grew filamentous materials out of barium salt in alkaline sodium silicate solutions under alkaline, mildly hydrothermal conditions. These initial materials and conditions, though uncommon on Earth today, are geochemically plausible during Archaean times [206]. French & Blake [202] similarly found a plausible abiotic formation mechanism for microfossils by examining submarine glasses from the western North Atlantic Ocean. By combining petrographic and electron microscopic observations with theoretical models of radiation damage from uranium and thorium decay, French & Blake [202] found that tubular and granular microfossils can be formed by preferential seawater corrosion of damage trails left by fission fragments.

Given the circumstances, it is difficult to be certain of a biological origin for microfossils without evidence for cell lumina and carbonaceous cell walls. The most recent studies have used state-of-the-art analysis techniques including laser Raman microspectroscopy, secondary ion mass spectrometry (SIMS), and transmission electron microscopy (TEM) to confirm these two traits. The oldest microfossils to meet these criteria are 3.2 [200], and 3.4 Gyr old [131]. In Figure 2.3, optical photomicrographs of several hollow, tubular microfossils from the 3.4 Gyr-old Strelley Pool Chert are displayed (figure from Wacey *et al.* [131]). The closely packed tubular microfossils in images (b), (d), and (e) are interpreted by Wacey *et al.* [131] to be much like the cells of prokaryotes within modern biofilms.

The 3.46 Gyr-old microfossil-like structures in the Apex chert were confirmed by De Gregorio *et al.* [207] to meet one of the two traits required for establishing

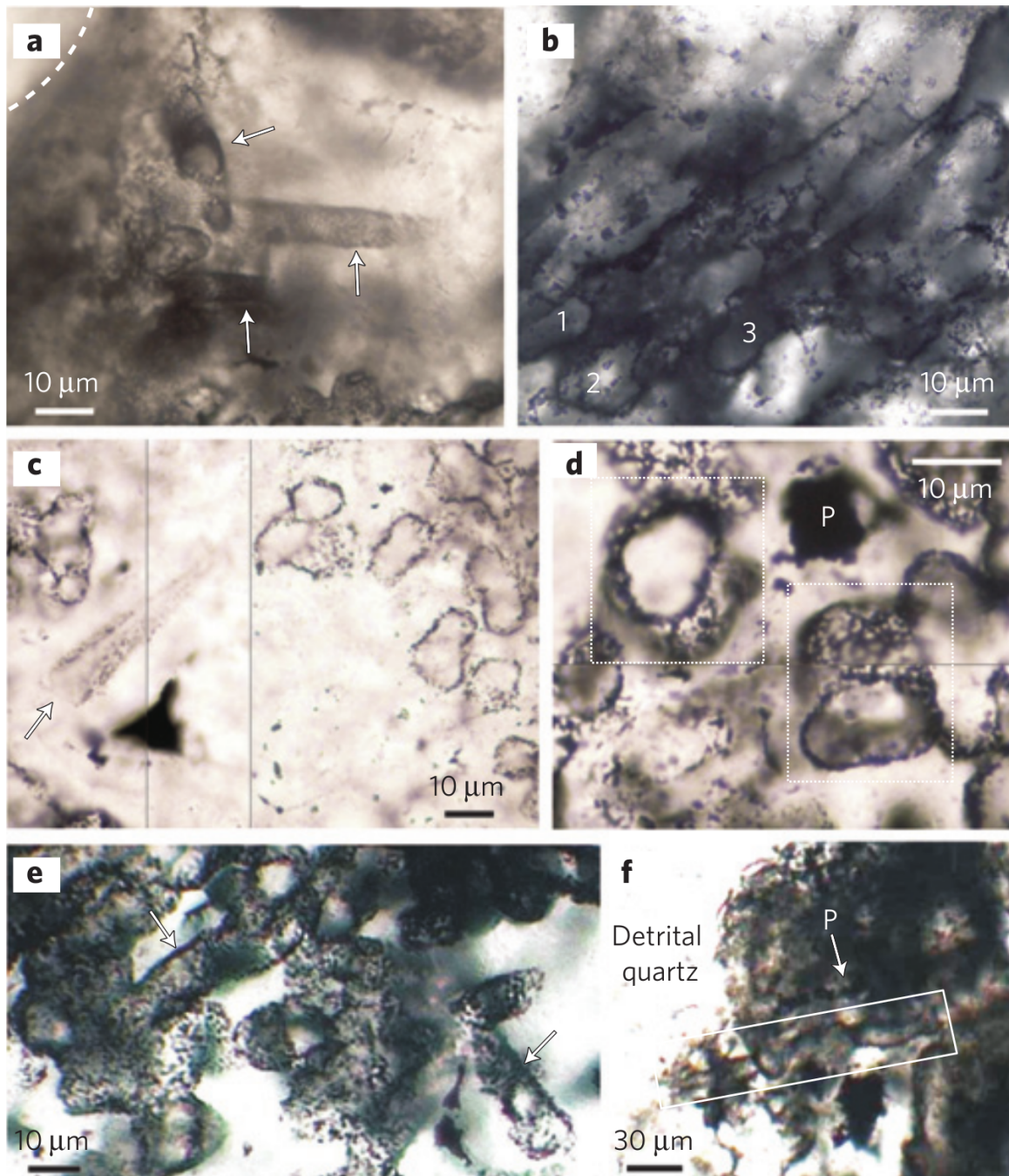


Figure 2.3: **(a) – (f)** Hollow, tubular microfossils from the 3.4 Gyr-old Strelley Pool formation (indicated by arrows, boxes, or numbers). A couple highlights are the tubular microfossil cross-sections in frame (d) and the dense patch of tubular microfossils in frame (e). P stands for pyrite. This figure is taken directly out of Wacey *et al.* [131].

authenticity (i.e. carbonaceous cell walls). However, Brasier *et al.* [178] examined thin slices of these microfossils with TEM and found at high spatial resolution, instead of cell lumina, the potential microfossils actually have a complex, incoherent spiky morphology, which is evidently formed by filaments of clay crystals coated with iron and carbon. This analysis led them to the conclusion that the multiple clay minerals within the thin slices are entirely compatible with chemistry in high temperature hydrothermal settings.

Lastly, although the recently discovered filamentary and tubular microfossil-like structures in the  $> 3.77$  Gyr-old Nuvvuagittuq belt co-occur with carbonaceous material [193], they do not exhibit carbonaceous cell walls and there is no evidence of cell lumina. Therefore these structures do not meet the most critical traits for establishing microfossil authenticity.

In light of all this evidence, in Figure 2.1, we date the oldest microfossils as 3.4 Ga, which matches the oldest microfossils exhibiting cell lumina and carbonaceous cell walls [131]. We now discuss the stromatolite macrofossils, which are also useful in constraining the biosignature boundary.

### 2.4.2 Stromatolites

The word ‘stromatolite’ in Greek literally means, layered rock. In general, stromatolites are layered, sheet-like, accretionary structures created by or resembling those created by microbial mats of microorganisms such as cyanobacteria. The suite of microbes that form stromatolites live in a biofilm bound by mucus or other adhesives that microbes produce. When photosynthetic microorganisms at the top of the mat get covered in naturally accumulating sedimentary grains and silt, and microbiologically induced carbonate precipitates, they migrate upwards towards the light. This creates a new microbial mat layer, with a calcium carbonate-cemented layer of sedimentary rock and silt left behind [208, 209]. Over thousands of years, layer upon layer of this combination of sedimentary rock, silt and carbonate builds up. These preserved structures are stromatolites.

The oldest stromatolite-like structures were recently discovered in the 3.7-Gyr-old Isua supracrustal belt in Greenland [104]. A photograph of these stromatolites along with the interpretation by Nutman *et al.* [104] and a comparison to similar, 2.03-Gyr-old stromatolites are shown in Figure 2.4. Previous to this discovery, the oldest widely accepted stromatolites were found in the Strelley Pool Chert [210], the contact

between the Strelley Pool Chert and Panorama Formation [211], and the Dresser Formation [212] in Western Australia. Rocks from these locations are U-Pb dated at ca. 3.43 Ga, 3.45 Ga and 3.48 Ga, respectively. Most recently, Djokic *et al.* [213] also discovered exceptionally well-preserved stromatolites in the 3.48 Gyr-old Dresser Formation. Nutman *et al.* [104] deduce that the 3.7-Gyr-old stromatolite forms match some of those discovered in the 3.43-Gyr-old Strelley Pool chert and the 2.03-Gyr-old Woolly Dolomite, implying a biological origin. Since the oldest stromatolites don't contain any fossil microbes, many assume that they are of biological origin due to morphological comparisons with modern, biological stromatolites [214]. Some key morphological indicators are wrinkly sequences of small-scale fine layers in cone, mat, peak and dome shapes and microbe-bound ripples in carbonate sand [104, 210, 215].

Just as with microfossils, there has also been some disagreement whether stromatolite rock formations are of biological origin. For example, Grotzinger & Rothman [214] deduce that these surfaces can be grown from chemical precipitation, diffusive rearrangement of suspended sediment, and uncorrelated random noise. Others defend that the distinct morphological attributes of stromatolites are inconsistent with purely mechanical deposition [104, 210]. For example, unlike crusts formed by mechanical deposition, the peaks of the 3.7 Ga stromatolite structures are inclined and asymmetrical, both dome- and peak-shaped structures are observed together, and there are no irregular projections normal to the growth surface (see Figure 2.4).

Non-morphological factors also indicate a biological origin of the oldest stromatolites. For example, there is a great diversity of stromatolites in the same location that all resemble known microbial mats, and none resemble any known structure formed abiotically [210]. This is consistent with the ecologically controlled growth of an Archean microbial reef [210]. These stromatolites also exist in a location where the shoreline moved inwards and deposited carbonates: a location where microbial mats exist today [216]. There is also an absence of ancient stromatolites in deep waters, where photosynthetic organisms wouldn't have had enough light to exist in microbial mats [210]. Altogether, the evidence that stromatolites are true biological fossils seems fairly strong.

With all of this evidence in hand, we are confident in pushing the biosignature boundary for the emergence of life outwards to the date of the oldest stromatolites, at 3.7 Ga.

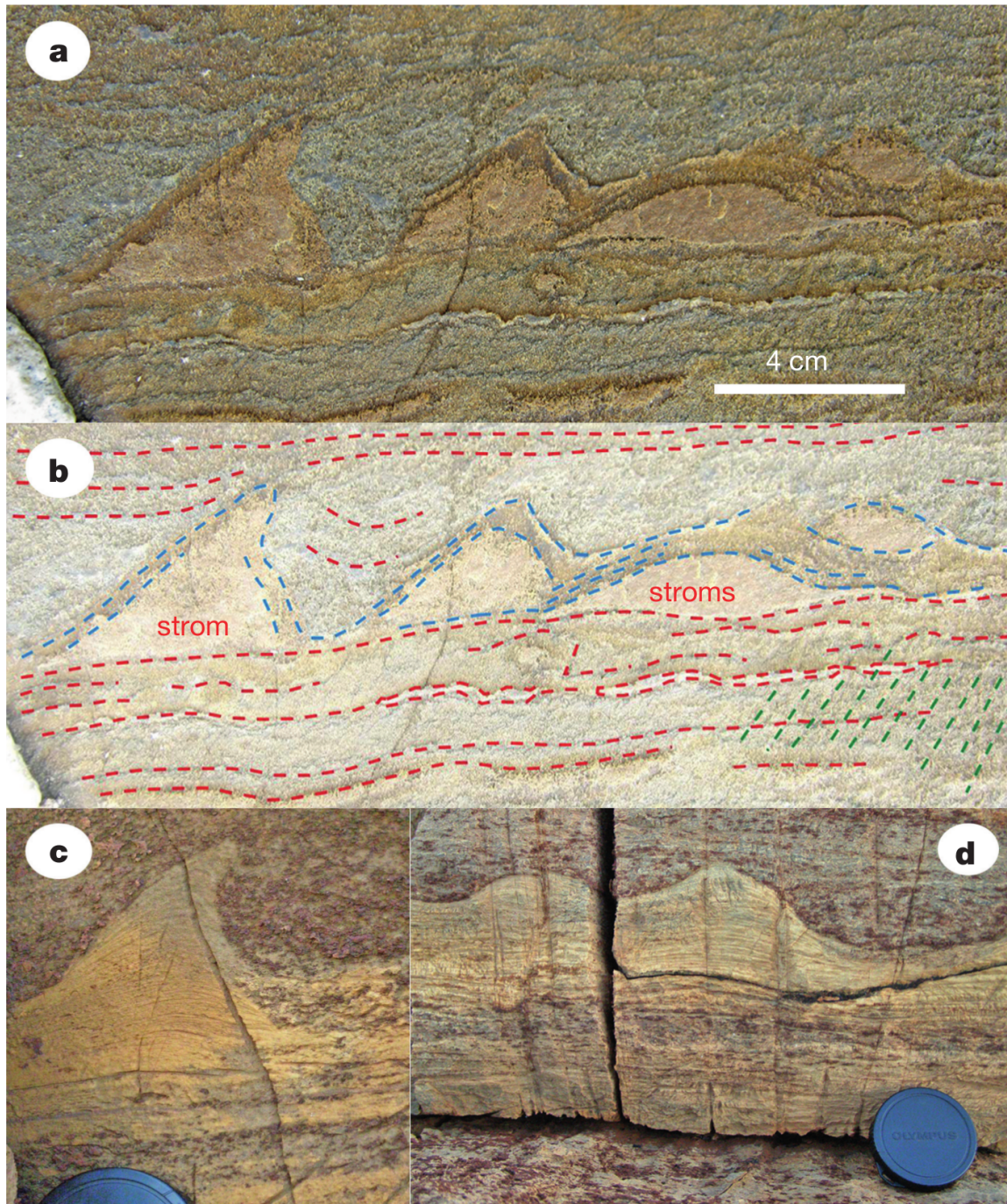


Figure 2.4: (a) Stromatolites in an exposed outcrop of 3.7-Gyr-old metacarbonate rocks in the Isua supracrustal belt in southwest Greenland. (b) Interpretation of (a), with both an isolated stromatolite (strom) and a conglomerate of stromatolites (stroms). (c) Asymmetrical, peak-shaped stromatolite and (d) linked, dome-shaped stromatolites from the 2-Gyr-old Woolly Dolomite carbonate platform in Western Australia. This figure is taken directly out of Nutman *et al.* [104].

## 2.5 Isotopic Signatures

### 2.5.1 Signatures for the Presence of Oxygen

Observations of sulfur and molybdenum isotopes and transition metals in ancient sedimentary rocks indicate that there was a so-called great oxidation event (GOE) around 2.4–2.3 Ga. The GOE is widely believed to have been produced by photosynthetic cyanobacteria [132, 133, 217, 218]. Although UV photodissociation of water vapour can produce  $O_2$  abiotically, unless one of the products of such a reaction is immediately removed, they will recombine to form water vapour [219]. Furthermore, water vapour would have been present in the atmosphere throughout the Hadean and Archean eons (see Section 2.3), and there is no known reason for the  $O_2$  produced via this mechanism to start building up around 2.4–2.3 Ga. This argument can also be used to explain why the photodissociation of atmospheric  $CO_2$  [220] is unlikely to have caused the GOE. Hence, the existence of  $O_2$  in the early atmosphere implies a rapid rate of creation of  $O_2$  by life that keeps the atmosphere out of equilibrium.

The fluctuations in atmospheric oxygen over geological time scales can be tracked by fluctuations in sulfur and molybdenum isotopes [132, 221] and enrichment of transition metals (e.g. chromium, molybdenum, rhenium) in the geologic record [222]. Sulfur isotopes are said to undergo mass independent fractionation (MIF) under anoxic conditions. However the term “MIF” can be misleading, as fractionation of sulfur isotopes is always dependent on the mass of the isotopes. Literally, MIF just means the isotopic signatures don’t obey the standard mass-dependent relationship (i.e.  $\delta^{33}S \sim 0.515\delta^{34}S$ ;  $\delta^{36}S \sim 1.91\delta^{34}S$ ) [223, 224]. The reason for this deviation from the standard isotopic relationship in anoxic environments, is that when sulfur rains out of the atmosphere or is deposited onto the surface, it does so in a variety of different oxidation states—leaving a variety of isotopic signatures in the sediments into which sulfur gets incorporated. In an oxygen atmosphere, even one as low as  $10^{-5}$  times the present atmospheric level of  $O_2$ , the clear majority of sulfur gets oxidized to  $H_2SO_4$ , which homogenizes the sulfur isotopes to match the standard mass-dependent relationship [224]. Therefore measuring such isotopes in old bioelemental sediments can be used to infer the oxygenation history of ancient seawater [225]. An accumulation of redox-sensitive transition metals in sedimentary rocks also signifies a necessity of oxygen in the early Earth seawater that deposited such rocks [222]. For example,

molybdenum, which currently exists in bodies of water as the unreactive molybdate ion ( $\text{MoO}_4^{2-}$ ), accumulates via oxidative weathering of molybdenum-bearing sulfide minerals in crustal rocks. Under anoxic conditions, molybdenum would instead be retained by these sulfide minerals and therefore would not accumulate in the oceans and be deposited into sediments [222].

MIF disappears completely from the geologic record before 2.4–2.3 Ga, providing the tightest constraint on the GOE [133]. A shift in sulfur isotopes [221] and an enrichment of transition metals [222] in 2.5-Gyr-old samples of shale from Mount MacRae in Western Australia indicates a presence of atmospheric oxygen even before the GOE. Moreover, Planavsky *et al.* [132] measured a large fractionation of molybdenum isotopes in 2.95-Gyr-old rocks from the Sinqeni Formation in South Africa. However in this case, molybdenum is used as a proxy for manganese (II), which requires free dissolved  $\text{O}_2$  to be oxidized. Planavsky *et al.* [132] inferred from these results that oxygen produced via photosynthesis began to accumulate in shallow marine settings at 2.95 Ga.

This is the kind of environment where we would expect stromatolites to grow, and as we saw in the previous section, evidence for stromatolites goes back to 3.7 Ga, about three-quarters of a billion years before the  $\text{O}_2$  signature is seen. These dates do not seem inconsistent to us. Stromatolites are presumed to be formed by photosynthetic bacteria, and modern stromatolites contain cyanobacteria that carry out oxygenic photosynthesis. However, there are several other groups of bacteria that carry out non-oxygenic photosynthesis (see Section 2.6 below). The earliest stromatolites might have been formed by bacteria such as these, or it may simply be that oxygenic photosynthesizers were present but not prolific enough to produce a detectable level of  $\text{O}_2$ . Thus, the evidence from  $\text{O}_2$ -dependent isotopic signatures seems to fit with that from the fossil record, but it does not push the biosignature boundary further back from what is known from stromatolites. In contrast, carbon isotope biosignatures extend further back in time and are currently a key piece of evidence that constrains the biosignature boundary, as we now discuss.

## 2.5.2 Carbon Isotope Biosignatures

Almost all rocks older than 3.6 Gyr, deposited just above the basement of the crust, underwent high-grade metamorphism (i.e. changed in mineral assemblage and structure due to high temperatures and pressures). Therefore fossils from before 3.6 Ga are

very unlikely to be preserved (which makes the 3.7-Gyr-old stromatolite discovery both remarkable and potentially controversial). This means typically, evidence for life beyond 3.6 Ga must include a geochemical component [102].

One isotope commonly used to infer evidence of biological activity is  $^{13}\text{C}$ .  $^{13}\text{C}$  is a stable isotope of carbon, and makes up approximately 1.1% of the natural carbon on Earth. The rest of the carbon is in the form of  $^{12}\text{C}$ , with only trace amounts existing of the short-lived radioactive  $^{14}\text{C}$ .

Two pioneering studies performed by Nier & Gulbransen [226] and Murphey & Nier [227] discovered that converting inorganic carbon to biological matter through biochemical reactions leads to an obvious fractionation of  $^{12}\text{C}$  and  $^{13}\text{C}$ . Subsequent works determined that photosynthetic reaction pathways discriminate against  $^{13}\text{C}$  because of its heavier mass. In general, isotopically light molecules are more mobile and tend to have greater velocities than their heavier counterparts [228]. As a result, not only does  $^{13}\text{C}$  diffuse slower than  $^{12}\text{C}$  through membranes, but certain enzymes fix lighter carbon faster, e.g. rubulose 1,5-bisphosphate carboxylase and pyruvate dehydrogenase [228–230]. However, not all enzymes prefer light carbon, for example, phosphoenolpyruvate carboxylase does not discriminate between  $^{12}\text{C}$  and  $^{13}\text{C}$  [229]. Because of discriminatory enzymes, molecules produced by living organisms are preferentially composed of light carbon, while heavy carbon is retained in the surface reservoir (mostly in the form of marine bicarbonate) [231]. It is unknown when these discriminatory enzymes were incorporated into life, therefore there may be a limit to the earliest organisms that can be detected using carbon isotopes.

The variable  $\delta^{13}\text{C}$  is used to determine how depleted or enriched a sample is in  $^{13}\text{C}$  (similarly to the  $\delta^{18}\text{O}$  variable from Equation 2.1).  $\delta^{13}\text{C}$  is calculated as

$$\delta^{13}\text{C} = \left( \frac{\left(\frac{^{13}\text{C}}{^{12}\text{C}}\right)_{\text{sample}}}{\left(\frac{^{13}\text{C}}{^{12}\text{C}}\right)_{\text{standard}}} - 1 \right) \times 1000\text{‰} \quad (2.2)$$

A comparison of the  $\delta^{13}\text{C}$  values of major groups of plants and autotrophic microbes, and inorganic carbon of the surface environment ( $\text{CO}_2$ ,  $\text{HCO}_3^-$ ,  $\text{CO}_3^{2-}$ ) are displayed in Figure 2.5 (figure from Schirrmeister *et al.* [201]). A negative  $\delta^{13}\text{C}$  value corresponds to a sample depleted in  $^{13}\text{C}$  (or enriched in  $^{12}\text{C}$ ) with respect to the inorganic, oxidized carbon sources.

Because molecules produced by modern living organisms are preferentially light in carbon, measuring highly negative  $\delta^{13}\text{C}$  values in organic matter within rocks of

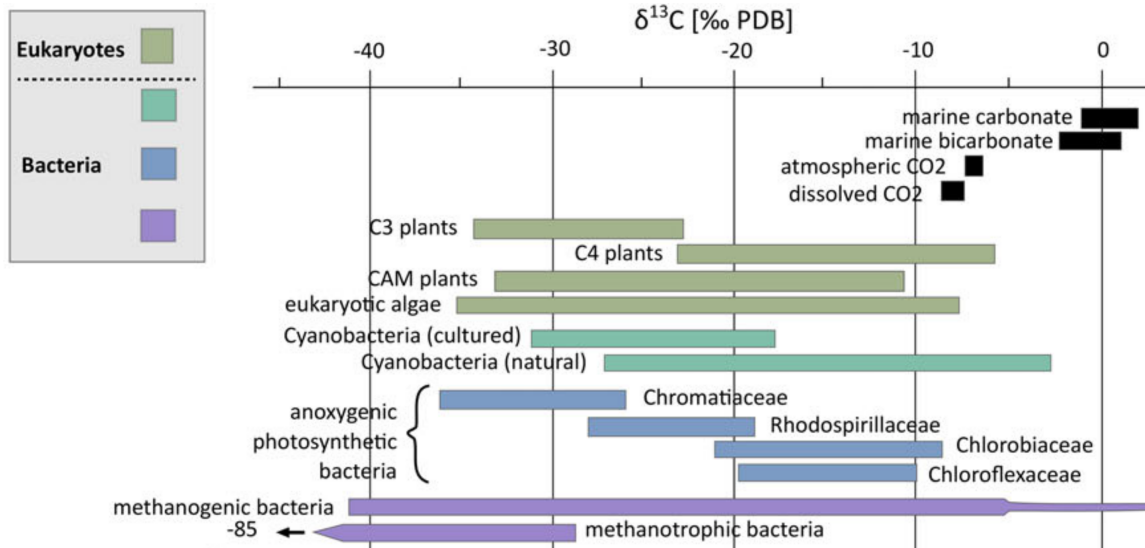


Figure 2.5: Isotopic carbon composition of various major groups of plants, protists, and bacteria compared with those of  $\text{CO}_2$ ,  $\text{HCO}_3^-$ , and  $\text{CO}_3^{2-}$  in the surface environment. Negative  $\delta^{13}\text{C}$  values correspond to  $^{13}\text{C}$  depletion relative to the Pee Dee Belemnite (PDB) standard. The positive extremes for methanogens were from experiments of cultures that were placed in conditions irrelevant to natural populations. This figure is taken directly out of Schirmer *et al.* [201].

sedimentary origin is suggestive of biological activity at the U-Pb date at which the rocks are aged. A sedimentary origin is an essential prerequisite for interpreting  $\delta^{13}\text{C}$  signatures to be biologically reduced, because there are abiotic mechanisms for reducing  $\delta^{13}\text{C}$  in rocks that are of non-sedimentary origin, and because a sedimentary origin provides evidence for a liquid water biosphere in a habitable temperature range. This is in contrast to rocks of metamorphic origin, which were formed by hot hydrothermal fluids reacting with rocks originally deposited by metamorphic or igneous fluids. Graphite, for example, is either formed by the metamorphism of carbon-rich sedimentary rocks or from the precipitation of carbon-bearing fluids or melts [232]. There are several high-temperature abiotic mechanisms that could produce light  $\delta^{13}\text{C}$  in rocks of non-sedimentary origin, including A) disproportionation of ferrous carbonates [233], B) decarbonation (the removal of  $\text{CO}_2$ ) during metamorphism accompanied by a Rayleigh distillation process or serpentinization (i.e. the addition of water into the crystalline structure of rock minerals) [234], C) Fischer-Tropsch reactions [235], D) diffusive fractionation [236], and E) degassing of basalts [237].

By sampling the  $\delta^{13}\text{C}$  value of graphite globules from sedimentary rocks from the

Isua supracrustal belt (ISB) in west Greenland, dated at 3.7 Ga, Rosing [102] deduced that they were biologically reduced. The low  $\delta^{13}\text{C}$  values within the globules ( $\sim -19\text{‰}$ ), are within the range of reduced C compositions from photosynthetic bacteria (i.e. approximately  $-10$  to  $-36\text{‰}$ , see Figure 2.5). The same 3.7-Gyr-old graphite globules were geochemically analyzed by Ohtomo *et al.* [103] to confirm whether they were of sedimentary origin, or instead deposited by metamorphic or igneous fluids. With the use of Raman spectroscopy, it was determined that the rocks containing the graphite globules were formed from marine sediments that were depleted in  $^{13}\text{C}$  at the time of their deposition. Furthermore, through the use of a transmission electron microscope, it was seen that the graphite globules are nanoscale polygonal and tube-like grains, which is unlike the flaky morphology of abiotic graphite in carbonate veins. Even more so, the graphite globules exhibited distorted crystal structures and disordered stacking of graphene, which is consistent with the thermochemical decomposition and pressurization of organics during metamorphism. Therefore the analysis by Ohtomo *et al.* [103] supports the claim by Rosing [102], that the 3.7-Gyr-old graphite globules are of biological origin.

Grassineau *et al.* [238] measured similarly low  $\delta^{13}\text{C}$  values ( $\sim -18.4$  to  $-14.7\text{‰}$ ) within samples obtained from a sedimentary outcrop in the ISB dated between 3.7–3.8 Ga, and stated that these samples might record biological activity as early as 3.8 Ga. However due to two high-grade metamorphic events in this outcrop at  $\sim 3.74$  Ga, metamorphic alteration could have overprinted the  $\delta^{13}\text{C}$  values within these samples. This means the low  $\delta^{13}\text{C}$  values in these samples could be a result of high temperature processes rather than the burial of organic matter.

Schidlowski [231] and Mojzsis *et al.* [239] measured mean  $\delta^{13}\text{C}$  values of approximately  $-13$  to  $-37\text{‰}$  in deposits of kerogen and grains of apatite from what they interpreted as banded iron formations (BIFs) in the ISB (U-Pb dated to be 3.8 Ga and 3.85 Ga). BIFs are  $\sim 4,280$ – $545$  Ma layered sedimentary rocks, whose successive layers contain high abundances ( $20$ – $40\%$ ) of iron [240, 241]. Both abiotic and biotic sources of the iron precipitate have been suggested, however iron-oxidizing bacteria have been gaining in popularity over the past decade as they can explain iron oxidation in anoxic environments [242]. The  $\delta^{13}\text{C}$  purported BIF signatures were initially interpreted to be evidence for early life at 3.8 Ga and 3.85 Ga. However, Fedo & Whitehouse [234] and van Zuilen *et al.* [233] challenged this interpretation by examining the claim that the purported BIF, from which the 3.8- and 3.85-Gyr-old samples of  $\delta^{13}\text{C}$

were obtained [231, 239], came from sedimentary rocks, chemically precipitated by seawater. They deduced, for various geological, petrological, and geochemical reasons, that the purported BIF rocks were most likely once metasomatic and igneous, and thus could have been reduced in carbon by one of the abiotic mechanisms listed above. Additionally, these previously molten rocks do not provide evidence for a habitable environment, and thus are unlikely to have hosted life.

Papineau *et al.* [243] measured  $\delta^{13}\text{C}$  values from -18.2 to -26.8 ‰ in graphite within the 3.75- to 4.28-Gyr-old Nuvvuagittuq BIF in northern Canada. These  $\delta^{13}\text{C}$  signatures may point to a biological origin for this carbon. However, the  $^{13}\text{C}$ -depleted graphite was deposited by hydrothermal or metamorphic fluids after peak metamorphism of the BIF [241, 243], therefore it could also have been reduced by one of the abiotic mechanisms above. Furthermore, it is uncertain whether this graphite is indigenous to the 3.75- to 4.28-Gyr-old rocks, as it has not undergone the same metamorphic history as the sedimentary host rock [241, 243].

Finally, preserved graphite encased in 4.1- and 4.25-Gyr-old zircon crystals from Jack Hills, Western Australia have been discovered to have a particularly low  $\delta^{13}\text{C}$  values [244, 245]. Though both studies could not rule out abiogenic sources, the simplest interpretation may be that the graphite represents organic carbon present at 4.1 and 4.25 Ga. Watson & Harrison [159] used a thermometer based on titanium content (a “zircon thermometer”) to measure the melt temperatures for 54 Jack Hills zircons, and found that they ranged from 644–801°C. At such high formation temperatures, the low  $\delta^{13}\text{C}$  value in the enclosed graphite could result from any of the five abiotic mechanisms listed above.

With the determination of a likely non-sedimentary origin for the oldest graphite samples described above (those with ages  $> 3.75$  Ga), along with several suggested abiotic mechanisms causing their low  $\delta^{13}\text{C}$  values, evidence is not strong for the existence of life before 3.7 Ga in Earth’s history.

There is also one universal potential abiotic source for low  $\delta^{13}\text{C}$  values in all old rock samples. This source is carbonaceous meteorites, whose  $\delta^{13}\text{C}$  contents range from +68 ‰ to -60 ‰ [244]. If the rock and graphite samples obtained in the ISB are actually fragments of early meteorite impacts, it is possible, given the meteorite fragments are on the low side of their  $\delta^{13}\text{C}$  range, that the samples are not indicative of biological activity at all. However, this possibility is more likely for rock samples older than  $\sim 3.8$  Ga, when the possible LHB (or the sustained, declining bombardment)

tapered off (see Figure 2.2). Furthermore, nearly all carbonaceous meteorites contain chondrules (previously molten spherical grains), which are not described to be present near the 3.7-Gyr-old sedimentary rock samples analyzed by Rosing [102] and Ohtomo *et al.* [103].

The general agreement of the sedimentary origin and biological reduction of  $^{13}\text{C}$  in the 3.7-Gyr-old graphite globules from Rosing [102] and Ohtomo *et al.* [103] makes us confident in maintaining the biosignature boundary for the emergence of life at 3.7 Ga, as we already concluded from the recently proposed stromatolites in Section 2.4.2. Although some isotopic evidence may suggest life existed as early as 3.8 Ga [238], due to the large uncertainty in dates for their sampled outcrop (3.7–3.8 Ga) and the possible metamorphic overprinting of their rock samples at  $\sim 3.74$  Ga, we are cautious to extend the inner boundary past 3.7 Ga.

## 2.6 Molecular Evolution and Phylogenetics

Another branch of evidence that can provide information about early evolutionary events on Earth is molecular phylogenetics: the use of gene sequences to determine evolutionary relationships among groups of organisms. Important early work on phylogenetics used ribosomal RNA (rRNA), which is one of the few kinds of genes found in all cellular organisms that can be reliably aligned even for the most divergent sequences. Woese & Fox [246] found that rRNA sequences formed three divergent groups, and thus established the idea that there are three domains of life: Bacteria, Archaea and Eukaryotes. It was also proposed early on, using sequences of pairs of paralogous genes that arose by gene duplication prior to the last common ancestor of the three domains, that the root of the tree of life lies on the bacterial branch [247, 248]. This implied that the fundamental split in the tree of life is the division between Bacteria and Archaea, with Eukaryotes arising as a sister group to Archaea at a later stage. It has since become apparent that the origin of Eukaryotes involves a fusion between a bacterial and an archaeal ancestor. Ideas of endosymbiosis were proposed very early on [249, 250], and whole-genome analysis in recent years has made it clear that Eukaryotes possess many genes that are of bacterial origin as well as archaeal origin [251, 252]. Nevertheless, the slowly evolving, highly conserved genes related to the gene-protein translation process show greater similarity between Eukaryotes and Archaea. This is consistent with a scenario in which the root of the translation-related

genes lies on the bacterial branch, as originally proposed, and in which other genes were transferred at a later date to the ancestral eukaryote by endosymbiosis. Recent work [253, 254] suggests that eukaryotes arose from within the archaea, not as a sister group. This means that archaea are paraphyletic, and that archaea and eukaryotes should be classed together as a single domain.

The last universal common ancestor of cellular organisms (LUCA) is the earliest point of division among prokaryotic lineages. Studies of early-duplicating paralogues [247, 248] suggest that this earliest division lies between bacterial and archeal domain, although an earlier division among lineages of bacteria may also be possible. At what time did this occur? Estimates of dates from phylogenetic trees requires some kind of molecular clock assumption, i.e. that mutations occur at a constant rate, so that the number of mutations by which two gene sequences differ is a straightforward function of the time since the species diverged. Geological evidence for species is then used as calibration points to place specific nodes of the tree into geological time. The dates of other points in the tree are then estimated consistently with these calibration points. Sheridan *et al.* [255] used rRNA sequences to create a phylogenetic tree of major archaeal and bacterial groups, and used a calibration point of 2.65 Ga for the origin of cyanobacteria, based on the detection of 2-methylhopanoids in sedimentary rocks of this age [256]. They estimated a time of 4.29 Ga for the LUCA and 3.46 Ga for both the earliest branch point within Archaea and the earliest branch point within Bacteria. These dates are consistent with other types of evidence that we discussed above. If stromatolites go back to 3.7 Ga, then there must have been a diversity of mat-forming organisms by then. Phylogenetic methods cannot give information prior to the root of the tree; therefore, the 4.29 Ga time estimate for the LUCA is the earliest point accessible from phylogenetics, and the origin of life must be before that. This point is consistent with the estimate of when Earth became habitable after the Moon-forming event (roughly 4.52–4.32 Ga) under the assumption that the LHB did not completely sterilize the Earth at a later date.

It should be realized, however, that there is a large margin for uncertainty in dates derived from molecular clocks, especially when pushing back these methods to the earliest points on the evolutionary tree. The rate of evolution varies substantially between organisms and between genes in the same organism, and these things can be accounted for, to some extent, in estimates of dates [257, 258]. However, these more sophisticated methods have not yet been attempted for estimating the age of the

LUCA, as far as we are aware.

Evolutionary studies of photosynthetic bacteria are particularly relevant to determining the biosignature boundary date because 1) stromatolites are formed by photosynthetic bacteria, 2) low  $\delta^{13}\text{C}$  signatures are taken as an indication of the existence of photosynthetic organisms which use  $\text{CO}_2$  from the air, and 3) the rise of  $\text{O}_2$  in the atmosphere is thought to derive from photosynthesis. Oxygenic photosynthesis today is carried out by Cyanobacteria, and by plants and algae which contain chloroplasts derived from Cyanobacteria. The date for the incorporation of plastids into eukaryotic cells is somewhere between 2.1 Ga and 1.2 Ga, depending on which group of fossils is taken to be the earliest eukaryotic algae [259]. This date is substantially later than the origin of Cyanobacteria.

Bacteria performing anoxygenic photosynthesis almost certainly existed before Cyanobacteria. Bacteria capable of anoxygenic photosynthesis include species from the following phyla: Chloroflexi, Chlorobi, Firmicutes, Proteobacteria, Gemmatimonadetes, Acidobacteria and possibly Actinobacteria (Rubrobacter). Gupta [260] has studied molecular signatures for these different phyla, and concludes that Chloroflexi were the earliest lineage in which photosynthetic ability was fully developed. Chloroflexi are filamentous bacteria, similar to the fossil organisms found in stromatolites. They carry out anoxygenic photosynthesis and could correspond to very early phototrophic microbial communities observed at 3.4 Ga [261, 262]. Olson [262] also discusses the geological evidence for the emergence of cyanobacteria carrying out oxygenic photosynthesis by 2.8 Ga, close to the calibration point used by Sheridan *et al.* [255] discussed above. The emergence of the Chloroflexi group is estimated as 3.1 Ga by Sheridan *et al.* [255], which fits reasonably with the scenario above. As we noted in Section 2.5.1, the dramatic rise in atmospheric oxygen occurring at the GOE, around 2.4–2.3 Ga seems to be somewhat after the first appearance of Cyanobacteria.

Now that many whole genomes have been sequenced for prokaryotic organisms, the process of genome evolution can be studied. Phylogenies for thousands of gene families have now been mapped to the Earth's geological timeline using models of gene gain and loss and horizontal transfer [263]. This shows that there was a period of innovation of new gene families in the Archaean eon between about 3.3 and 2.8 Ga, which corresponds to a period of diversification among prokaryotic lineages. Several time-calibration points were used. They chose to set the date for LUCA as  $< 3.85$  Ga, based on carbon isotope evidence for the earliest life that we discussed above

[102, 239]. They were also able to follow the change in frequency of genes involved in pathways linked to molecular oxygen, which occurs over the period during which the oxygen level increases in the atmosphere.

Overall, although molecular phylogenetic methods are perhaps not the most reliable way to estimate dates, the molecular studies seem to be consistent and to add some further support to the conclusions derived from geological evidence.

## 2.7 Discussion - How Quickly Did Life Emerge on Earth?

The timeline that illustrates the essential measurements and the resulting constraints on the emergence of life is detailed in Figure 2.1. The Earth formed  $\sim 24$  Myr after the first solids condensed in the Solar System (the latter of which occurred at  $\sim 4.568$  Ga). The impact of Theia with the proto-Earth, which led to the complete melting of the Earth's surface and the formation of the Moon occurred  $\sim 28$ – $128$  Myr after that. Finally, the Earth's magma ocean cooled to form a solid surface, leading to a potentially habitable world another  $\sim 0.02$ – $100$  Myr later. The absolute earliest the Earth could have been habitable is therefore  $\sim 4.5$  Ga. On the other hand, the absolute latest the Earth could have been habitable is  $\sim 3.9$  Ga, as the habitability boundary depends strongly on whether life could emerge during a sustained, declining asteroid bombardment, or survive the potential LHB.

Once life emerged, the first solid imprints of its existence appear in 3.7-Gyr-old rocks of sedimentary origin in a location which is exposed today in southwest Greenland. The imprints of life at 3.7 Ga come in two forms: 1) graphite globules formed out of sedimentary rock which included the remains of organisms with biologically depleted  $\delta^{13}\text{C}$  signatures, and 2) fossilized stromatolite-like structures that formed from photosynthetic organisms in microbial mats. At 3.43–3.48 Ga, more photosynthetic organisms left behind their fossilized imprint in the form of stromatolites. And at 3.4 Ga, the first spheroidal/ellipsoidal, and tubular single-celled organisms imprinted their shapes into the geological record. The rise in atmospheric oxygen due to oxygenic photosynthetic organisms did not begin to leave an imprint in the rock record until 2.95 Ga. This is when oxygenic photosynthesizers likely began to accumulate in shallow marine settings. Finally, at 2.4–2.3 Ga, the oxygen levels in the atmosphere rose in a

great oxidation event as the oxygenic photosynthesizers proliferated.

There is a large range for the outer boundary for the origin of life (4.5–3.9 Ga). Thus in order to analyze this time frame, we will explore two cases. (1) Asteroidal impacts on the Hadean Earth did not postpone or reset the origin of life. (2) Asteroidal impacts continuously postponed the emergence of life, or, specifically in the case of the LHB, reset the entire process. This removes the necessity to debate which scenario for asteroid bombardment occurred on the early Earth, and focuses instead on how asteroid impact frequency may affect the process of forming life.

In case 1, life emerged in the wide time frame of 4.5–3.7 Ga. The outer boundary in this case is based on the earliest estimate for the Moon-forming impact, around 4.516 Ga, followed by efficient radiative cooling to clement temperatures (taking  $\sim 0.02$ –16 Myr). Based on the consolidated evidence in this review, this case represents the widest, and therefore the most conservative time interval for the origin of life. In this case, it would have taken  $\sim 800$  million years to go from a habitable world to a population of organisms that can imprint their  $\delta^{13}\text{C}$  signature in rocks and form domical stromatolite-like structures. 800 million years is a short period, astronomically speaking, but a long period, evolutionarily speaking. In an RNA world setting [8], life emerged through the Darwinian evolution of chemically produced RNA molecules. If this process—beginning with prebiotic chemistry and ending at the LUCA—took 800 million years, perhaps life could be a rare occurrence. After all, 800 million years is 15 % of the time our planet has to be habitable (assuming our oceans boil away due to the greenhouse effect in 1 Gyr ([264])).

In case 2, life emerged in the shorter time interval of 3.9–3.7 Ga. This is the narrow time frame scenario, which assumes that either the LHB wiped clean any life or pre-life molecules that emerged before 3.9 Ga, or that asteroid impacts were too disruptive for life to emerge during a sustained, declining bombardment period from 4.5–3.9 Ga. If the evolutionary process forming life on a newly habitable planet took  $< 200$  million years, is there a better chance that life exists pervasively throughout the Universe? In truth we cannot make this conclusion, as the Earth is a sample size of  $n = 1$ . In other words, there is a selection bias in estimating the probability of life emerging elsewhere in the Universe.

But is the oldest evidence of life yet to be found? Have all sedimentary rocks older than 3.7 Ga been melted into magma? Have we reached our limit for using  $\delta^{13}\text{C}$  signatures and need to develop a different technique to find evidence for earlier life?

Because biosignatures are detected in the oldest preserved sedimentary rocks, we know that life existed prior to their formation time. And although the 3.8 Ga and 3.85 Ga rock samples from Isua Greenland are not of sedimentary origins, and therefore their low  $\delta^{13}\text{C}$  content could be explained by high-temperature, abiotic processes [234], do they still hint at the existence of life at this time? Perhaps an advancement in techniques will ultimately distinguish the low  $\delta^{13}\text{C}$  values in these samples from the known abiotic mechanisms. The farther we are able to confidently push the inner boundary towards earlier dates, the more encouraging the prospect for the emergence of life elsewhere in the Universe seems.

Based on the recent activity in the research fields of biogenic isotopes, stromatolites, and microfossils [103, 104, 132, 178, 191–193, 212, 213], it would seem that researchers are still actively looking for older evidences of life’s existence on Earth. If a high level of interest sustains in these fields, it would not be surprising to see the 3.7 Ga biosignature boundary being pushed to earlier dates in the next decade. However, it is also possible that in the same time, abiotic processes will be revealed to explain both the stromatolite morphologies and the low  $\delta^{13}\text{C}$  values in old rocks of sedimentary origin.

Whether the LHB occurred has not yet reached consensus. Researchers are still asking whether a single cataclysm occurred [167], and more evidence will be needed to sway the consensus in either direction. Planet formation theorists are actively improving models for the formation of our solar system [122, 265], which could eventually constrain the inwards and outwards migration of Jupiter to better understand the likelihood of a late lunar cataclysm being caused by such an event.

Finally, many researchers such as Rugheimer *et al.* [51], Mollière *et al.* [266], Hu & Seager [267], Kaltenegger *et al.* [268] are improving atmospheric models, which may someday be sophisticated enough to include  $\text{CO}_2$  subduction and degassing from meteorites. These models could better constrain the cooling time for the Earth’s magma mantle, and the likelihood of the Earth losing all of its atmosphere and freezing over.

As a final thought, we note that even the shorter 200-million-year time frame is very much longer than the life times of individual biomolecules. A key step for the origin of life is the creation of an autocatalytic, self-replicating chemical system. We envisage a ‘searching and waiting period’ in which chemical synthesis generates and explores a diversity of random, non-functional biopolymer sequences, until a rare

event occurs that establishes a stable small group of replicators. Our understanding of molecular evolution, the nature of the earliest replicators and the environment in which they existed is not good enough to make a first-principles prediction of how long a search period would have been required. The time interval between the habitability and biosignature boundaries, which we have been considering in this paper, tells us some information about how long the search period might have been, but it should be remembered that the time resolution of our biological and geochemical records is poor, and there remains the possibility that the search and wait period could have been much shorter than 200 million years. The initiation of life may be considered as a rare event on a biochemical and evolutionary timescale, and at the same time very rapid on the scale of planetary lifetimes. A key goal of the field of astrobiology and the origin of life is to estimate the average searching and waiting period on habitable planets, and hence to be able to give reliable estimates of the frequency of life on other worlds.

## **2.8 Acknowledgments**

We are grateful to two anonymous referees whose reports helped considerably to clarify the text. We are especially grateful to Allyson Brady, Greg Slater, and Radhey Gupta for their invaluable comments on the various topics in this review. We thank Steve Janzen - at McMaster Media Resources - for his superb work in rendering Figure 2.1. This work was supported by the NSERC discovery grants of P.G.H. and R.E.P. Finally, B.K.D.P was supported by a NSERC Canada graduate scholarship (CGS-M) and an Ontario graduate scholarship (OGS).

## **Author Disclosure Statement**

No competing financial interests exist.

## Chapter 3

# Origin of the RNA World: The Fate of Nucleobases in Warm Little Ponds

**Ben K. D. Pearce, Ralph E. Pudritz, Dmitry A. Semenov & Thomas K. Henning**

*N.B. This chapter was revised in accord with the favourable reviews of 2 referees and resubmitted to PNAS on July 28<sup>th</sup>, 2017. This chapter constitutes part II of this thesis.*

### Abstract

Prior to the origin of simple cellular life, the building blocks of RNA (nucleotides) had to form and polymerize in favourable environments on the early Earth. At this time, meteorites and interplanetary dust particles delivered organics such as nucleobases (the characteristic molecules of nucleotides) to warm little ponds whose wet-dry cycles promoted rapid polymerization. We build a comprehensive numerical model for the evolution of nucleobases in warm little ponds leading to the emergence of the first nucleotides and RNA. We couple Earth's early evolution with complex prebiotic chemistry in these environments. We find that RNA polymers must have emerged very quickly after the deposition of meteorites (< a few years). Their constituent

nucleobases were primarily meteoritic in origin and not from interplanetary dust particles. Ponds appeared as continents rose out of the early global ocean but this increasing availability of “targets” for meteorites was offset by declining meteorite bombardment rates. Moreover, the rapid losses of nucleobases to pond seepage during wet periods, and UV photodissociation during dry periods means that the synthesis of nucleotides and their polymerization into RNA occurred in just one to a few wet-dry cycles. Under these conditions, RNA polymers likely appeared prior to 4.17 billion years ago.

### 3.1 Introduction

One of the most fundamental questions in science is how life first emerged on the Earth. Given its ubiquity in living cells and its ability to both store genetic information and catalyze its own replication, RNA probably formed the basis of first life [7]. RNA molecules are made up of sequences of 4 different nucleotides, the latter of which can be formed through reaction of a nucleobase with a ribose and a reduced phosphorous (P) source [22, 26]. The evidence suggests that first life appeared earlier than 3.7 Gyr ago (Ga) [103, 104] and thus the RNA world would have developed on a violent early Earth undergoing meteoritic bombardment at a rate of  $\sim 1\text{--}1000 \times 10^{12}$  kg/yr [269], which is approximately 8–11 orders of magnitude greater than today [61]. At this time, the atmosphere was dominated by volcanic gases, and dry land was scarce as continents were rising out of the global ocean. What was the source of the building blocks of RNA? And what environments enabled nucleotides to polymerize and form the first functioning RNA molecules under such conditions? Although experiments have produced simple RNA strands in highly idealized laboratory conditions [60, 270], the answer to this question is largely unknown.

As to the sources of nucleobases, the early Earth’s atmosphere was likely dominated by  $\text{CO}_2$ ,  $\text{N}_2$ ,  $\text{SO}_2$ , and  $\text{H}_2\text{O}$  [34]. In such a weakly reducing atmosphere, Miller-Urey type reactions are not very efficient at producing organics [33]. One solution is that the nucleobases were delivered by interplanetary dust particles (IDPs) and meteorites. Intact carbon influxes of  $\sim 6 \times 10^7$  kg yr<sup>-1</sup>, and  $\sim 2 \times 10^3$  kg yr<sup>-1</sup>, respectively are estimated for these early times [33]. Although nucleobases have not been identified in IDPs yet, three of the five nucleobases (uracil, cytosine, and thymine) have been formed on the surfaces of icy IDP analogues in the lab through exposure to UV

radiation [76]. Nucleobases are found in meteorites (guanine, adenine, and uracil) with concentrations of 0.25–515 parts-per-billion (ppb) [36, 70]. The ultimate source of nitrogen within them could be molecules such as ammonia and HCN that are observed in the disks of gas and dust around all young stars [42, 78, 83]. A second possible source of nucleobases is synthesis in hydrothermal vents that well up from spreading cracks on the young Earth’s ocean floors [44]. A potential problem here is the lack of concentrated and reactive nitrogen sources in these environments [44].

A central question concerning the emergence of the RNA world is how the polymerization of nucleotides occurred. Warm little ponds (WLPs) are excellent candidate environments for this process because their wet and dry cycles have been shown to promote the polymerization of nucleotides into chains possibly greater than 300 links [60]. Furthermore, clay minerals in the walls and bases of WLPs promote the linking of chains up to 55 nucleotides long [275]. Conversely, experiments simulating the conditions of hydrothermal vents have only succeeded in producing RNA chains a few monomers long [89]. A critical problem for polymerizing long RNA chains near hydrothermal vents is the absence of wet-dry cycles.

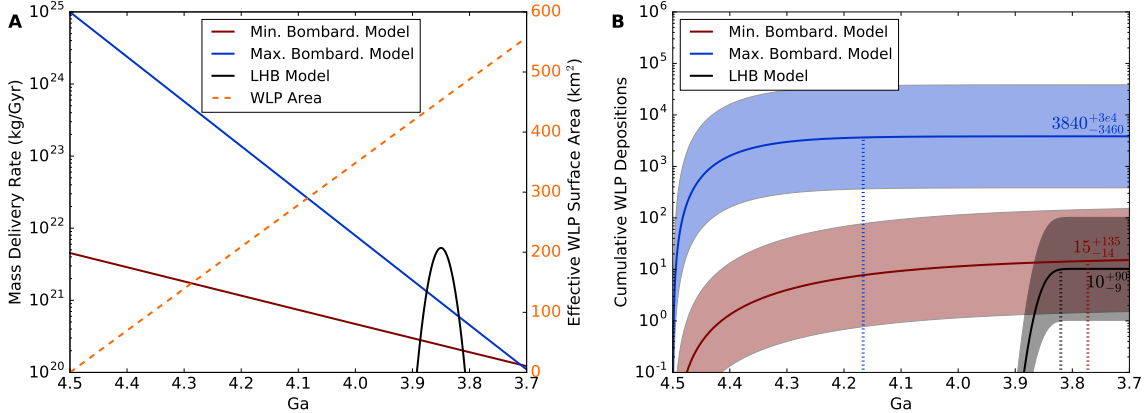


Figure 3.1: **History of carbonaceous meteorite deposition in warm little ponds:** (A) History of mass delivery rate to the early Earth and of effective warm little pond (WLP) surface area. Three models for mass delivered to the early Earth are compared: a Late Heavy Bombardment model, and a minimum and maximum bombardment model. All mass delivery models are based on analyses of the lunar cratering record [269, 271]. The effective WLP surface area during the Hadean eon is based on a continental crust growth model [272], the number of lakes and ponds per unit crustal area [273], and the lake and pond size distribution [273]. (B) Cumulative WLP depositions for the small fragments of carbonaceous meteoroids of diameter 40–80 m landing in any 1–10 m-radius WLP on the early Earth. A deposition is characterized as a meteoroid debris field that overlaps with a WLP. We assume the ponds per area during the Hadean eon is the same as today, and that all continental crust remains above sea-level, however we vary the ponds per area by  $\pm 1$  order of magnitude to obtain error bars. 95% of WLP depositions in each model occur before the corresponding dotted vertical line. 40–80 m is the optimal range of carbonaceous meteoroid diameters to reach terminal velocity, while still landing a substantial fraction of mass within a WLP area. 1–10 m is the optimal range of WLP radii to avoid complete evaporation within a few months, while also allowing non-negligible nucleobase concentrations to be reached upon meteorite deposition. The numbers of carbonaceous meteoroid impactors in the 20–40 m-radius range are based on the mass delivery rate, the main-belt size-frequency distribution, and the fraction of impactors that are of type CM, CR or CI [269, 271, 274] (see SI Text).

## 3.2 Model: Fates of Nucleobases in Evolving WLPs

We compute a well posed model for the evolution of WLPs, the fates of nucleobases delivered to them, and the emergence of RNA polymers under early Earth conditions. The sources of nucleobases in our model are carbonaceous meteorites and IDPs whose delivery rates are estimated using the lunar cratering record [33, 269, 271], the distribution of asteroid masses [271], and the fraction of meteorites reaching terminal velocity that are known to be nucleobase carriers [36, 274]. The WLPs are “targets” in which molecular evolution of nucleobases into nucleotides and subsequent polymerization into RNA occurs. The evolution of ponds due to precipitation, evaporation, and seepage constitute the immediate environments in which the delivered nucleobases must survive and polymerize<sup>1</sup>. The data for these sources and sinks are gathered from historical precipitation records [57], or are measured experimentally [53, 54]. Sinks for these molecules include destruction by unattenuated UV rays (as the early Earth had no ozone), hydrolysis in the pond water, as well as seepage from the bases of ponds. The data for these sinks are measured experimentally [54, 90, 91]. The nucleobases that survive go on to form nucleotides that ultimately polymerize.

To calculate the number of carbonaceous meteorite source depositions in target WLPs on the early Earth, we combine a continental crustal growth model [272], the lake and pond size distribution and ponds per unit crustal area estimated for ponds on Earth today [273], the asteroid belt mass distribution [271] and three possible mass delivery models based on the lunar cratering record [269, 271]. This results in a first order linear differential equation (Equation 3.18), which we solve analytically. The details are in the SI Text, and the main results are discussed in the following section.

Nucleobase abundances in WLPs from IDPs and meteorites are described in our model by first order linear differential equations (Equations 3.34 and 3.38, respectively). The equations are solved numerically (see SI Text for details).

Our fiducial model WLPs are cylindrical (because sedimentation flattens their initial bases) and have a 1 m radius and depth. We find these ponds to be optimal because they are large enough to not dry up too quickly but small enough that high

---

<sup>1</sup>We don’t emphasize groundwater-fed ponds (hot springs) because their small number on Earth today ( $\sim$ thousands) compared to regular lakes/ponds ( $\sim$ 304 million [273]) suggests they didn’t contribute greatly to the combined WLP target area for meteorite deposition.

nucleobase concentrations can be achieved (see SI Text).

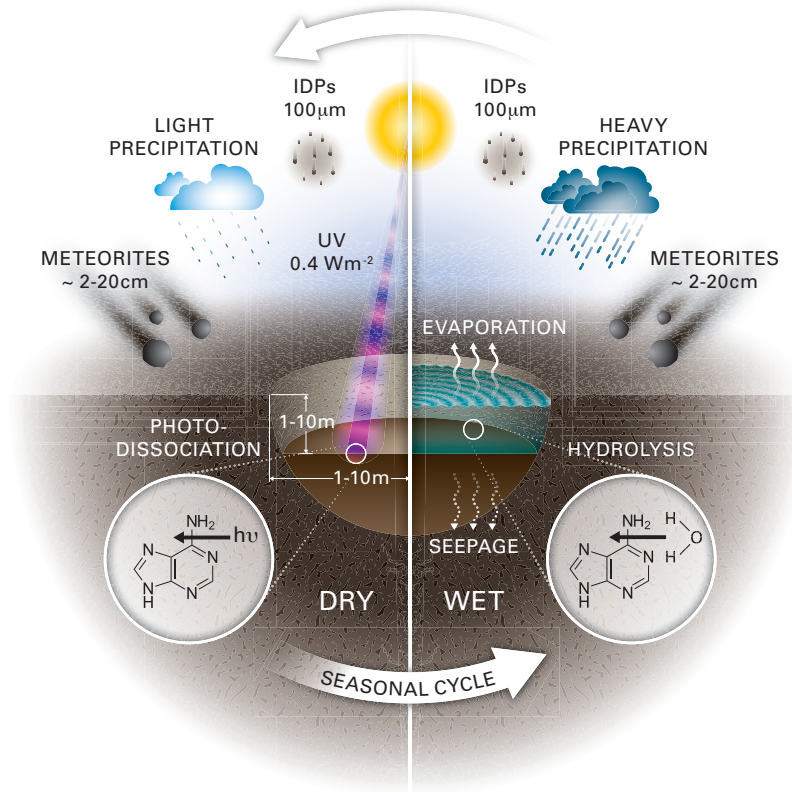


Figure 3.2: An illustration of the sources and sinks of pond water and nucleobases in our model of isolated warm little ponds on the early Earth. The only water source is precipitation. Water sinks include evaporation and seepage. Nucleobase sources include carbonaceous IDPs and meteorites, which carry up to  $\sim 1$  picogram and  $\sim 3$  mg of each nucleobase, respectively. Nucleobase sinks include hydrolysis, UV photodissociation, and seepage. Nucleobase hydrolysis and seepage are only activated when the pond is wet, and UV photodissociation is only activated when the pond is dry.

### 3.3 Meteorite Sources and Targets

In Figure 3.1A, we show the history of meteoritic mass delivery rates on the early Earth, and of WLP targets. From total meteoritic mass, we extract just the nucleobase sources, i.e. only carbonaceous meteoroids whose fragments slow to terminal velocity in the early atmosphere. In Figure 3.1B we show the history of depositions of such nucleobase sources into 1–10 m radius WLP targets from 4.5–3.7 Ga.

The lunar cratering record shows either a continuously decreasing rate of impacts from 4.5 Ga forwards, or a brief outburst beginning at  $\sim 3.9$  Ga known as the Late Heavy Bombardment (LHB). Due to the lack of lunar impact melts with ages prior to  $\sim 3.92$  Ga, the rate of mass delivered to the early Earth preceding this date is uncertain [114]. Therefore we compare three models for mass delivery to the early Earth based on analytical fits to the lunar cratering record [269, 271]: a LHB, a minimum and a maximum bombardment model. The latter two models represent lower and upper limit fits for a sustained declining bombardment, and are subject to considerable uncertainty [276]. The total target area of WLPs increases as the rising continents provide greater surface area for pond sites. An ocean world, in this view, is an implausible environment for the emergence of an RNA world. Iron and rocky bodies impact the solid surface at speeds high enough to form small craters [66]; contributing to the WLP population.

Our calculations show that 10–3840 terminal velocity carbon-rich meteoroids would have deposited their fragments into WLPs on the Earth during the Hadean eon. Given the large uncertainty of the ponds per unit area and the growth rate of continental crust, we vary the WLP growth function by  $\pm 1$  order of magnitude. From this we get a minimum of 1–384 depositions and a maximum of 100–38,400 WLP depositions from 4.5–3.7 Ga. The optimal model for WLP depositions—the maximum bombardment model—suggests the majority of depositions occurred prior to 4.17 Ga. The less optimal models for WLP depositions, the LHB and minimum bombardment models, suggest the majority of depositions occurred before 3.82 Ga and 3.77 Ga, respectively.

### 3.4 Life Cycles of WLPs

Figure 3.2 illustrates the variation of physical conditions for WLPs during the Hadean eon, approximately 4.5–3.7 Ga. Annual rainfall varies sinusoidally [57], creating seasonal wet and dry environments. The increased heat flow from greater abundances of radiogenic sources at this time [55] causes temperatures of around 50–80 °C [56]. The various factors that control the water level and thus the wet-dry cycles of WLPs are precipitation, evaporation, and seepage (through pores in the ground).

In Figure 3.3A, we present the results of these calculations. We select two different temperatures (65°C, and 20°C) as analogues for hot and warm early Earths. For each of these, we examine three different environments: dry, intermediate, and wet (see Table 3.1 for details). The water levels in the wet environment WLPs range from

approximately 60–100% full. WLPs experiencing dry states of approximately half (intermediate environment) and three-quarters of a year (dry environment) only fill up to 20% and 10%, respectively. These results clearly establish the existence of seasonal wet-dry cycles.

### 3.5 Nucleobase Evolution in WLPs

As shown in Figure 3.2, the build up of nucleobases in WLPs is offset by losses due to hydrolysis [90], seepage [54], and dissociation by UV radiation that was incident on the early Earth in the absence of ozone [51, 91]. Some protection would be afforded during WLP wet phases, as a 1 m column of pond water can absorb UV radiation up to  $\sim 95\%$  [277]. It is of particular interest that sediment, which collects at the base of WLPs, also attenuates UV radiation. Studies show it only takes a  $\sim 0.6$  mm layer of basaltic sediment to attenuate UV radiation by  $>99.99\%$  [278].

Nucleotide formation and stability are sensitive to temperature. Phosphorylation of nucleosides in the lab is slower at low temperatures, taking a few weeks at  $65^\circ\text{C}$  compared to a couple hours at  $100^\circ\text{C}$  [279]. The stability of nucleotides on the other hand, is favoured in warm conditions over high temperatures [280]. If a WLP is too hot ( $>80^\circ\text{C}$ ), any newly formed nucleotides within it will hydrolyze in several days to a few years [280]. At temperatures of  $5\text{--}35^\circ\text{C}$  that either characterize more temperate latitudes or a post-snowball Earth, nucleotides can survive for thousand-to-million-year timescales. However at such temperatures, nucleotide formation would be very slow. Considering this temperature sensitivity, we model the evolution of nucleobases in WLPs in matching warm ( $5\text{--}35^\circ\text{C}$ ) and hot ( $50\text{--}80^\circ\text{C}$ ) early Earth environments. Hotter ponds evaporate quicker, therefore we choose rainier analogue sites on a hot early Earth to maintain identical pond environments to our warm early Earth sites.

In Figure 3.3B, we focus on the adenine concentrations in WLPs from only IDP sources. The combination of spikes, flat tops, and troughs in Figure 3.3B reflects the variations of adenine concentration in response to drying, balance of input and destruction rates, and precipitation during wet periods. In any environment and at any modeled temperature, the maximum adenine concentration from only IDP sources remains below  $2 \times 10^{-7}$  ppb (see Figure 3.10). This is two orders of magnitude below current detection limits [70], making subsequent reactions negligible. The nucleobase mass fraction curves are practically independent of pond size ( $1\text{m} < r_p \leq 10\text{m}$ ) once

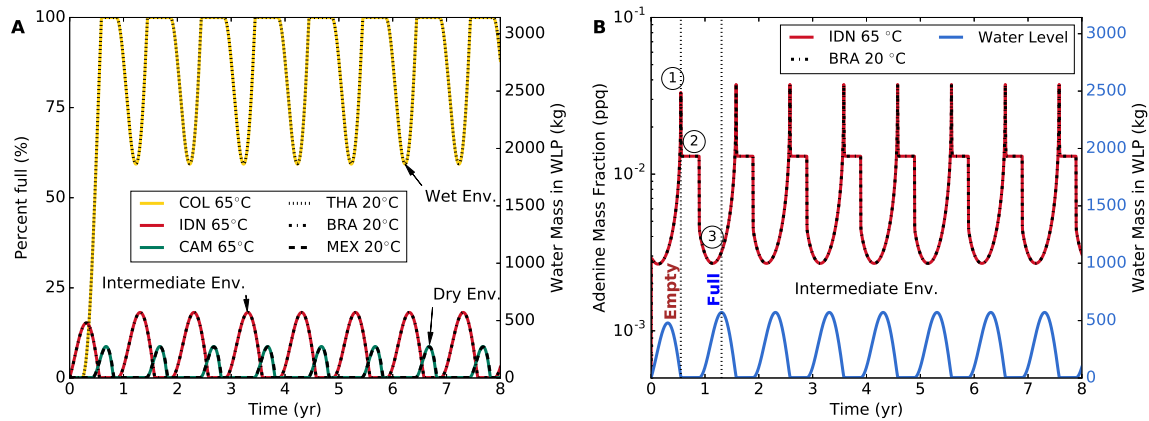


Figure 3.3: **Histories of pond water and adenine concentration from interplanetary dust particles:** (A) The change in water level over time in our fiducial dry, intermediate, and wet environment WLPs due to evaporation, seepage, and precipitation. Precipitation rates from a variety of locations on Earth today are used in the models, and represent 2 classes of matching early Earth analogues: hot (Columbia, Indonesia, Cameroon), and warm (Thailand, Brazil, and Mexico) (for details see Table 3.1). All models begin with an empty pond, and stabilize within 2 years. (B) The red and black-dotted curves represent the adenine concentrations over time from carbonaceous interplanetary dust particles (IDPs) in our fiducial WLPs. The degenerate intermediate WLP environment used in this calculation is for a hot early Earth at 65 °C and a warm early Earth at 20 °C. The blue curve represents the corresponding water level in the WLP, with initial empty and full states labeled in brown and blue text. Three features are present: 1) The maximum adenine concentration at the onset of the dry phase. 2) A flat-top equilibrium between incoming adenine from IDPs and adenine destruction by UV irradiation. 3) The minimum adenine concentration just before the pond water reaches its highest level.

Table 3.1: Precipitation models matching dry, intermediate, and wet environments on a warm (5–35°C) and hot (50–80°C) early Earth. Precipitation data from a variety of locations on Earth today [57, 281] represent 2 classes of matching early Earth analogues: warm (Thailand, Brazil, and Mexico) and hot (Columbia, Indonesia, Cameroon). For example, the conditions in Mexico on a warm early Earth match the conditions in Cameroon on a hot early Earth.  $\bar{P}$  is the mean precipitation rate,  $\delta_p$  is the seasonal precipitation amplitude, and  $s_p$  is the phase shift.

Model	Environment	Analogue Site	$\bar{P}$ (m yr <sup>-1</sup> )	$\delta_p$	$s_p$ (yr)
Warm early Earth (5–35°C)	Dry	Mexico (MEX)	0.94	1.69	0.3
	Intermediate	Brazil (BRA)	1.8	0.50	0.85
	Wet	Thailand (THA)	3.32	0.91	0.3
Hot early Earth (50–80°C)	Dry	Cameroon (CAM)	3.5	0.5	0.3
	Intermediate	Indonesia (IDN)	4.5	0.2	0.85
	Wet	Columbia (COL)	6.0	0.5	0.3

To obtain the rate of the decrease in pond water for a given analogue site, table values are input into this equation:

$$\frac{dL}{dt} = 0.83 + 0.06T - \bar{P} \left[ 1 + \delta_p \sin \left( \frac{2\pi(t-s_p)}{\tau_s} \right) \right] \text{ (see SI Text).}$$

a stable, seasonal pattern is reached (< 35 years). This is because although larger ponds have a larger collecting area for IDPs, they have an equivalent larger area for collecting precipitation and seeping nucleobases.

### 3.6 Dominant Source of Surviving Nucleobases

In Figure 3.4 we assemble all of these results and compare carbonaceous IDPs to meteorites as sources of adenine to our fiducial WLPs. Small meteorite fragments (1 cm in radius) are compared with IDPs in panel A. The effects of larger meteorite fragments (5 cm and 10 cm) on adenine concentration are displayed in panel B.

The maximum adenine concentration in our model WLPs from carbonaceous meteorites is 10 orders of magnitude higher than the maximum adenine concentration from carbonaceous IDPs. The reason for this huge disparity is simply that carbonaceous meteoroid fragments—each carrying up to a few mg of adenine—are deposited into a WLP in a *single event*. This allows adenine to reach ppb–ppm-level concentrations before seepage and UV photodissociation efficiently remove it from the WLP in one to a few wet-dry cycles. The maximum guanine and uracil accumulated in our

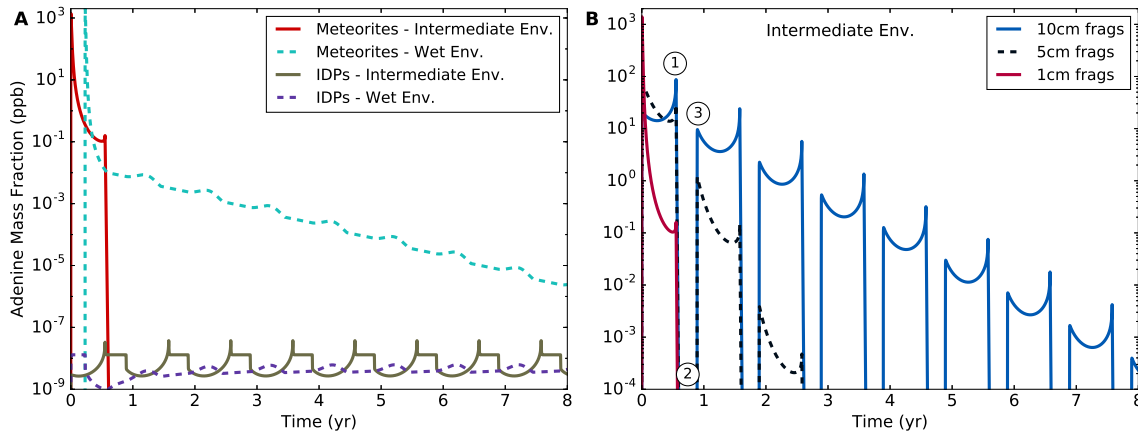


Figure 3.4: **Comparative histories of adenine concentrations from interplanetary dust particles and meteorites:** (A) A comparison of the accumulation of adenine from carbonaceous IDPs and meteorites in our fiducial WLPs. The meteorite fragments are small (1 cm), and originate from a 40 m-radius carbonaceous meteoroid. Adenine concentrations for intermediate (wet-dry cycle) and wet environments (never dry) are compared and correspond to both a hot early Earth at 65 °C and a warm early Earth at 20 °C (for details see Table 3.1). (B) The effect of meteorite fragment sizes on adenine concentration. The degenerate intermediate WLP environment used in these calculations is for a hot early Earth at 65 °C and a warm early Earth at 20 °C. The fragments are either only small in size (1 cm in radius), only medium in size (5 cm in radius), or only large in size (10 cm in radius). Three features are present: 1) Adenine is at its highest concentration at the onset of the pond’s dry phase. 2) Upon drying, adenine ceases to outflow from large fragments, and UV radiation rapidly destroys all previously released adenine. 3) Re-wetting allows the remaining adenine within large fragment pores to continue to outflow. The U-shape is due to the increase and decrease in water level.

model WLPs from meteorites are also more than 10 orders of magnitude higher than those accumulated from IDPs. A maximum adenine concentration of 2 ppm is still  $\sim 1$ – $2$  orders of magnitude lower than the initial adenine concentrations in aqueous experiments forming adenosine and AMP [22], however these experiments only ran for an hour.

Adenine within larger fragments diffuses over several wet-dry cycles, and during the dry phase no outflow occurs. For fragments 1, 5, and 10 cm in radius, 99% of the adenine is released into the pond water within  $\sim 10$  days, 8 months, and 32 months, respectively. Only the adenine that has already flowed out of the fragments gets rapidly photodestroyed, therefore, adenine within larger fragments can survive up to  $\sim 7$  years.

Thus, even though the carbon delivery rates from IDPs to the early Earth vastly exceed those from meteorites, it is the meteoritic material that is the dominant source of nucleobases for RNA synthesis.

### 3.7 Nucleotide and RNA Synthesis

To form nucleotides in WLPs, ribose and a reduced P source must be available. Ribose may have formed and stabilized in borate-rich WLPs via the formose reaction (polymerization of  $\text{H}_2\text{CO}$ ) [282]. Additionally, phosphite has been detected in a pristine geothermal pool representative of early earth, suggesting the potential availability of reduced P to WLP environments [283]. Only the AMP nucleotide has been experimentally synthesized in a single step involving ribose, reduced P and UV radiation [22].

Because of the rapid rate of seepage ( $\sim 1.0$ – $5.1$  mm day $^{-1}$  [54]), nucleotide synthesis would need to be fast, occurring within a half-year to a few years after nucleobase deposition, depending on meteoroid fragment sizes. This is ample time given that lab experiments show hour-to-week-long timescales are sufficient to form adenosine and AMP [22, 26].

Nucleotides, once synthesized using meteorite-delivered nucleobases, are still subject to seepage, regardless of the temperature. Therefore nucleotide polymerization into RNA would also need to be fast, occurring within one to a few wet-dry cycles, in order to reduce their likelihood of seeping through the estimated 0.001–400  $\mu\text{m}$ -sized pores at the WLP base [92]. Experiments show that nucleotides can polymerize into RNA chains possibly greater than 300 monomers by subjecting them to just 1–16 wet-dry

cycles [60].

### 3.8 Discussion and Conclusions

Seepage is one of the dominant nucleobase sinks in WLPs. It will be drastically reduced if nucleobases are encapsulated by vesicles (spheres of size 0.5-5  $\mu\text{m}$  that form spontaneously upon hydration, whose walls consist of lipid bilayers derived from fatty acids within meteorites) [284]. However, even if seepage is turned off, maximum adenine concentrations from IDPs are still negligible ( $\lesssim 150$  ppq) (see Figure 3.12).

Also, we note that a cold early Earth (if it occurred [114]) with seasonal or impact-induced freeze-thaw cycles could also be suitable for RNA polymerization and evolution for reasons similar to those we have analyzed for WLPs. The cyclic thawing and freezing resembles wet-dry cycles [60].

We conclude that the physical and chemical conditions of WLPs place strong constraints on the emergence of an RNA world. A hot early Earth (50–80°C) favours rapid nucleotide synthesis in WLPs [279]. Meteorite-delivered nucleobases could react with ribose and a reduced P source to quickly ( $<$  a few years) create nucleotides for polymerization. Polymerization then occurs in one to a few wet-dry cycles to reduce the likelihood that these molecules are lost to seepage. This rapid process also reduces the likelihood of setbacks for the emergence of the RNA world due to frequent large impacts, a.k.a. impact frustration [285]. Sedimentation would be of critical importance as UV protection for nucleobases, nucleotides, and RNA [91, 286, 287].

The mass-delivery model providing the most WLP depositions indicates that the majority of meteorite depositions occurred prior to 4.17 Ga. The first RNA polymers would have formed in WLPs around that time, prefiguring the emergence of the RNA world. This implies that the RNA world could have appeared within  $\sim 200$ –300 million years after the Earth became habitable.

### 3.9 Acknowledgments

This research is part of a collaboration between the Origins Institute and the Heidelberg Initiative for the Origins of Life. We thank the referees for their thoughtful insights. We thank M. Rheinstädter for providing valuable comments on the manuscript. BKDP thanks MPIA for their hospitality during his summer abroad, supported by an NSERC

Michael Smith Foreign Study Supplement. REP thanks MPIA and ITA for their support during his sabbatical leave. The research of BKDP was supported by an NSERC Canada Graduate Scholarship and Ontario Graduate Scholarship. REP is supported by an NSERC Discovery Grant.

## 3.10 Supporting Information (SI)

### 3.10.1 Calculating WLP Surface Area on the Early Earth

The earliest fairly conclusive evidences of life are in the form of light carbon signatures in graphite globules formed from marine sediments, and stromatolite fossils, both which are dated to be 3.7 Gyr old [103, 104]. Therefore nucleobase deposition in WLPs and subsequent reactions to form nucleotides and RNA, would have occurred sometime between  $\sim 4.5$ –3.7 Ga.

Once Theia impacted the proto-Earth  $\sim 50$  Myr after Solar System formation, it may have only taken 10–100 Myr for the magma mantle to cool [114]. Furthermore, basic evidence (from the zircon oxygen isotope record) exists of crustal material interacting with liquid water at or near the Earth’s surface since 4.3 Ga [288]. Such evidence makes it clear that the Earth had a hydrosphere at that point, and therefore could have formed WLPs on any rising continental crust.

An estimate of the surface area of WLPs on the early Earth has not been previously attempted, however it is often suggested that they were typical on early Earth continents [55, 284, 288]. Water-deposited sediments dated at 3.8 Ga indicate early erosion and transport of sediment, therefore at least some continental mass must have been exposed above sea level at that time, on which WLPs could have formed [55].

#### 3.10.1.1 Continental Crust Growth Model

The number of WLPs present at any given time depends on the fraction of continental crust above sea level. Calculations from a continental crust growth model shows a linear formation of early crust, increasing from 0 to 12.8% of today’s crustal surface area from 4.5–3.7 Ga [272]. This is expressed in the equation below.

$$f_{cr} = 0.16t \tag{3.1}$$

where  $f_{cr}$  is the fraction of today's crustal surface area, and  $t$  is the time in Gyr ( $t = 0$  starts at 4.5 Ga).

We assume the number of bodies of water per unit area of continental crust is constant over time, thus by multiplying Equation 3.1 by the number of lakes and ponds on Earth today, we get the number of bodies of water on Earth at any date from 4.5–3.7 Ga. The number of lakes and ponds on Earth today (down to 0.001 km<sup>2</sup>) is estimated to be 304 million [273], therefore the equation becomes:

$$N_t = 4.864 \times 10^7 t \quad (3.2)$$

where  $N_t$  is the total number of bodies of water on Earth for times  $0 \text{ Gyr} \leq t \leq 0.8 \text{ Gyr}$  ( $t = 0$  starts at 4.5 Ga).

### 3.10.1.2 Lake and Pond Size Distribution

The size distribution of lakes and ponds on Earth today follows a Pareto distribution function [273].

$$dN_A = N_t c k^c A^{-(c+1)} dA, \quad (3.3)$$

where  $dN_A$  is the number of bodies of water in the km<sup>2</sup> area range  $A$  to  $A + dA$ ,  $N_t$  is the total number of bodies of water on Earth,  $c$  is the dimensionless shape parameter, and  $k$  is the smallest lake/pond area in the distribution. The shape parameter was calculated for lakes and ponds down to 0.001 km<sup>2</sup> to be  $c = 1.06$  [273].

The total area of ponds on Earth in a given size range can then be calculated by multiplying Equation 3.3 by  $A$  and integrating from  $A_{min}$  to  $A_{max}$ , which gives

$$A_{tot} = \frac{c}{-c+1} N_t k^c \left[ A_{max}^{(-c+1)} - A_{min}^{(-c+1)} \right] \quad [\text{km}^2]. \quad (3.4)$$

There is an upper size limit on WLPs in which substantial concentrations of nucleobases from meteorites can be deposited. If the surface area of a WLP is comparable to the area of a meteoroid's strewnfield, then partial overlapping of the strewnfield and WLP is probable. This would lead to fewer fragment depositions per unit pond area, and lower nucleobase concentrations. For this reason, we choose the upper limit on WLP radii to be 10 m. This equates to pond areas that are <0.04 % of the strewnfield area of typical carbonaceous meteoroids (the latter of which are  $\sim 0.785$

km<sup>2</sup>).

There is also a lower size limit as ponds that evaporate too quickly spend the majority of their time in the dry state. This would prevent nucleobase outflow from the pores of meteorites. Moreover, the probability of meteorite deposition in WLPs decreases for decreasing pond radii. A cylindrical WLP at 65 °C with a radius and depth of < 1 metre will likely evaporate in less than 3 months without replenishment from rain or geysers [53]. Therefore we set the lower WLP radius and depth limit for our interests at 1 m.

### 3.10.1.3 Total WLP Surface Area

From Equations 3.2 and 3.4, the total surface area of cylindrical, 1–10 m-radii WLPs on the early Earth at time  $0 \text{ Gyr} \leq t \leq 0.8 \text{ Gyr}$  is

$$A_{tot}(t) = 651t \text{ [km}^2\text{]}. \quad (3.5)$$

For this calculation, we choose  $c = 1.06$  and  $k = 3.14 \times 10^{-6} \text{ km}^2$ . Note  $t = 0$  starts at 4.5 Ga.

## 3.10.2 Calculating Carbonaceous Meteorite Depositions in WLPs

Aerodynamic forces fragment meteoroids that enter the atmosphere, which increases their total meteoroid cross-section, and thus their aerodynamic braking [66]. Numerical simulations show that the fragments of carbonaceous meteoroids with initial diameters up to 80 metres and atmospheric entry velocities near the median value (15 km/s [276]) reach terminal velocity [66]. These fragments do not produce craters upon impact [67] and can be intactly deposited into WLPs. Larger meteoroids produce fragments with impact speeds too fast to avoid cratering and partial or complete melting or vapourization of the impactor. The same numerical simulations calculate the largest fragments from a 80-metre-diameter carbonaceous meteoroid of initial velocity 15 km/s to be  $\sim 20$  cm in diameter [66]. (This roughly makes sense as the biggest carbonaceous meteorite recovered, the Allende, is only 110 kg—corresponding to a  $\sim 40$  cm-diameter sphere [289]).

The optimal diameter range for carbonaceous meteoroids to deposit a substantial

fraction of mass into WLPs at terminal velocity is therefore 40–80 m. We base our calculation of carbonaceous meteoroid fragment depositions on this range.

### 3.10.2.1 Mass Delivery Models

The lunar cratering record analyzed by the Apollo program has revealed a period of intense lunar bombardment from  $\sim 3.9$ – $3.8$  Ga [290]. Whether a single lunar cataclysm (lasting  $\sim 10$ – $150$  Myr) or a sustained declining bombardment preceded 3.9 Ga is still debated [114]. We choose three models for the rate of mass delivered to the early Earth: a LHB model, and a minimum and maximum bombardment model. All models are based on analyses of the lunar cratering record [269, 271].

Analyses from both dynamic modeling and the lunar cratering record estimate the total mass delivered to the early Earth during the LHB to be  $\sim 2 \times 10^{20}$  kg [271]. We assume a Gaussian curve for the rate of impacts during the LHB [114], which centers on 3.85 Ga, integrates to  $2 \times 10^{20}$  kg, and drops to nearly zero at 3.9 and 3.8 Ga. Thus,

$$dm_{LHB}(t) = 5.33 \times 10^{21} e^{-\frac{(t-0.65)^2}{2(0.015)^2}} dt \quad [\text{kg}], \quad (3.6)$$

where  $dm_{LHB}$  is the total mass from  $t$  to  $t + dt$  (Gyr) ( $t = 0$  starts at 4.5 Ga).

Equations for the minimum and maximum mass delivered to the early Earth, given a sustained declining bombardment preceded 3.9 Ga, are displayed below [269].

$$m_{minB}(t) = 1 \times 10^{21} - 0.76 \left[ 4.5 - t + 4.57 \times 10^{-7} \left( e^{(4.5-t)/\tau_a} - 1 \right) \right] m_2^{1-b} 4\pi R_{moon}^2 \Sigma \quad [\text{kg}]. \quad (3.7)$$

$$m_{maxB}(t) = 7 \times 10^{23} - 0.4 \left[ 4.5 - t + 5.6 \times 10^{-23} \left( e^{(4.5-t)/\tau_c} - 1 \right) \right] m_2^{1-b} 4\pi R_{moon}^2 \Sigma \quad [\text{kg}]. \quad (3.8)$$

where  $m_{minB}$  and  $m_{maxB}$  are the total mass delivered from  $t = 0$  to  $t = t$  ( $t = 0$  starts at 4.5 Ga),  $\tau_a$  and  $\tau_b$  are decay constants ( $\tau_a = 0.22$  Gyr,  $\tau_b = 0.07$  Gyr),  $m_2$  is the maximum impactor mass ( $m_2 = 1.5 \times 10^{18}$  kg),  $b = 0.47$ ,  $R_{moon}$  is the mean radius of the moon ( $R_{moon} = 1737.1$  km), and  $\Sigma$  is the ratio of the gravitational cross sections of the Earth and Moon ( $\Sigma \sim 23$ ).

Taking the derivatives of Equations 3.7 and 3.8 gives us the corresponding rates of mass delivered to the early Earth.

$$dm_{minB}(t) = 0.76 \left( 1 + \frac{4.57 \times 10^{-7}}{\tau_a} e^{(4.5-t)/\tau_a} \right) m_2^{1-b} 4\pi R_{moon}^2 \Sigma dt \quad [\text{kg}]. \quad (3.9)$$

$$dm_{maxB}(t) = 0.4 \left( 1 + \frac{5.6 \times 10^{-23}}{\tau_c} e^{(4.5-t)/\tau_c} \right) m_2^{1-b} 4\pi R_{moon}^2 \Sigma dt \quad [\text{kg}]. \quad (3.10)$$

See Figure 3.1 in the main text for a plot of the three mass delivery models.

### 3.10.2.2 Impactor Mass Distribution

Chemical analyses of lunar impact samples, and crater size distributions suggest that the impactors of the Earth and Moon before  $\sim 3.85$  Ga were dominated by main-belt asteroids [290]. It is also likely that the size-frequency distribution of impactors on the early Earth is similar to that of the main-belt asteroids today [291]. Though there is no conclusive evidence to constrain the fraction of early Earth impactors that were of cometary origin, some suggest approximately 10% of the total accreted mass was from comets [269].

The early-Earth impactor mass distribution for impactors with radii 20–40 m, adjusted for the total mass delivered during the LHB, follows the linear relation

$$dm_{LHB}(r) = [7.5 \times 10^{13}r + 3 \times 10^{15}] dr \quad [\text{kg}], \quad (3.11)$$

where  $dm$  is the mass of impactors with radii  $r$  to  $r + dr$  (m) [271].

To get the impactor mass distributions for the mass delivered between  $t$  and  $t + dt$  in each of our three models, we multiply Equation 3.11 by Equation 3.6, 3.9, or 3.10, and divide by  $2 \times 10^{20}$  kg.

$$dm_i(t, r) = [7.5 \times 10^{13}r + 3 \times 10^{15}] \frac{dm_i(t)}{2 \times 10^{20}} dr \quad [\text{kg}], \quad (3.12)$$

where  $i$  is the model (LHB, minB, or maxB).

### 3.10.2.3 Impactor Number Distribution

Equation 3.12 can be turned into a number distribution (from  $t$  to  $t + dt$ ) for asteroids of a specific size and type (e.g. carbonaceous chondrites, ordinary chondrites, irons) by multiplying by the fraction of impactors that are asteroids ( $f_a$ ) and the fraction of asteroid impacts that are of a specific meteorite parent body-type ( $f_t$ ), and then dividing by the volume and average density of such asteroids. After simplification, this is

$$dN_i(t, r) = \frac{3f_a f_t}{4\pi\rho} \left[ \frac{7.5 \times 10^{13}}{r^2} + \frac{3 \times 10^{15}}{r^3} \right] \frac{dm_i(t)}{2 \times 10^{20}} dr, \quad (3.13)$$

where  $i$  is the model (LHB, minB, or maxB).

### 3.10.2.4 Total Number of Carbonaceous Impactors

Although some carbonaceous chondrites may have originated from comets [292], for this calculation we conservatively assume that all carbonaceous meteorites originated from asteroids.

Integrating Equation 3.13 from  $r_{min}$  to  $r_{max}$  gives the total number of meteoroids in that radii range to have impacted the early Earth, from  $t$  to  $t + dt$ , for each model.

$$dN_i(t) = \frac{3f_a f_t}{4\pi\rho} \left[ 7.5 \times 10^{13} \left( \frac{1}{r_{min}} - \frac{1}{r_{max}} \right) + \frac{3 \times 10^{15}}{2} \left( \frac{1}{r_{min}^2} - \frac{1}{r_{max}^2} \right) \right] \frac{dm_i(t)}{2 \times 10^{20}}, \quad (3.14)$$

where  $i$  is the model (LHB, minB, or maxB).

### 3.10.2.5 Probability of WLP Deposition

The probability of an infinitesimally small object hitting within a target area, given the probability of hitting anywhere within the total area is equal, is the geometric probability,

$$P_g = \frac{A_{targ}}{A_{tot}}. \quad (3.15)$$

This equation can be used to estimate the probability of blindly hitting the bull's eye on a dart board from relatively close in, where  $A_{targ}$  is the area of the bull's eye and  $A_{tot}$  is the area of the dart board. In this case, since the tip of a dart is relatively small with respect to the bull's eye, the approximation is relatively accurate. In the case of estimating the probability of meteoroid fragments falling into a WLP, the tip of the "dart" (i.e. the debris area of meteoroid fragments) is not always going to be larger than the "bull's eye" (i.e. the total surface area of WLPs at any time). For example, the probability of fragments from a single meteoroid falling into a WLP at  $\sim 4.5$ - $4.45$  Ga, when there was a small fraction of continental crust and few WLPs, is more analogous to the probability of blindly hitting the bull's eye with a small ball; which would be slightly more likely than with a dart. Any large enough part of the ball overlapping with the bull's eye counts as a hit, as does any large enough part of

the debris field overlapping with the combined WLP surface area. “Large enough” in our case corresponds to the area of the largest WLP for which the meteoroid fragment deposition probability is being calculated (or equivalently 100 of the smallest WLP in our study). (This minimum area is necessary in order to assume a homogeneous surface deposition when calculating the total mass of meteoroid fragments to have entered a WLP.)

In order to use Equation 3.15 to calculate the probability for the fragments of a single meteoroid landing in a primordial WLP,  $A_{targ}$  must be the *effective* target area. The effective target area is illustrated in Figure 3.5 below. Any meteoroid that enters the atmosphere within the effective target area (of radius  $d$ ), disperses its fragments over at least one WLP’s entire surface.

The area of the asymmetric “lens” in which any two circles intersect is

$$A = r^2 \cos^{-1} \left( \frac{d^2 + r^2 - R^2}{2dr} \right) + R^2 \cos^{-1} \left( \frac{d^2 + R^2 - r^2}{2dR} \right) - \frac{1}{2} \sqrt{(-d + r + R)(d + r - R)(d - r + R)(d + r + R)}, \quad (3.16)$$

for circles of radii  $r$  and  $R$ , and distance between their centers  $d$  [293].

In Figure 3.5, the asymmetric lens created by the intersection of the combined WLP surface area at a given time and the meteoroid fragment debris area corresponds to the area of the largest individual WLP in our distribution. Because the effective target area radius,  $d$ , grows linearly with total WLP surface area radius,  $R$ , we can plot Equation 3.16 at  $t = 1$  Gyr to solve for  $d$ , and input the linear time dependence afterwards. For this calculation,  $A = 3.14 \times 10^{-4} \text{ km}^2$ ,  $r = r_g = 0.5 \text{ km}$ , and  $R = \sqrt{\frac{651 \text{ km}^2}{\pi}} = 14.4 \text{ km}$ . This gives us the effective target radius,  $d = 14.9 \text{ km}$ , and corresponds to an effective target area:

$$A_{eff}(t) = 697t \text{ [km}^2\text{]}. \quad (3.17)$$

See Figure 3.1 in the main text for a plot of the effective WLP surface area over time.

Finally, the probability of the fragments from all CM-, CI-, or CR-type meteoroids with radii  $r_{min} = 20 \text{ m}$  to  $r_{max} = 40 \text{ m}$  landing in WLPs on the early Earth of radii 1–10 m from time  $t$  to  $t + dt$  is the product of Equations 3.14 and 3.15.

$$dP_i(t) = \frac{697t}{4\pi R_{\oplus}^2} dN_i(t), \quad (3.18)$$

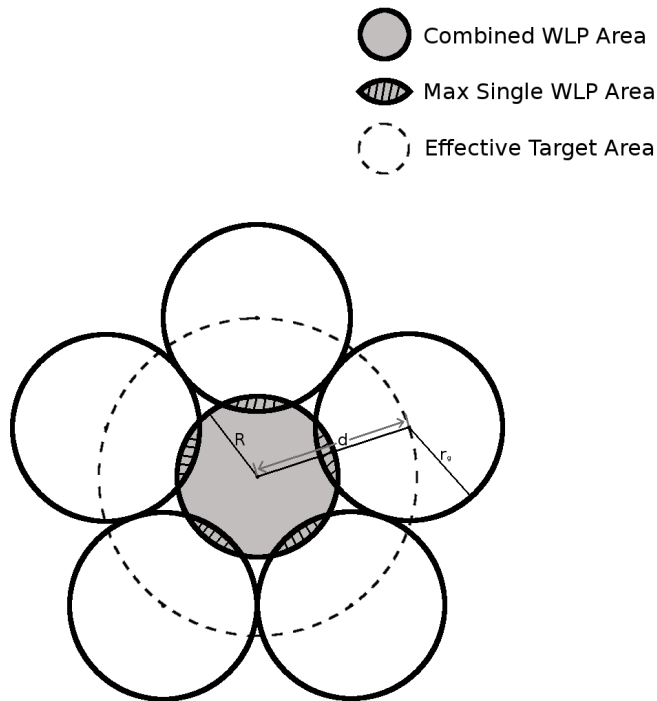


Figure 3.5: The dotted circle represents the target area for landing the dispersed fragments from a single meteoroid into any WLP on the early Earth. The smaller, light grey circle in the center is the total combined WLP surface area on the early Earth at a given time (WLPs would have been individually scattered, however for a geometric probability calculation they can be visualized as a single pond cross-section). The larger, surrounding circles represent the area of debris when the fragments of the meteoroid hit the ground. Shortly after 4.5 Ga, the area of debris from a single meteoroid would be large compared to the the combined WLP surface area. At any time, the target area for a meteoroid to deposit fragments homogeneously into at least 1 WLP is slightly larger than the combined area of WLPs. The effective target area grows linearly with total WLP surface area. The diagonally striped intersections between the circles represent the largest individual WLP for which the meteoroid fragment deposition probability is being calculated. The logic is that if a meteoroid enters the atmosphere at distance  $d$  from the center of the combined pond cross-section, at least 1 pond of any size in the WLP distribution will completely overlap with the area of debris.

where  $i$  is the model (LHB, minB, or maxB).

In Figure 3.6, we plot the normalized probability distributions ( $dP_i/dt$ ) for the deposition of carbonaceous meteorites into WLPs from 4.5–3.7 Ga. The LHB, the minimum and the maximum bombardment models are compared. For the LHB model,

there are 10 WLP depositions from 3.9–3.8 Ga. 95% of these depositions occur between 3.88–3.82 Ga. For the minimum bombardment model, there are 15 WLP depositions during the entire Hadean eon, however 95% of these depositions occur between 4.47–3.77 Ga. Finally, for the maximum bombardment model, there are 3840 depositions during the Hadean eon, with 95% of these depositions occurring between 4.50–4.17 Ga. See Figure 3.1 in the main text for cumulative deposition distributions.

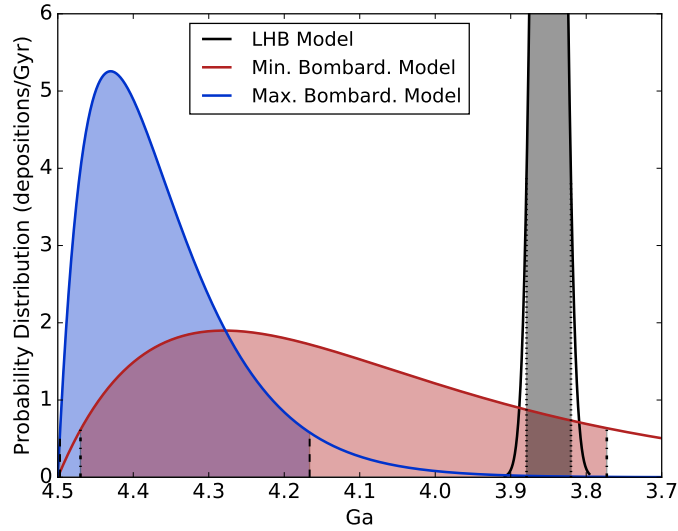


Figure 3.6: Normalized probability distributions of fragments from CM-, CI-, and CR-type meteoroids with radii 20–40 m landing in WLPs on the early Earth of radii 1–10 m. Three models for mass delivery are compared: the Late Heavy Bombardment model, and minimum and maximum mass models for a sustained, declining bombardment preceding 3.9 Ga. All models are based on analyses of the lunar cratering record [269, 271]. See Figure 3.1 in the main text for display of mass delivery rates. The 95% confidence intervals are shaded, and correspond to the most likely deposition intervals for each model.

One assumption is made in our deposition probability calculation, which is, given that the largest WLP considered is completely within the carbonaceous meteoroid’s strewnfield, at least one fragment will land in the WLP. (An equivalent assumption would be, given that 100 of the smallest WLPs considered are completely within the meteoroid’s strewnfield, at least one fragment will deposit into one of the ponds.) To determine whether this is the case, we need a good estimate for the number of fragments that spread over a debris field from a single carbonaceous meteoroid. For the Pultusk stony meteoroid, which entered Earth’s atmosphere above Poland in 1868

[294], the number of fragments is estimated to be 180,000 [294]. Although the Pultusk meteorites may not represent the typical fragmentation of stony meteoroids, since this meteoroid is about 1.6 times denser than the average carbonaceous meteoroids in our study [295], we would expect a carbonaceous meteoroid to fragment more than the typical stony meteorite. If meteoroid fragments are randomly spaced within a strewnfield, then Equation 3.15 multiplied by the the number of meteoroid fragments will give us roughly the number of fragments that will enter a WLP. (In this case  $A_{targ}$  is the area of the cylindrical pond, and  $A_{tot}$  is the area of the strewnfield.) From this calculation, given a 10 m-radius WLP is within a 180,000-fragment strewnfield of radius 500 m, roughly 72 carbonaceous meteoroid fragments will land in the pond. In fact, as long as 40–80 m carbonaceous meteoroids fragment into at least 2500 pieces, fragment deposition into a 10 m-radius WLP is probable. We therefore consider this assumption reasonable.

### 3.10.2.6 Sensitivity Analysis

In our estimate of the number of carbonaceous meteoroids that led to WLP depositions on the early Earth, we assume that from 4.5–3.7 Ga, the continental crust grows at 16%/Gyr [272], and the ponds per unit area is the same as today. However, the uncertainty in the growth rate of continental crust and the WLPs per unit area on the early Earth is high. For example, the number of WLPs per unit area was probably higher on the above-sea-level crust of the Hadean Earth than it is on Earth’s continents now. The greater rate of asteroid bombardment during the Hadean [114] would have created many small craters, which over a few rain cycles could fill to become ponds. On the other hand, geophysical models suggest the surface ocean was increasing in volume from  $\sim$ 4.5–4.0 Ga [296]. This would slow the growth rate of above sea-level crust. Because of these uncertainties, we adjust the growth rate of WLPs on the early Earth by  $\pm 1$  order of magnitude to obtain error bars. Because the probability of deposition (Equation 3.18) is directly proportional to the number of WLPs on the early Earth, varying the growth rate of WLPs by  $\pm 1$  order of magnitude equates to a  $\pm 1$  order of magnitude uncertainty in the WLP deposition expectation values (see Figure 3.1 in the main text).

### 3.10.3 Sources and Sinks Model Overview

Calculating the water and nucleobase content in WLPs over time is a problem of sources and sinks. These sources and sinks are illustrated in Figure 3.2 in the main text, and displayed in Table 3.2 below.

Table 3.2: Sources and sinks of pond water and nucleobases in our model of early Earth WLPs.

	Sources	Sinks
Pond water	Precipitation	Evaporation Seepage
Nucleobases	IDPs Meteorites*	Hydrolysis* Seepage* Photodissociation <sup>†</sup> Forming nucleotides <sup>‡</sup>

\*Only when pond is wet

† Only when pond is dry

‡ To be added in a future model

Because nucleobase diffusion from carbonaceous meteorite fragments is slow (see section on nucleobase outflow and mixing below), this source is only turned on in the wet phase. Although it may be possible for nucleobases to occasionally enter WLPs from runoff, we do not consider this as a source. IDPs that fall on dry land are the most likely nucleobase source to be carried by runoff into WLPs (because of their low mass). However, these IDPs are exposed to photodissociating UV light until they are picked up by a runoff stream, by which time few, if any enclosed nucleobases likely remain. Hydrolysis of nucleobases only occurs in the presence of liquid water, therefore we only turn on this sink when our ponds are wet. Similarly, seepage of nucleobases through the pores in the bases of WLPs only occurs during the wet phase. A 1 m column of pond water can absorb UV radiation up to  $\sim 95\%$  [277], therefore as a first order approximation, we only turn on UV photodissociation when our WLPs are in the dry phase. We do not consider cosmic rays as a sink for nucleobases, as a study has shown that adenine has a half-life of millions of years from cosmic ray dissociation at 1 AU [297]. This is several orders of magnitude greater than the timescales of nucleobase decay from the other sinks. Finally, since we are interested in accumulating

nucleobases in WLPs so that they can react to form nucleotides, a future model will include such reactions as a sink.

### 3.10.4 Pond Water Sources and Sinks

#### 3.10.4.1 Evaporation

There are many variables that could go into a pond evaporation calculation. However, a simple relation was obtained by measuring the depth and temperature of a  $\sim 1$  m-radius lined pond (to prevent seepage) and a class-A cylindrical evaporation pan over time:

$$\frac{dE}{dt} = -9.94 + 5.04T \quad [\text{mm month}^{-1}], \quad (3.19)$$

where  $dE$  is the drop in pond depth, and  $T$  is the pond temperature in  $^{\circ}\text{C}$  [53].

This relation is converted to  $\text{m yr}^{-1}$  below.

$$\frac{dE}{dt} = -0.12 + 0.06T \quad [\text{m yr}^{-1}]. \quad (3.20)$$

#### 3.10.4.2 Seepage

Unless the material (e.g. basalt, soil, clay) at the base of a WLP is saturated in water, gravity will cause pond solution to seep through the pores in this material. The average seepage rate of 55 small ponds in Auburn, Alabama was measured to be  $5.1 \text{ mm day}^{-1}$  [54]. This value is high compared to the average seepage rates from small ponds in North Dakota and Minnesota ( $1.0 \text{ mm day}^{-1}$ ), and the Black Prairie region of Alabama ( $1.6 \text{ mm day}^{-1}$ ) [54]. These seepage rates are comparable in magnitude to the pond evaporation rates above, and therefore must be considered as a sink for water and nucleobases in our WLP model. We take an average of the above three values and apply a constant seepage rate of  $2.6 \text{ mm day}^{-1}$  to our WLP water evolution calculations.

$$\frac{dS}{dt} = 0.95 \quad [\text{m yr}^{-1}]. \quad (3.21)$$

We assume that the majority of seepage occurs from the base of the pond, where the water pressure is the highest. The effect of seepage on nucleobase mass loss is handled in the nucleobase sinks section below.

### 3.10.4.3 Precipitation

If we ignore the possibility of local water geysers, the main source of pond water is likely to be precipitation. It has been shown that the vast majority of monthly precipitation climates around the world can be adequately described by a sinusoidal function with a 1 year period [57]. That is,

$$\frac{dP}{dt} = \bar{P} \left[ 1 + \delta_p \sin \left( \frac{2\pi(t - s_p)}{\tau_s} \right) \right] \quad [\text{m yr}^{-1}], \quad (3.22)$$

where  $dP$  is the amount of precipitation,  $\bar{P}$  is the mean precipitation rate ( $\text{m yr}^{-1}$ ),  $\delta_p$  is the dimensionless seasonal precipitation amplitude,  $s_p$  is the phase shift of precipitation (yrs),  $t$  is the time (yrs), and  $\tau_s$  is the duration of the seasonal cycle (i.e. 1 yr) [57].

From 1980–2009, the mean precipitation on the Earth ranged from  $\sim 0.004$ – $10$   $\text{m yr}^{-1}$  (with a global mean of  $\sim 0.7$   $\text{m yr}^{-1}$ ), the seasonal precipitation amplitudes ranged from  $\sim 0$ – $4.7$ , and the latitude-dependent phase shift ranged from  $0$ – $1$  year [57].

### 3.10.4.4 Summary

The evaporation and seepage rates minus the rate of water rise due to precipitation gives us the overall rate of water decrease in a WLP.

$$\frac{dL}{dt} = 0.83 + 0.06T - \bar{P} \left[ 1 + \delta_p \sin \left( \frac{2\pi(t - s_p)}{\tau_s} \right) \right] \quad [\text{m yr}^{-1}]. \quad (3.23)$$

Equation 3.23 is too complex to be solved by standard analytical techniques or mathematical software, therefore we solve it numerically using a forwards time finite difference approximation with the boundary conditions  $0 \leq L(T, t) \leq r_p$ . We then convert the drop in pond depth as a function of time,  $L(t)$ , to the mass of water in the WLP using the water density and the volume of a cylindrical portion. This equates to:

$$m(t) = \pi \rho_w r_p^2 (r_p - L) \quad [\text{kg}]. \quad (3.24)$$

For our models we assume pond water of density  $\rho_w = 1000$   $\text{kgm}^{-3}$ .

### 3.10.5 Nucleobase Sinks

#### 3.10.5.1 Hydrolysis

The first-order hydrolysis rate constants for adenine (A), guanine (G), uracil (U), and cytosine (C) have been measured from decomposition experiments at pH 7 [90]. These rate constants are expressed in the Arrhenius equations below.

$$k_A = 10^{\frac{-5902}{T} + 8.15} \quad (3.25)$$

$$k_G = 10^{\frac{-6330}{T} + 9.40} \quad (3.26)$$

$$k_U = 10^{\frac{-7649}{T} + 11.76} \quad (3.27)$$

$$k_C = 10^{\frac{-5620}{T} + 8.69} \text{ [s}^{-1}\text{]}. \quad (3.28)$$

The nucleobase decomposition rate due to being dissolved in water can then be obtained by plugging Equations 3.25–3.28 into the first-order reaction rate law below.

$$\frac{dm_i}{dt} = -m_i \gamma k \text{ [kg yr}^{-1}\text{]}, \quad (3.29)$$

where  $\gamma = 3600 \cdot 24 \cdot 365.25 \text{ s yr}^{-1}$ .

The hydrolysis rates of adenine, guanine, and cytosine remain relatively stable in solutions with pH values from 4.5–9 [90, 298]. WLPs may have been slightly acidic (from pH 4.8–6.5) due to the higher partial pressure of CO<sub>2</sub> in the early Earth atmosphere [56].

#### 3.10.5.2 UV photodissociation

The photodestruction of adenine has been studied by irradiating dried samples under Martian surface UV conditions [91]. This quantum efficiency of photodecomposition (from 200–250 nm)—which is independent of the thickness of the sample—was measured to be  $1.0 \pm 0.9 \times 10^{-4} \text{ molecule photon}^{-1}$  [91].

For the calculation of the quantum efficiency of adenine, a beam of UV radiation was focused on a thin compact adenine sample formed through sublimation and recondensation [91]. In this case, all the photons in the beam of UV radiation were incident on the nucleobases. In the WLP scenario, not all the incoming UV photons will be incident on nucleobases. Instead, large gaps can exist between nucleobases

that collect at the base of the pond. Therefore the number of photons incident on the pond area is not the same as those incident on the scattered nucleobases unless there are at least enough nucleobases present to cover the entire pond area. Since the nucleobases are mixed well into the pond water before complete evaporation, we assume nucleobases will spread out evenly as they collect on the base of the pond. This means we assume that all locations on the base of the pond are covered in nucleobases before nucleobases stack on top of one another. For low abundances of total nucleobases in a WLP, this approach will lead to a slightly higher estimate for the rate of photodissociation than expected. We deem this acceptable for a first-order estimate of nucleobase photodissociation.

The mass of nucleobases photodestroyed per year, per area covered by nucleobases (i.e. the photodestruction flux), is constant over time and is dependent on the experimentally measured quantum efficiency of photodecomposition.

$$\dot{M}_i = \frac{\Phi F \lambda \gamma \mu_i}{hc N_A} \text{ [kg yr}^{-1} \text{ m}^{-2}\text{]}, \quad (3.30)$$

where  $\Phi$  is the quantum efficiency of photodecomposition of the molecules (molecules photon<sup>-1</sup>),  $F$  is the UV flux incident on the entire pond area (W m<sup>-2</sup>),  $\lambda$  is the average wavelength of UV radiation incident on the sample (m),  $\gamma$  is 3600 · 24 · 365.25 s yr<sup>-1</sup>,  $\mu_i$  is the molecular weight of the irradiated molecules (kg mol<sup>-1</sup>),  $h$  is Planck's constant (m<sup>2</sup> kg s<sup>-1</sup>),  $c$  is the speed of light (ms<sup>-1</sup>), and  $N_A$  is Avogadro's number (molecules mol<sup>-1</sup>).

Our estimation of the photodestruction rate of a nucleobase depends on the total mass of the nucleobase within the WLP. If there is enough of the nucleobase present for the entire base of the pond to be covered, we can multiply the photodestruction flux by the entire pond area. Otherwise, we must multiply the photodestruction flux by the combined cross-sectional area of the nucleobase present in the WLP to get the photodestruction rate.

$$\frac{dm_i}{dt} = \begin{cases} -\dot{M}_i \frac{m_i}{\rho_i d}, & \text{if } \frac{m_i}{\rho_i d} < A_p \\ -\dot{M}_i A_p, & \text{otherwise} \end{cases} \text{ [kg yr}^{-1}\text{]}, \quad (3.31)$$

where  $m_i$  is the mass of the sample (kg),  $\rho_i$  is the mass density of the nucleobase (kg m<sup>-3</sup>),  $d$  is the distance between two stacked nucleobases in the solid phase (m), and

$A_p$  is the area of the WLP ( $\text{m}^2$ ).

Assuming cloudless skies, an upper limit on the early Earth integrated UV flux from 200–250 nm is  $\sim 0.4 \text{ W m}^{-2}$  [51, 299]. UV wavelengths  $< 200 \text{ nm}$  would be completely attenuated by  $\text{CO}_2$  and  $\text{H}_2\text{O}$  in the early atmosphere [51]. The mass density of solid adenine is  $1470 \text{ kg m}^{-3}$ , making the distance between two stacked adenine molecules in the solid phase  $\sim 6.6 \text{ \AA}$ . For guanine, uracil, and cytosine, we take the mass densities to be  $2200 \text{ kg m}^{-3}$ ,  $1320 \text{ kg m}^{-3}$ , and  $1550 \text{ kg m}^{-3}$ , respectively.

### 3.10.5.3 Seepage

The constant pond water seepage  $\dot{S} = 0.95 \text{ m yr}^{-1}$  was determined in the pond water source and sinks section above. This can be used to calculate the nucleobase seepage rate via the equation:

$$\frac{dm_i}{dt} = w_i \rho_w A_p \dot{S} \quad [\text{kg yr}^{-1}], \quad (3.32)$$

where  $w_i$  is the nucleobase mass fraction,  $\rho_w$  is the density of water ( $\text{kg yr}^{-1}$ ), and  $A_p$  is the area of the WLP ( $\text{m}^2$ ).

### 3.10.6 Nucleobase Outflow and Mixing

Chondritic IDPs and meteorites are porous [75, 300, 301]. With the exception of the nucleobases potentially formed due to surface photochemistry [76], any soluble nucleobases delivered to the prebiotic Earth by carbonaceous IDPs and meteorites would have layed frozen in the pores of these sources upon them entering the atmosphere. Pulse heating experiments show approximately  $\sim 1\text{--}6\%$  of the organics within IDPs could have survived atmospheric entry [75]. And, based on their presence in carbonaceous chondrites today, nucleobases in carbonaceous meteorites evidently would have also survived atmospheric entry heating. Therefore both sources, upon entering WLPs on the prebiotic Earth, would have slowly released their remaining soluble nucleobases into the surrounding pond water. These nucleobases would then slowly homogenize into the pond solution.

We model the outflow of nucleobases from carbonaceous IDPs and meteorites and the mixing of a local concentration of nucleobases into a WLP using finite difference approximations of the one-dimensional advection-diffusion equation (see Appendix A

for complete details).

Our model of nucleobase outflow is run for average-sized IDPs ( $r = 100\mu\text{m}$ ), and for small ( $r = 1\text{ cm}$ ), medium ( $r = 5\text{ cm}$ ) and large ( $r = 10\text{ cm}$ ) carbonaceous meteorites. The fraction of nucleobases remaining in each of these sources as a function of time is plotted in Figure 3.7 below.

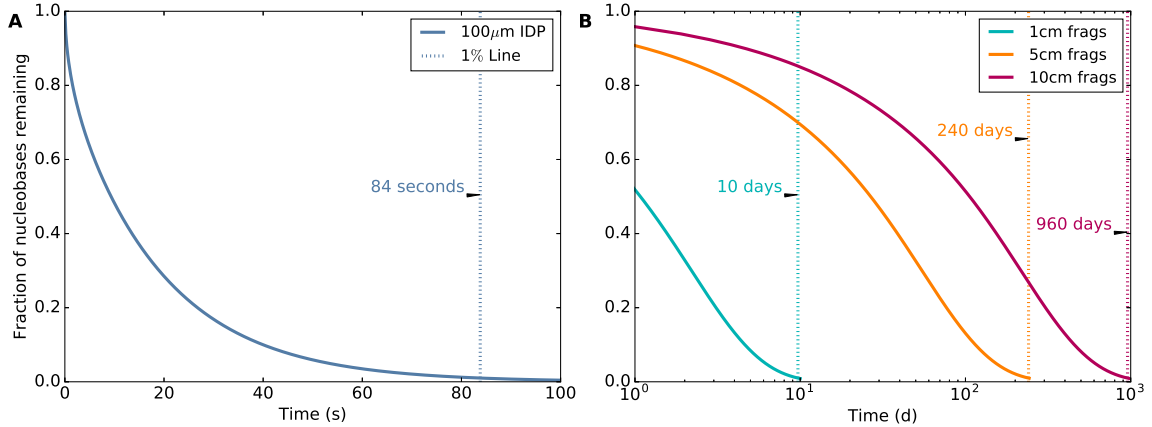


Figure 3.7: Fraction of the total initial nucleobases remaining in **(A)** a  $100\mu\text{m}$ -radius IDP and **(B)** 1 cm-, 5 cm-, and 10 cm-radii meteorites over time as a result of diffusion across a rock-pond boundary. The IDP and meteorites are considered to be laying on the bottom of a WLP, and are diffusing nucleobases symmetrically in the radial direction. The times at which 99% of the initial contained nucleobases have diffused into the WLP are labeled on the plots.

Our models show that the duration of nucleobase diffusion from carbonaceous IDPs and meteorites into WLPs is mostly determined by the radius of the source. For typical,  $100\mu\text{m}$ -radius carbonaceous IDPs laying at the bottom of a WLP, it takes  $< 2$  minutes for  $> 99\%$  of the soluble nucleobases to diffuse into the surrounding pond water. For 1 cm-radius carbonaceous meteorites, this time increases to 10 days. For the largest carbonaceous meteoroid fragments, with radii of 5 cm and 10 cm, this duration increases to approximately 8 and 32 months, respectively.

For nucleobase mixing, we model a base-to-surface convection cell within cylindrical ponds with equal radii and depths of 1 m, 5 m, and 10 m. This model gives us the timescale of mixing a local concentration of nucleobases within WLPs. The maximum percent local nucleobase concentration difference from the average is plotted as a function of time in Figure 3.8. This metric allows us to characterize the nucleobase homogeneity in a convection cell of the WLP.

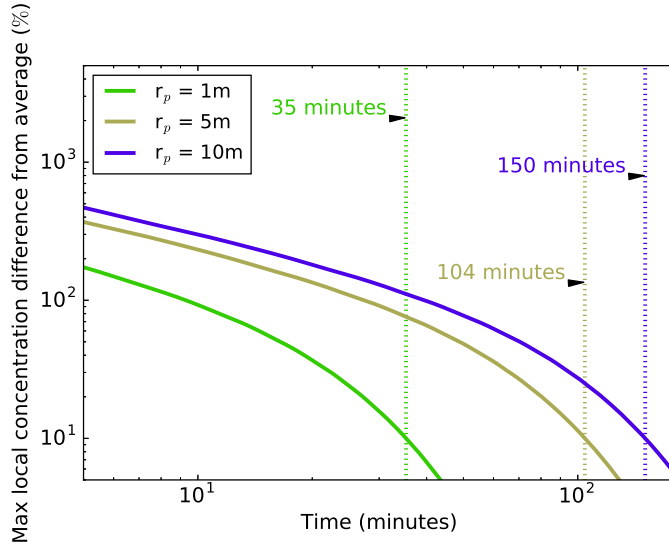


Figure 3.8: The nucleobase mixing time in a base-to-surface convection cell (length =  $2r_p$ ) within 1 m-, 5 m-, and 10 m-deep WLPs, beginning from a local concentration at the base of the pond. Nucleobase mixing is measured using the maximum percent local nucleobase concentration difference from the average. The time at which the maximum local nucleobase concentration difference from the average drops to 10% is labeled on the plot for each pond size. At this time, we consider the nucleobases in the WLP to be well mixed. For WLPs with radii 1 m, 5 m, and 10 m, the convection cell nucleobase mixing times are 35 minutes, 104 minutes, and 150 minutes, respectively.

Our simulations suggest that the mixing of local deposits of nucleobases in WLPs, resulting from their diffusion out of carbonaceous IDPs and meteorites, is a very efficient process. For a cylindrical WLP 1 m in depth, it will take about 35 minutes for a local deposition to homogenize in a convection cell within the pond. For larger WLPs, with 5 m and 10 m depths, the nucleobase mixing time increases to 104 and 150 minutes, respectively. These short mixing times make it clear that, for carbonaceous meteorites  $\geq 1$  cm in radius, nucleobase deposition and homogenization in WLPs is dominated by the nucleobase outflow time from these bodies. In contrast, being that carbonaceous IDPs are much smaller than meteoroid fragments, the nucleobase outflow time from IDPs is negligible compared to the nucleobase homogenization time in WLPs.

### 3.10.7 Nucleobase Evolution Equation From IDPs

It is estimated that at 4 Ga, approximately  $6 \times 10^8 \text{ kg yr}^{-1}$  of carbonaceous IDPs were being accreted onto the Earth [33]. Since IDPs are tiny (typically  $\sim 100 \mu\text{m}$  in radius), they are circulated by the atmosphere upon accretion and thus likely reached almost everywhere on the prebiotic Earth. Approximately 1–6% of the organic content within IDPs could have survived the pulse heating of atmospheric entry [75]. Assuming IDPs accreted uniformly, the surface nucleobase mass accretion per square area would be

$$\frac{dm_i}{dt dA} = \frac{w_i \dot{m}_I f_s}{4\pi R_{\oplus}^2} \quad [\text{kg yr}^{-1} \text{m}^{-2}], \quad (3.33)$$

where  $w_i$  is the nucleobase mass fraction within IDPs for nucleobase  $i$ ,  $\dot{m}_I$  is the mass accretion rate of IDPs on the prebiotic Earth ( $\text{kg yr}^{-1}$ ), and  $f_s$  is the average fraction of nucleobases that survive pulse heating from atmospheric entry.

IDPs are thought to correspond to origins of asteroids or comets [33], therefore at best, the average nucleobase abundances in IDPs could match the average nucleobase content within the nucleobase-rich CM, CR, and CI meteorites. The average abundances of adenine, guanine, and uracil in CM, CR, and CI meteorites are listed in Table 3.3 along with the weighted averages based on relative fall frequencies. These abundances might be an upper limit for the guanine, adenine, and uracil content of IDPs because unlike the interior of large meteorites, molecule-dissociating UV radiation can penetrate everywhere within  $\mu\text{m}$ – $\text{mm}$ -sized pieces of dust.

Table 3.3: Average guanine, adenine and uracil abundances (in ppb) in the CM, CR, and CI carbonaceous chondrites. Abundances obtained from [36]. Some CM and CR meteorite analyses found no adenine or uracil, these samples were excluded from the average. Weighted nucleobase averages are also displayed based on relative fall frequencies [274]. Uracil has not been measured in CR meteorites. Cytosine has not been measured in any meteorites.

	Guanine	Adenine	Uracil
CM	183.5	69.8	50.0
CR	1.8	9.3	-
CI	81.5	60.5	73.0
Weighted Avg	141.3	60.7	48.6

The amount of cytosine that could have formed on the surfaces of primordial IDPs

is not well constrained. Cytosine has been detected in experiments exposing IDP analogs to UV radiation, but hasn't been quantified [76]. Furthermore, these analog experiments formed cytosine via photoreactions involving pyrimidine: a molecule that has no measured abundance in IDPs or meteorites. For this analysis we explore a best-case scenario, and set the maximum cytosine IDP abundance to 141.3 ppb (the possible upper limit of guanine in carbonaceous IDPs).

In the nucleobase outflow and mixing section above we learned that nucleobase diffusion from IDPs is quick (lasting  $< 2$  minutes), and nucleobase homogenization in WLPs takes one to a few hours, depending on the pond size. If we spread out the  $6 \times 10^8$   $\text{kg yr}^{-1}$  accretion rate of IDPs uniformly across the surface of the Earth—assuming IDPs are all  $100 \mu\text{m}$ -radius spheres of CI, CM, and CR type ( $\rho = \sim 2185 \text{ kg m}^{-3}$ )—then IDPs would drop into 1–10 m-radius primordial WLPs at approximately 0.05–5 per hour. Since each carbonaceous IDP can only carry a tiny mass in nucleobases ( $\sim 1$  picogram), nucleobase inhomogeneities within WLPs would be a maximum of  $\sim 15$  picograms. This abundance of nucleobases is negligible, therefore for our calculations of nucleobase accumulation in WLPs from IDP sources, we can assume that nucleobase deposition and pond homogenization is instantaneous.

Thus, the differential equation for the mass of nucleobase  $i$  accumulated in a WLP from IDP sources over time is the sum of the nucleobase mass accretion rate from IDPs, the nucleobase mass decomposition rate, the nucleobase mass seepage rate, and the nucleobase photodissociation rate:

$$\frac{dm_{i,IDP}(t)}{dt} = \frac{w_i \dot{m}_I f_s A_p}{4\pi R_{\oplus}^2} - \gamma m_i k_i - w_i \rho_w A_p \dot{S} - \begin{cases} \dot{M}_i \frac{m_i}{\rho_i d}, & \text{if } \frac{m_i}{\rho_i d} < A_p \\ \dot{M}_i A_p, & \text{otherwise} \end{cases} \quad [\text{kg yr}^{-1}]. \quad (3.34)$$

The second and third terms after the equal sign are only activated when the pond is wet, and the fourth term is only activated when the pond is dry. The first term is always activated as recently accreted nucleobases are susceptible to UV dissociation while still laying in the pores of IDPs, and they effectively instantaneously outflow from IDPs upon wetting.

Using Equation 3.34, we compute the nucleobase mass as a function of time numerically using a forwards time finite difference approximation. We then divide the nucleobase mass by the water mass at each time step to obtain the nucleobase mass

concentration over time. Because some ponds are seasonally dry, we freeze the water level at 1 mm during the dry phase in order to calculate a nucleobase concentration during this phase.

### 3.10.8 Nucleobase Evolution Equation From Meteorites

Simulations show the fragments from carbonaceous meteoroids with diameters from 40–80 m and initial velocities of 15 km/s will expand over a radius of  $\sim 500$  m, and  $\sim 32\%$  of the original meteoroids will survive ablation [66]. Since a single meteoroid impacting the atmosphere may break up into 180,000 fragments before spreading across its strewnfield, it is probable that a meteorite deposition event involves multiple meteorites landing in a single WLP. The best estimate of the total nucleobase mass deposited into a WLP is thus calculated assuming the ablated meteoroid mass is spread uniformly over its strewnfield. Considering this, the total nucleobase mass to deposit into a WLP from a meteoroid would be

$$m_{i0} = \frac{4}{3} \frac{w_i f_s r^3 \rho A_p}{r_g^2} \quad [\text{kg}], \quad (3.35)$$

where  $w_i$  is the nucleobase mass fraction within the meteoroid for nucleobase  $i$ ,  $f_s$  is the fraction of the meteoroid to survive ablation,  $r$  is the meteoroid radius as it enters Earth's atmosphere (m),  $\rho$  is the density of the meteoroid ( $\text{kg m}^{-3}$ ),  $r_g$  is the radius of the debris when the meteoroid fragments hit the ground (m), and  $A_p$  is the area of the WLP ( $\text{m}^2$ ).

After the deposition of meteoroid fragments into a WLP, the frozen meteorite interiors will thaw to pond temperature, allowing hydrolysis to begin inside the fragments' pores. This means the total mass of nucleobases that diffuse from the fragments' pores into the pond will be less than the total initial nucleobase mass within the deposited fragments. By integrating the nucleobase hydrolysis rate (Equation 3.29), we obtain the mass of nucleobase  $i$  remaining after a given time of hydration  $t_h$ ,

$$m_i = m_{i0} e^{-\gamma k_i t_h} \quad [\text{kg}]. \quad (3.36)$$

Note that  $t_h$  (yr) may be different than  $t$ , as the hydration clock is paused when WLPs are dry.

Unlike carbonaceous IDPs, which unload their nucleobases into a WLP in seconds,

nucleobases may not completely outflow from all deposited carbonaceous meteoroid fragments before the WLP evaporates. (However, the nucleobases that do outflow from the meteorites will mix homogeneously into the WLP within a single day-night cycle.) Thus, we calculate the nucleobase outflow time constants for 1 cm-, 5 cm-, and 10 cm-radius carbonaceous meteorites by performing least-squares regressions of our nucleobase diffusion simulation results to the function below.

$$f(t_h) = \alpha \left( 1 - e^{-\frac{t_h}{\tau_d}} \right). \quad (3.37)$$

This equation shows that as time increases, the mass of nucleobases that have flowed out of a single meteorite, into the WLP, approaches the coefficient  $\alpha$ —which represents the total initial nucleobase mass contained in the meteorite. Since nucleobase outflow is mass-independent, we can use an arbitrary initial total nucleobase mass for  $\alpha$  in our simulations to obtain the nucleobase outflow time constants.

The results of the fits give diffusion time constants for 1 cm-, 5 cm-, and 10 cm-radius fragments of  $\tau_d = 4.9 \times 10^{-3}$  yr, 0.12 yr and 0.48 yr, respectively.

Adding up the sources and sinks gives us the nucleobase mass within the WLP from meteorite sources as a function of time and hydration time.

$$\begin{aligned} \frac{dm_{i,Met}(t, t_h)}{dt} = & \frac{m_{i0}}{\tau_d} e^{-t_h \left( \gamma k_i + \frac{1}{\tau_d} \right)} - \gamma m_i k_i - w_i \rho_w A_p \dot{S} \\ & - \begin{cases} \dot{M}_i \frac{m_i}{\rho_i d}, & \text{if } \frac{m_i}{\rho_i d} < A_p \\ \dot{M}_i A_p, & \text{otherwise} \end{cases} \quad [\text{kg yr}^{-1}]. \end{aligned} \quad (3.38)$$

The first three terms after the equal sign are only activated when the pond is wet, and the fourth term is only activated when the pond is dry.

Since there are many possibilities for the sizes of meteoroid fragments that will enter a WLP, we consider 3 simplified models: all fragments that enter a WLP from a meteoroid of radius 20–40 m are either 1 cm in radius, 5 cm in radius, or 10 cm in radius. These three models represent a local part of the strewnfield that deposited either many small fragments, mostly medium-sized fragments, or just a couple to a few large fragments.

Cytosine is unlikely to have sustained within meteorite parent bodies long enough to be delivered to the early Earth by meteorites [42], therefore we only model the accumulation of adenine, guanine, and uracil in WLPs from meteorite sources.

We solve Equation 4 numerically using a forwards time finite difference approximation. Nucleobase concentration is then obtained by dividing the nucleobase mass by the water mass in the WLP at each time step.

### 3.10.9 Additional results

#### 3.10.9.1 Pond Water

In Figure 3.9 we explore the effects of changing temperature on wet environment WLPs of 1 m radius and depth (see Table 3.1 in main text for wet environment model details). To do this, we vary our fiducial model temperatures (65°C for a hot early Earth and 20°C for a warm early Earth) by  $\pm 15^\circ\text{C}$ . As temperature increases, evaporation becomes more efficient, however the wet environment WLPs never dry completely.

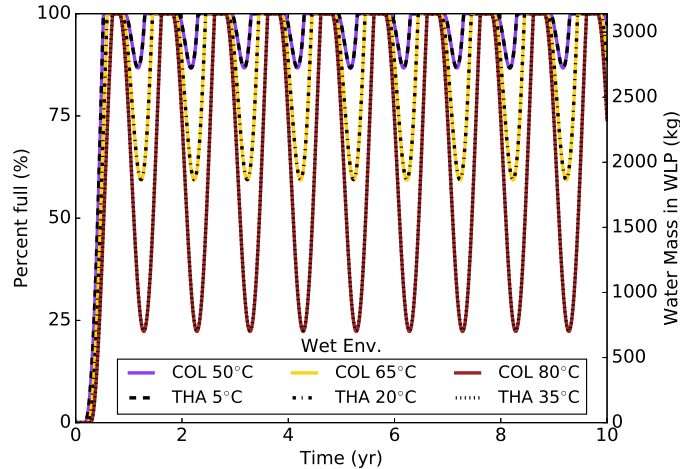


Figure 3.9: The effect of temperature on the change in water mass over time in wet environment cylindrical WLPs with radii and depths of 1 m. Temperatures are varied for a hot early Earth model (50 °C, 65 °C, and 80 °C) and a warm early Earth model (5 °C, 20 °C, and 35 °C). Precipitation rates from Columbia and Thailand on Earth today are used to represent the hot, and warm early Earth analogues, respectively (for details see Table 3.1 in the main text).

#### 3.10.9.2 Nucleobase Accumulation from IDPs

In Figure 3.10 we explore the evolution of adenine concentration from only IDP sources in WLPs of 1 m radius and depth. We model the adenine accumulation in three environments (dry, intermediate, and wet) on a hot and warm early Earth (see Table 3.1

in the main text for precipitation model details). The left panel is for 65°C on a hot early Earth and 20°C on a warm early Earth, and the left panel is for 50°C on a hot early Earth and 5°C on a warm early Earth.

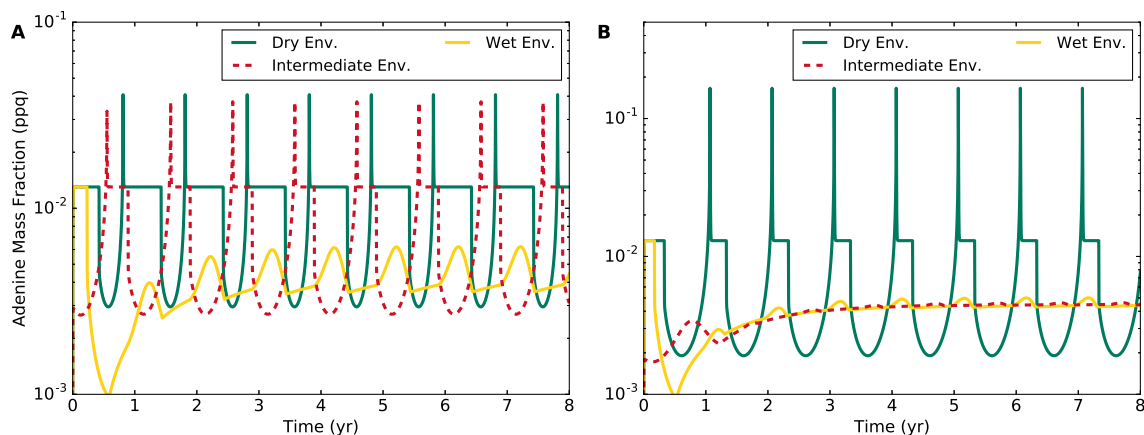


Figure 3.10: The accumulation of adenine from only carbonaceous IDP sources in cylindrical WLPs with radii and depths of 1 m. The three curves (dry, intermediate, and wet environments) differ by their precipitation rates, which are from a variety of locations on Earth today, and represent 2 classes of matching early Earth analogues: hot (Columbia, Indonesia, Cameroon), and warm (Thailand, Brazil, and Mexico) (for details see Table 3.1 in the main text). **(A)** The degenerate WLP models used for these calculations correspond to a hot early Earth at 65 °C and a warm early Earth at 20 °C. **(B)** The degenerate WLP models used for these calculations correspond to a hot early Earth at 50 °C and a warm early Earth at 5 °C.

All adenine concentration curves reach a stable seasonal pattern within  $\sim 5$  years. The highest adenine concentrations occur for models with a dry phase (i.e. the dry and intermediate models at 65°C, and the dry model at 50°C.) The lower maximum concentrations in the models without a dry phase are due to the sustained high water levels. The maximum adenine to accumulate in any model from IDP sources is  $\sim 0.2$  ppq. This occurs just before the pond dries. Upon drying, UV photodissociation immediately drops the adenine concentration to an amount which balances the incoming adenine from IDP accretion. The curves in Figure 3.10 do not change drastically with increasing pond radius and depth once a stable seasonal pattern is reached. This is because although ponds of increasing surface area collect more nucleobases, these ponds have an equivalent increase in area to nucleobase seepage.

In Figure 3.11 we explore guanine, uracil, and cytosine accumulation in degenerate dry environment WLPs for a hot early Earth at 65 °C and a warm early Earth at 20

$^{\circ}\text{C}$  (See Table 3.1 in main text for details). The differences in each nucleobase mass fraction over time is caused by the different initial abundances of each nucleobase in IDPs (see Table 3.3). Although hydrolysis rates differ between nucleobases, decay due to hydrolysis is negligible over  $< 10$  year periods at temperatures lower than  $\sim 70$   $^{\circ}\text{C}$ .

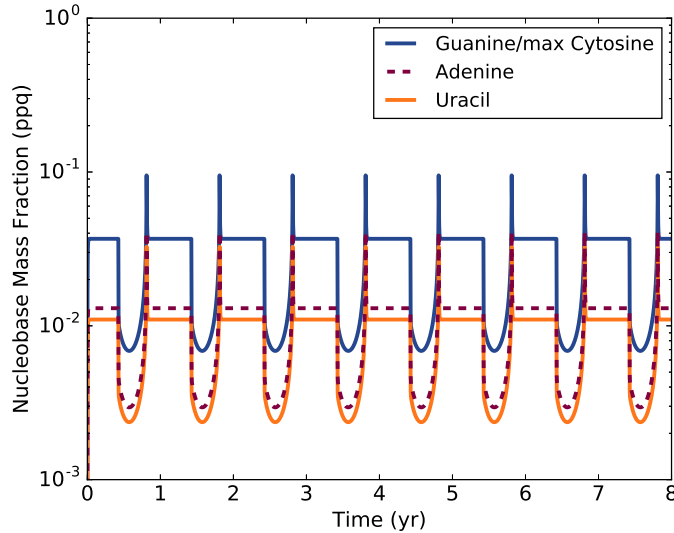


Figure 3.11: The accumulation of guanine, adenine, uracil, and cytosine from only carbonaceous IDP sources in cylindrical WLPs with radii and depths of 1 m. The degenerate dry WLP models used for these calculations correspond to a hot early Earth at  $65$   $^{\circ}\text{C}$  and a warm early Earth at  $20$   $^{\circ}\text{C}$ . Precipitation rates from Cameroon and Mexico on Earth today are used to represent the hot, and warm early Earth analogues, respectively (for details see Table 3.1 in the main text). The cytosine abundance in IDPs used to calculate the max cytosine curve, matches the average abundance of guanine in IDPs (see Table 3.3). The curves are obtained by numerically solving Equation 3.34.

In Figure 3.12 we turn off seepage, e.g. resembling a scenario where a lipid biofilm has covered the WLP base, and explore the evolution of adenine concentrations from IDP sources. This model is displayed for a hot early Earth at  $65$   $^{\circ}\text{C}$  and a warm early Earth at  $20$   $^{\circ}\text{C}$  (See Table 3.1 in main text for details). UV photodissociation is always the dominant nucleobase sink for the dry and intermediate environments, therefore for this model we only display the evolution of adenine in the wet environment, where hydrolysis takes over as the dominant nucleobase sink.

In the absence of seepage, adenine concentrations can build up in wet environment WLPs until the rate of incoming adenine from IDPs matches the decay rate due to hydrolysis. Hydrolysis rates are faster at hotter temperatures, therefore maximum

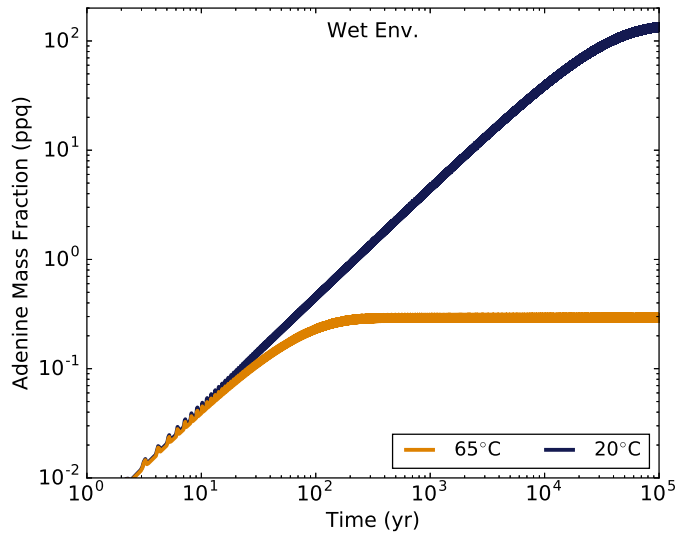


Figure 3.12: **The no seepage limit:** The accumulation of adenine from only carbonaceous IDP sources in cylindrical WLPs with radii and depths of 1 m. The two curves represent the adenine concentrations in a wet environment pond on a hot (65 °C), and warm (20 °C) early Earth (for details see Table 3.1 in the main text). The thickness of the lines is due to the seasonal oscillations in adenine concentrations.

adenine concentrations are higher and take longer to converge in the 20 °C pond compared to the 65 °C pond. However, these maximum adenine concentrations are 145 and 0.3 ppq, respectively, which are negligible in comparison to the ppb–ppm-level adenine concentrations reached in WLPs from carbonaceous meteorite sources.

### 3.10.9.3 Nucleobase Accumulation from Meteorites

In Figure 3.13 we explore the evolution of adenine concentration in WLPs with radii and depths of 1 m, from 1-cm fragments of an initially 40 m-radius carbonaceous meteoroid. The models correspond to degenerate environments on a hot (65 °C) and warm (20 °C) early Earth. The maximum adenine concentration in the intermediate environment is  $\sim 1.4$  ppm, and occurs 16 hours after the fragments deposit into the nearly empty pond. The dry and wet environments allow for a maximum adenine concentration of  $\sim 2$  ppm. Because adenine outflow from 1 cm-sized meteorites occurs in just 10 days, only adenine sinks exist from 10 days onwards. As the ponds wet, the adenine concentrations decrease exponentially, and as the ponds dry again, the curves flatten out and ramp up slightly before the ponds completely dry up. When

the ponds dry, UV radiation quickly wipes out the adenine at the base of the ponds. Since the wet environment doesn't have a dry phase, the adenine concentration slowly diminishes in this model due mainly to seepage.

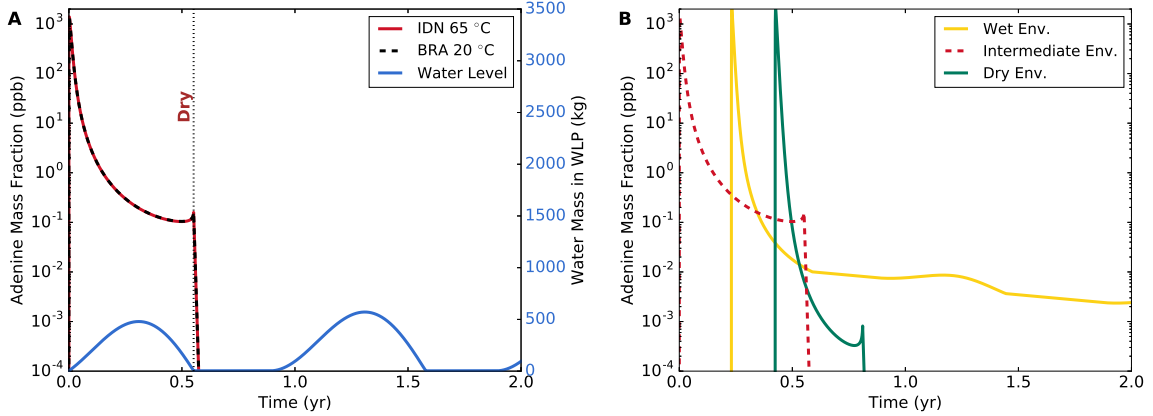


Figure 3.13: The accumulation of adenine from 1 cm fragments of an initially 40 m-radius carbonaceous meteoroid in a cylindrical WLP with a radius and depth of 1 m. The degenerate WLP models used for these calculations correspond to a hot early Earth at 65 °C and a warm early Earth at 20 °C. **(A)** The accumulation of adenine from carbonaceous meteorites in an intermediate environment (for details see Table 3.1 in the main text). The wet-dry cycles of the pond are also shown to illustrate the effect of water level on adenine concentration. **(B)** The three curves (dry, intermediate, and wet environments) differ by their precipitation rates, which are from a variety of locations on Earth today, and represent 2 classes of matching early Earth analogues: hot (Columbia, Indonesia, Cameroon), and warm (Thailand, Brazil, and Mexico) (for details see Table 3.1 in the main text). The curves are obtained by numerically solving Equation 3.38.

The adenine mass fraction curves in Figure 3.13, over a 2 year period, do not change as pond radii and depths increase equally. This is because, although the mass of water in a WLP increases for larger collecting areas, larger pond areas also collect more meteorite fragments, which counterbalances the water mass and keeps the nucleobase concentration the same.

In Figure 3.14 we explore how initial meteoroid radius affects the maximum concentration of adenine accumulated (from its fragments) in WLPs with radii and depths of 1 m. The maximum adenine concentration only differs by at most a factor of 8 when varying the initial meteoroid radius from 20–40 m. This is because the nucleobase mass to enter a WLP scales with the meteoroid mass, i.e.  $\propto r^3$ .

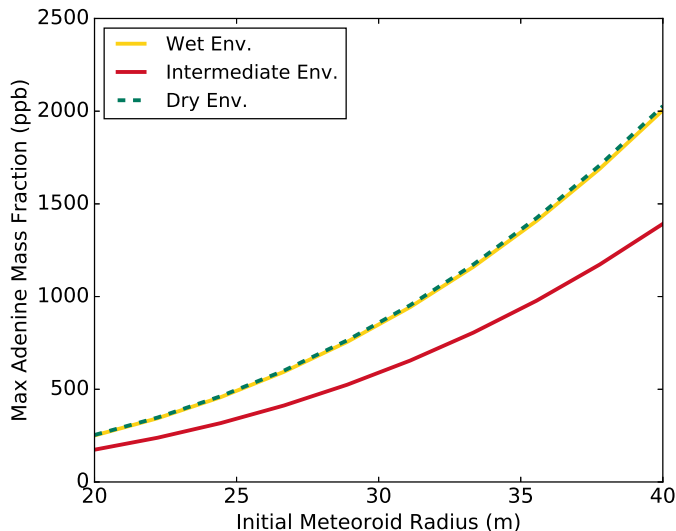


Figure 3.14: The maximum concentration of adenine accumulated from 1 cm fragments of a carbonaceous meteoroid 20–40 m in radius in cylindrical WLPs with radii and depths of 1 m. The degenerate WLP models used for these calculations correspond to a hot early Earth at 65 °C and a warm early Earth at 20 °C. The three curves (dry, intermediate, and wet environments) differ by their precipitation rates, which are from a variety of locations on Earth today, and represent 2 classes of matching early Earth analogues: hot (Columbia, Indonesia, Cameroon), and warm (Thailand, Brazil, and Mexico) (for details see Table 3.1 in the main text). The curves are obtained by numerically solving Equation 3.38.

Finally, in Figure 3.15 we explore guanine and uracil accumulation in intermediate and wet environment WLPs with radii and depths of 1 m. These models correspond to a hot early Earth at 65 °C and a warm early Earth at 20 °C. The small differences between each nucleobase mass fraction over time is due to the different initial nucleobase abundances in the deposited meteorite fragments (see Table 3.3). Although each nucleobase has a different hydrolysis rate (see Equation 3.25), the decay of guanine, adenine, and uracil due to hydrolysis is negligible in < 10 years for temperatures < 65°C.

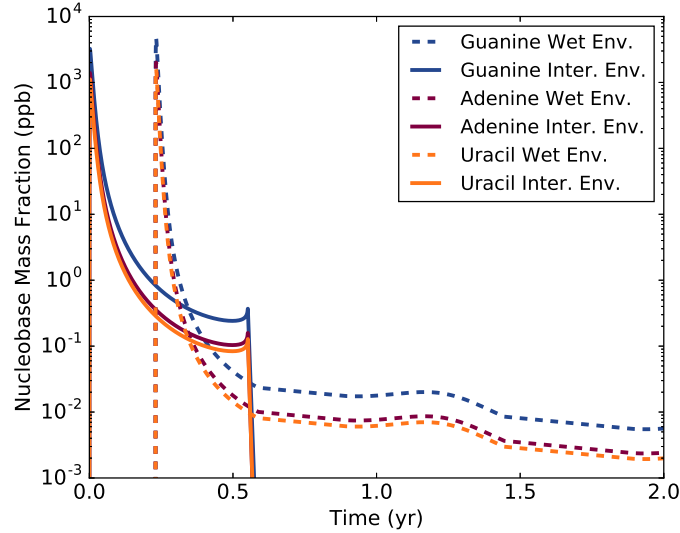


Figure 3.15: The accumulation of guanine, adenine, and uracil from 1 cm fragments of an initially 40 m-radius carbonaceous meteoroid in cylindrical WLPs with radii and depths of 1 m. The degenerate WLP models used for these calculations correspond to a hot early Earth at 65 °C and a warm early Earth at 20 °C. The two curves for each nucleobase differ by their precipitation rates, which create intermediate (solid lines), and wet (dotted lines) environments, and are from a variety of locations on Earth today representing 2 classes of matching early Earth analogues: hot (Columbia, Indonesia), and warm (Thailand, Brazil) (for details see Table 3.1 in the main text). The curves are obtained by numerically solving Equation 3.38.

### 3.10.10 Appendix A: Advection and Diffusion Model

Advection and diffusion are the two main considerations of solute transport in water. Because nucleobases will diffuse out of the pores of carbonaceous IDPs and meteorites at a different rate than they will mix homogeneously in the WLP, we separate our nucleobase transport model into two distinct parts. In part one, we model the outflow of nucleobases from carbonaceous IDPs and meteorites. In part two, we model the mixing of a local concentration of nucleobases into a WLP.

Both parts of our simulation can be modeled with the advection-diffusion equation below, with either one or both RHS terms “turned on.”

$$\phi \frac{\partial C_i}{\partial t} = \nabla \cdot [D_{eff} \nabla C_i] - \nabla \cdot [u C_i], \quad (3.39)$$

where  $\phi$  is the porosity of the medium,  $C_i$  is the mass concentration of the species,

$D_{eff}$  is the effective diffusion coefficient (often in  $\text{m}^2\text{s}^{-1}$ ), and  $u$  is the convective fluid velocity [302].

For a 1D case, where the diffusion coefficient and fluid velocity are constant along the simulated path, the advection-diffusion equation can be written as,

$$\phi \frac{\partial C_i}{\partial t} = D_{eff} \frac{\partial^2 C_i}{\partial r^2} - u \frac{\partial C_i}{\partial r}. \quad (3.40)$$

For part one of our nucleobase transport model (the nucleobase outflow portion), we set  $u = 0$ . This is because carbonaceous IDPs and meteoroid fragments are likely too small to attain noticeable interior pressure differences (thus the convective velocity within these bodies is probably negligible).

We do not consider hydrolysis in our nucleobase transport model, as we only intend on estimating nucleobase outflow and mixing timescales from these models (rather than the nucleobases remaining after these processes). Since nucleobase decay is uniform within the carbonaceous sources and WLPs, and is also very slow at WLP temperatures ( $t_{1/2} \sim$  tens to hundreds of years [42]), it is not likely to affect the timescales of complete nucleobase outflow from the source or homogenization within the WLP. A non-zero amount of nucleobases will decompose during diffusion from the source, and during mixing within the WLP. However, this is considered in the final calculations of nucleobase accumulation within WLPs from each source (see Sections 3.10.7 and 3.10.8).

The advection-diffusion equation also does not include adsorption or formation reactions. However, for the diffusion of *soluble* nucleobases from small porous environments which previously reached chemical equilibrium, the effects of these extra sources and sinks will probably be minimal. Also, to adjust the diffusion equation for a free-water medium, one simply needs to set  $\phi = 1$ , and  $D_{eff} = D_{fw}$ .

The effective diffusion coefficient of a species is proportional to, but smaller than its free water diffusion coefficient. Many equations exist for modeling the effective diffusion coefficient in porous media [303–306]. These equations depend on variables such as the porosity, tortuosity, and constrictivity of the medium, which represent the void space fraction, the curves in the pores, and the bottleneck effect, respectively. These equations are listed in Table 3.4.

Carbonaceous meteorites of type CM, CR, and CI have average porosities of 24.7%, 9.5%, and 35.0% [308]. Based on the relative fall frequency of these meteorites on Earth [274], the weighted average porosity of these meteorite types is  $\sim 25\%$ . Chondritic

Table 3.4: Different equations for modeling the effective diffusion coefficient of species in porous media. Estimates of the effective diffusion coefficients of single nucleobases through the pores of carbonaceous IDPs and meteorites are also calculated for each model. The free water diffusion coefficient,  $D_0$ , represents the unobstructed diffusion of a species, the porosity factor,  $\phi$ , represents the void fraction of the medium, the constrictivity factor,  $\delta$ , represents the bottleneck effect due to small pore diameters, and the tortuosity factor,  $\tau$ , represents the restriction in diffusive flow due to curves in the pores. Estimates of these factors, and the empirical exponent,  $m$ , for carbonaceous IDPs and meteorites are,  $D_0 = 4 \times 10^{-10} \text{m}^2 \text{s}^{-1}$ ,  $\phi = 0.25$ ,  $\delta = 1$ ,  $\tau = 1.45$ , and  $m = 2$  [306–309].

$D_{eff}$	Source	Estimate for this work ( $\times 10^{-11} \text{m}^2 \text{s}^{-1}$ )
$\frac{\phi\delta}{\tau} D_{fw}$	Saripalli <i>et al.</i> [303]	6.90
$\frac{\phi\delta}{\tau^2} D_{fw}$	van Brakel and Heertjes [304]	4.76
$\frac{2\phi}{3-\phi} D_{fw}$	Caré [305]	7.27
$\phi^m D_{fw}$	Boving and Grathwohl [306]	2.50

$D_{fw}$  = free water diffusion coefficient

$\phi$  = porosity

$\delta$  = constrictivity

$\tau$  = tortuosity

$m$  = empirical exponent

IDPs have similar porosities to carbonaceous chondrites [300], therefore a 25% porosity may also well represent nucleobase-containing IDPs.

The constrictivity of a porous medium is only important when the size of the species is comparable to the diameter of the pores [306]. Therefore given that nucleobases are  $< 1$  nm in diameter and the bulk of pore diameters in, for example, the Acfer 094 carbonaceous chondrite, range from 20–200 nm [301], we can neglect  $\delta$  from the listed models.

Tortuosities of chondritic meteorites have an average value of 1.45 [309], and the empirical exponent  $m$  for carbonaceous meteorites might be similar to that of nearshore sediments with a value of 2 [306].

Finally, the free water diffusion coefficient of a single nucleobase has not been measured, however the free water diffusion coefficient of a single nucleotide is 400

$\mu\text{m}^2\text{s}^{-1}$  [307]. Since nucleotides are heavier than nucleobases by a ribose and phosphate molecule, they will likely diffuse slower than nucleobases. Therefore  $400 \mu\text{m}^2\text{s}^{-1}$  is a good estimate of the lower limit of the free water diffusion coefficient of a single nucleobase.

Using the above estimates, we calculate the effective diffusion coefficients for nucleobases in carbonaceous meteorites and IDPs using each of the four models and display them in their respective columns in Table 3.4. The average value of the effective diffusion coefficient across all four models is  $5.36 \times 10^{-11} \text{ m}^2\text{s}^{-1}$ .

As previously stated, convective velocity within the pores of carbonaceous IDPs and meteorites is considered negligible. However, this is not the case within 1–10 m-radius WLPs. Due to the day-night cycles of the Earth, WLPs likely experienced a temperature gradient from the atmospherically exposed top of the pond to the constant geothermally heated base. Since convection is likely the dominant form of heat transport within hydrothermal ponds [310], convection cells would have formed, with warm (higher pressure) parcels of water flowing upwards and recently cooled (lower pressure) parcels flowing downwards.

The convective fluid velocity can be estimated with the equation

$$u = \sqrt{g\beta\Delta TL} \quad [\text{m s}^{-1}], \quad (3.41)$$

where  $g$  is the gravitational acceleration experienced by the fluid ( $\text{m s}^{-2}$ ),  $\beta$  is the fluid's volumetric thermal expansion coefficient ( $\text{K}^{-1}$ ), and  $\Delta T$  is the temperature difference (K) over a scale length  $L$  (m) [311]. The volumetric thermal expansion coefficients for water at 50, 65, and 80 °C, are 4.7, 5.6, and  $6.5 \times 10^{-4} \text{ K}^{-1}$  respectively [312].

Small ponds and even lakes can experience a temperature difference of 1–5 °C over the course of a day-night cycle [313]. However, convection begins cycling water well before temperature differences of this magnitude are reached. To estimate the lower bound of a constant temperature difference between the surface and the base of a WLP during a day-to-night period, we assume that each convection cycle cools a surface parcel of water by  $\Delta T$ . Then, given  $\Delta T$ , we match the corresponding cycle length and number of cycles with the approximate 12 hour period required for a 1 °C change in pond temperature. The equation for this calculation is summarized below.

$$\Delta T = \left( \frac{2LT_c}{P_{dn}\sqrt{g\beta L}} \right)^{\frac{2}{3}} \text{ [K]}, \quad (3.42)$$

where  $T_c$  is the change in pond temperature over a day-to-night period (K) and  $P_{dn}$  is the duration of that period (s).

Using Equation 3.42, the minimum constant temperature difference between the surface and the base of a cylindrical WLP with a radius and depth of 1 m, at 65 °C is  $\sim 0.007$  K. For a WLP with a radius and depth of 10 m, this minimum constant temperature difference increases to  $\sim 0.016$  K. However, given that smaller ponds experience greater temperature changes than larger ponds due to faster heat transfer, a  $\Delta T$  of  $\sim 0.01$  K may be a reasonable lower-bound estimate for all WLPs in the 1–10 m-radius/depth range.

Given a constant temperature difference of 0.01 K between the base and surface of 1 m-, 5 m-, and 10 m-deep WLPs at around 65 °C, the convective flow velocities would be approximately 0.7, 1.7, and 2.4  $\text{cms}^{-1}$ , respectively.

Due to the 1D nature of our simulations, we are assuming a radially symmetric outflow of nucleobases from spherical carbonaceous IDPs and meteorites. We also assume that local concentrations of nucleobases recently flowed out of these sources will remain within a single convection cell. Lastly, we assume that the nucleobase homogenization timescale within a 1D convection cell of a WLP is mostly representative of the nucleobase homogenization timescale within the entire WLP. Though the 1D handling of this part of our model is a simplification of advection and diffusion within WLPs, since we are only attempting to estimate nucleobase homogenization timescales to within a few factors, a 1D model is probably sufficient.

For both model parts we use a backward time, centered space (BTCS) finite difference method for the diffusion term in the advection-diffusion equation. For part two of the model, we use the upwind method to approximate the additional advection term. The BTCS method was selected over the more accurate Crank-Nicolson method based on the former's stability for sharply edged initial conditions and convergence for increasing levels of refinement. However, differences in diffusion timescales are found to be within rounding error upon comparison of these methods for a 100  $\mu\text{m}$  carbonaceous IDP. The upwind method was selected over higher-order advection approximation methods (e.g. Beam-Warming, Lax-Wendroff) due to its lack of spurious oscillations, lowest error accumulation in mass conservation tests and convergence for increasing

levels of refinement. These two models are summarized in Table 3.5 below.

Table 3.5: Summary of parts one and two of our 1D nucleobase transport model. Part one is a model of nucleobase outflow from carbonaceous IDPs and meteorites while they lay at the base of a WLP. Part two is the mixing (i.e. homogenization) of a local concentration of nucleobases throughout the WLP.

Part	Model Description	Num. Method	Boundaries	Initial condition	$\phi$	$D_{eff}$ ( $\text{m}^2\text{s}^{-1}$ )
1	Nucleobase outflow from carbonaceous IDPs and meteorites	BTCS	Neumann and open	See Figure 3.16a	0.25	$5.36 \times 10^{-11}$
2	Nucleobase mixing in WLPs	BTCS and upwind	Cyclic	See Figure 3.16b	1	$4.0 \times 10^{-10}$

For part one of our nucleobase transport model, the simulation frame starts at the center of the IDP or meteorite, and ends at the rock-pond interface. The left ( $r = 0$ ) boundary is Neumann (i.e.  $\frac{\partial C_i}{\partial t} = 0$  across the boundary), simulating zero inflow, and the right boundary is open (i.e.  $\frac{\partial C_i}{\partial t}$  before the boundary equals  $\frac{\partial C_i}{\partial t}$  after the boundary), simulating outflow into the WLP. The nucleobase content of the modeled sources are initially homogeneous, but drop sharply to zero at the open boundary (i.e. the initial condition represents an exponentially smoothed step function). This is made to represent the searing of the outermost layer of carbonaceous IDPs and meteorites from atmospheric entry heating.

For part two, the simulation frame is an eccentric 1D convection cell, which loops between the bottom and the top of the WLP (length =  $2r_p$ ). The convection cell is modeled with cyclic boundaries, i.e., continuous nucleobase flow, and no nucleobases exit the convection cell. The initial concentration of nucleobases is a sharp Gaussian beginning at the base of the pond. The width of the spike is  $\sim 1\%$  of the WLP's radius.

Example simulations, including initial conditions, for parts one and two of our nucleobase transport model are plotted in Figure 3.16. Because the time it takes for complete nucleobase outflow from a source, or complete nucleobase homogenization in a WLP, is independent of initial nucleobase abundance, the solution to the diffusion equation at each grid point is displayed as a fraction of the total initial nucleobase concentration. For ease of viewing, part two of the model is displayed in the convection cell's moving frame, with coordinate  $r' = r - u\Delta t$ .

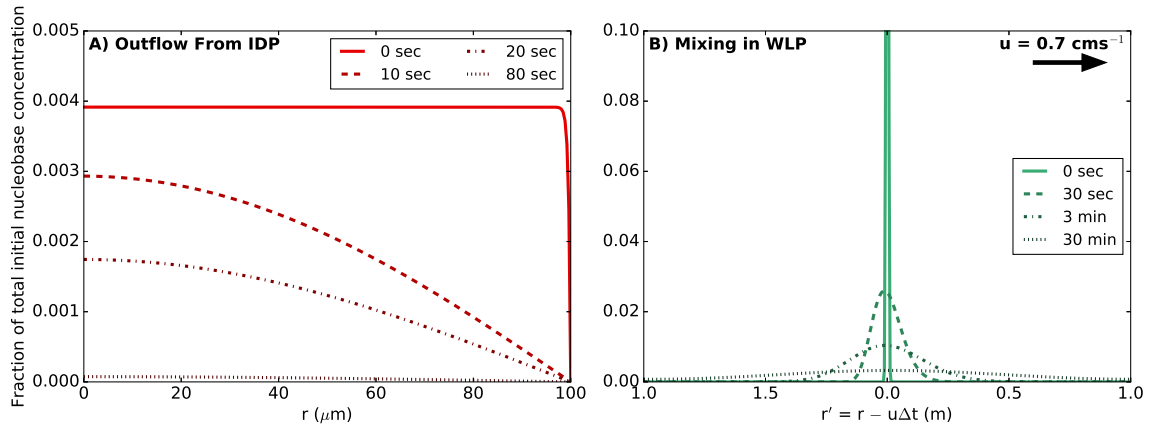


Figure 3.16: Example simulations, including the initial conditions, for our two part nucleobase transport model. Each line represents a different snapshot in time. **(A)** Initially homogeneous nucleobase diffusion from a 100  $\mu\text{m}$ -radius carbonaceous IDP. **(B)** Initially locally concentrated nucleobase mixing in a convection cell within a 1 m-deep WLP. The convection cell is a  $L = 2r_p$  eccentric loop flowing between the bottom to the top of the WLP. This loop is sliced at  $r' = 1$  m in the convection cell's moving frame and unraveled for display in the above 1D plot.

# Chapter 4

## Conclusions & Future Work

The topic of this thesis is on the emergence of the RNA world on the early Earth, with a focus on the time frame and the environmental conditions in which it occurred. These two research focuses are, for the most part, separated into Chapters 2 and 3.

In Chapter 2 we searched the literature and collected all the evidence that could be used to constrain the time interval for the emergence of life. The time interval has two boundaries: a habitability boundary, i.e. the earliest time at which life could exist on the Earth, and a biosignature boundary, i.e. the earliest time at which there is clear evidence that life existed. The habitability boundary is constrained by the formation of the Solar System, the Earth and the Moon, the timescale for the cooling of the Earth's magma ocean, and the possible LHB. The biosignature boundary is constrained by stromatolites, microfossils, light carbon isotopes, the GOE, and molecular phylogenetics. This review lead to the following conclusions:

- Life could have emerged as early as 4.5 Ga, the earliest possible point at which the Earth had a solid crust and stable hydrosphere, and as late as 3.9 Ga, the end of the possible LHB.
- There is still no consensus as to whether the LHB occurred. More evidence is required to sway the consensus in one direction or the other.
- Stromatolites and light carbon isotopes in sedimentary rocks point to the presence of life as early as 3.7 Ga.
- The time it took life to emerge could be as short at 200 Myr, or as long as 800 Myr.

- A 200 Myr timescale for life's emergence, which is only 4% of the total time the Earth has to be habitable, suggests life may have emerged many times within the Galaxy. A 800 Myr timescale for life's emergence, which is 15% of the total time the Earth has to be habitable, suggests life could be a rarer occurrence.

In Chapter 3 we presented a model for the survival and evolution of nucleobases in WLPs, leading to the emergence of nucleotides and their polymerization into RNA. This model functions on the basis of sources and sinks for both pond water and nucleobases. The only source of water is precipitation, and the sinks are evaporation and seepage through pores in the base of the pond. The nucleobase sources are carbonaceous IDPs and meteorites, and the sinks are seepage, hydrolysis and UV photodissociation. Diffusive nucleobase outflow from meteoritic and IDP sources and nucleobase mixing within WLPs are also modeled. To obtain the nucleobase concentration in WLPs over time, we numerically solve the source and sink differential rate equations, where rates are either gathered historically, measured experimentally, or estimated based on the lunar cratering record. We also calculate the expectation value for the number of carbonaceous meteoroids to deposit their fragments into WLPs on the Earth from 4.5–3.7 Ga. To perform this calculation, we use a continental crust growth model, three mass delivery models based on analytical fits to the lunar cratering record, pond and asteroid size and mass distribution functions, and a pond per crustal area similar to today's. The conclusions from these models are summarized below.

- Meteorites, not IDPs, are the key sources of nucleobases that can survive to form nucleotides and RNA within WLPs. Meteorites provide ppb–ppm-level nucleobase concentrations within WLPs for half a year to a few years. Whereas IDPs provide maximum concentrations 10 orders of magnitude lower than those provided by meteorites.
- Nucleotide synthesis in WLPs was fast, as nucleobases are lost to seepage and UV photodissociation within a few years. These loss times are long compared to the hour-to-week-long lab experiments that have successfully synthesized adenosine and AMP [22, 26].
- Nucleotide polymerization into RNA was also fast, occurring within 1–3 wet-dry cycles, as making long chains is a good way to avoid being lost to seepage. This number of wet-dry cycles agrees with nucleotide polymerization experiments [60].

- Seepage can be drastically reduced if nucleotides get encapsulated by vesicles, i.e. 0.5–5 $\mu$ m-diameter lipid bilayer spheres that form upon WLP hydration [284].
- Nucleobases and nucleotides laying at the base of dry WLPs require sediment for protection against destructive UV irradiation. It only takes a  $\sim$ 0.6 mm layer of basaltic sediment to attenuate UV radiation by  $>99.99\%$  [278].
- Approximately 10–3840 carbonaceous meteoroids likely deposited their fragments into WLPs from 4.5–3.7 Ga.
- Our optimal mass-delivery model indicates that the first RNA molecules emerged prior to 4.17 Ga. If the earliest evidences of life from 4.1–4.28 Ga [193, 244, 245] are indeed biological in origin, then the RNA world would have appeared within  $\sim$ 40–300 years after the Earth became habitable.
- The RNA world could have emerged on a cold early Earth subjected to freeze-thaw cycles. Freeze-thaw cycles promote the polymerization of nucleotides via the RNA chaperone effect [314], and ice provides protection from destructive UV radiation and a possible way to avoid nucleobase loss to seepage.

As we move closer to understanding when and how the RNA world emerged on Earth, it becomes clearer that such timescales and processes would not be unique to our solar system. Potentially habitable terrestrial planets exist in many solar systems in the Milky Way [97], and these planets would also have been bombarded by meteoroids at a higher rate during the early stages of their lives. Some of these meteoroids would have initially contained HCN, CO, NH<sub>3</sub> and water in their interiors, leading to the production of nucleobases through universal Fischer-Tropsch-type and HCN-based chemical reactions [42]. If some of these potentially habitable planets are watery and have plate tectonics, they could have formed WLPs on their emerging crusts. Then carbonaceous meteorites could have delivered nucleobases to these environments for subsequent nucleotide and RNA formation. Given 200–800 Myr is required for life as we know it to emerge, only a small fraction of solar systems wouldn't exist long enough to support life (those surrounding short-lived O-, B-, and A- type stars). It is still unknown if an improbable event would need to have occurred on Earth to allow the RNA world to emerge, e.g., there is no evidence to suggest that ribose was delivered to WLPs by the same carbonaceous meteorites that contain nucleobases, perhaps

suggesting a subsequent ribose delivery in a short time interval. However, our estimate of 10–3840 carbonaceous meteoroid deposition events suggests several opportunities were available for nucleobases to react to form nucleotides and RNA in WLPs on the prebiotic Earth.

A formal debate recently occurred at the 2017 Astrobiology Science Conference, where WLPs were compared to hydrothermal vents as sites for the origin of life. No clear winner emerged from this debate, as both sites still have problems. For hydrothermal vents, it is the difficulty of nucleotide polymerization in constant aqueous environments. Only dimers of AMP have been formed in laboratory environments simulating hydrothermal vents [89]. Nucleotide polymerization in WLPs on the other hand is favourable due the periodic wet and dry cycles in such environments. Experiments simulating these wet-dry cycles have polymerized nucleotides into RNA chains possibly  $> 300$  monomers long [58–60]. For WLPs, the major problem is the unknown constant source of organics (although, hydrothermal vents also have this problem with regards to a source of reactive nitrogen [44]). One favourable feature of hydrothermal vents is that they provide a constant source of magmatic  $\text{CO}_2$  [39] and  $\text{H}_2$  from serpentinization [40], which react favourably together to produce methane and acetate, or  $\text{CO}$  and  $\text{H}_2\text{O}$  [39]. WLPs near volcanically active areas however could provide a constant source of  $\text{H}_2$  from the same processes and dissolved  $\text{CO}_2$  from equilibrium with the early atmosphere [34, 51]. Furthermore, a reactive constant source of nitrogen ( $\text{NH}_3$ ) could enter WLPs from a reaction pathway beginning with the oxidation of  $\text{N}_2$  by lightning [63]. This suggests FTT synthesis (Equation 1.1) of nucleobases may be possible within WLPs [36]. HCN-based reactions (Equations A.2–A.5) and formamide reactions (Equation A.6) may also produce nucleobases within WLPs, as a small abundance of atmospheric HCN can dissolve in these environments from the photodissociation products of methane reacting with nitrogen in the atmosphere [41, 63].

The results of Chapter 3 suggests it is improbable that a single pond will have been subjected to more than one meteorite deposition event. But is a single deposition of concentrated nucleobases enough to kick-start the RNA world? For future work, I am interested to expand the WLP model developed in Chapter 3 to include a non-equilibrium chemical reaction network. This network will include FTT, HCN-based, and formamide-based synthesis of nucleobases [36], and will help us constrain the concentrations of nucleobases that can be reached in WLPs in absence of meteoritic

sources.

Finally, we showed in Chapter 3 that RNA polymers emerged rapidly in WLPs, thus the natural next step is to understand how ribozymes emerged. Damer & Deamer [284] describe a model where the coupled wet-dry phases of ponds allow for selection of RNA polymers by their encapsulation in vesicles. During the dry phase, lipids accumulate at the sides and bases of ponds, creating a multi-layered biofilm. This biofilm clogs up rock pores, and allows RNA to accumulate between layers. Upon rewetting, layers fold upwards creating vesicles that contain concentrated solutions of RNA polymers. Favourable RNA polymers, e.g. polymers that stabilize the lipid membrane, can then be selected by remaining within the vesicles until subsequent drying, where they can be redistributed into the next generation. These cycles would occur indefinitely, leading to the selection of ribozymes, and to increasingly complex systems.

To gauge whether this model is likely, in future work, we intend to calculate the area of WLPs that can be covered in layered fatty acid biofilms from meteorite sources. Carboxylic acids with straight-chain and branch-chain structures ranging from 2–12 carbon atoms have been measured in various carbon-rich meteorites with abundances from  $10^{-4}$ –10 % [71, 315, 316]. Thus it is conceivable that the meteoritic sources that delivered prebiotic nucleobases could have also delivered the prebiotic fatty acids that produced the first protocells.



# Bibliography

- [1] Oldroyd D. R. “Charles Darwin’s theory of evolution: A review of our present understanding”. In: *Biol Philos* 1 (1986), pp. 133–168 (cit. on p. 1).
- [2] R. Shapiro. “The Oparin-Haldane Hypothesis”. In: *Origins: A Skeptic’s Guide to the Creation of Life on Earth*. Toronto: Bantam Books, 1987, pp. 109–111 (cit. on p. 1).
- [3] S. A. Benner. “Defining Life”. In: *Astrobiology* 10 (2010-12), pp. 1021–1030. DOI: 10.1089/ast.2010.0524 (cit. on pp. 1, 3).
- [4] C. Woese. “The genetic code”. In: New York: Harper and Row, 1967, p. 179 (cit. on p. 2).
- [5] F. H. C. Orgel. “Evolution of the genetic apparatus”. In: *J Mol Biol* 38 (1968), p. 381 (cit. on p. 2).
- [6] F. H. C. Crick. “The Origin of the Genetic Code”. In: *J Mol Biol* 38 (1968), p. 367 (cit. on p. 2).
- [7] W. Gilbert. “Origin of life: The RNA world”. In: *Nature* 319 (1986-02), p. 618. DOI: 10.1038/319618a0 (cit. on pp. 2, 58).
- [8] M. Neveu, H.-J. Kim, and S. A. Benner. “The “Strong” RNA World Hypothesis: Fifty Years Old”. In: *Astrobiology* 13 (2013-04), pp. 391–403. DOI: 10.1089/ast.2012.0868 (cit. on pp. 2, 4, 33, 54, 146).
- [9] P. G. Higgs and N. Lehman. “The RNA World: molecular cooperation at the origins of life”. In: *Nat Rev Genet* 16 (2015), pp. 7–17 (cit. on p. 2).
- [10] Blausen.com staff. “Medical gallery of Blausen Medical 2014”. In: *WikiJournal of Medicine* 1 () (cit. on p. 2).

- [11] Pinterest. *Explore Amino Acid Sequence, Nucleic Acid, and more!* 2017-06. URL: <https://www.pinterest.com/pin/503347695822737964/> (cit. on p. 2).
- [12] D. A. Drummond and C. O. Wilke. “The evolutionary consequences of erroneous protein synthesis”. In: *Nat Rev Genet* 10 (2009), pp. 715–724 (cit. on p. 3).
- [13] M. Kreysing, L. Keil, S. Lanzmich, and D. Braun. “Heat flux across an open pore enables the continuous replication and selection of oligonucleotides towards increasing length”. In: *Nat Chem* 7 (2015), pp. 203–208 (cit. on p. 4).
- [14] J. Pampel. *Polymerases*. 2016-03. URL: <http://www.genomics-online.com/resources/16/5013/polymerases/> (cit. on p. 4).
- [15] J. Attwater, A. Wochner, and P. Holliger. “In-ice evolution of RNA polymerase ribozyme activity”. In: *Nat Chem* 5 (2013), pp. 1011–1018 (cit. on pp. 4, 33).
- [16] A. Wochner, J. Attwater, A. Coulson, and P. Holliger. “Ribozyme-Catalyzed Transcription of an Active Ribozyme”. In: *Science* 332 (2011), pp. 209–212 (cit. on p. 4).
- [17] T. A. Lincoln and G. F. Joyce. “Self-Sustained Replication of an RNA Enzyme”. In: *Science* 323 (2009), pp. 1229–1232 (cit. on p. 5).
- [18] Y. E. Kim and P. G. Higgs. “Co-operation between Polymerases and Nucleotide Synthetases in the RNA World”. In: *PLoS Comput Biol* 12 (2016), e1005161 (cit. on p. 5).
- [19] A. S. Tupper and P. G. Higgs. “Error Thresholds for RNA Replication in the Presence of Both Point Mutations and Premature Termination Errors”. In: *Life, submitted* () (cit. on p. 5).
- [20] McKay C. P. “What Is Life—and How Do We Search for It in Other Worlds?” In: *PLoS Biol* 2 (2004), e302 (cit. on p. 6).
- [21] M. W. Powner, B. Gerland, and J. D. Sutherland. “Synthesis of activated pyrimidine ribonucleotides in prebiotically plausible conditions”. In: *Nature* 459 (2009-05), pp. 239–242 (cit. on p. 6).
- [22] C. Ponnampertuma, C. Sagan, and R. Mariner. “Synthesis of Adenosine Triphosphate Under Possible Primitive Earth Conditions”. In: *Nature* 199 (1963-07), pp. 222–226. DOI: 10.1038/199222a0 (cit. on pp. 6, 58, 68, 106).

- [23] C. Ponnampereuma, R. Mariner, and C. Sagan. “Formation of Adenosine by Ultra-violet Irradiation of a Solution of Adenine and Ribose”. In: *Nature* 198 (1963-06), pp. 1199–1200. DOI: 10.1038/1981199a0 (cit. on p. 6).
- [24] W. D. Fuller, R. A. Sanchez, and L. E. Orgel. “Studies in Prebiotic Synthesis VI. Synthesis of Purine Nucleosides”. In: *J Mol Biol* 67 (1972), pp. 25–33 (cit. on p. 6).
- [25] C. Ponnampereuma and R. Mack. “Nucleotide Synthesis under Possible Primitive Earth Conditions”. In: *Science* 148 (1965-05), pp. 1221–1223. DOI: 10.1126/science.148.3674.1221 (cit. on p. 6).
- [26] M. Gull, M. A. Mojica, F. M Fernández, D. A. Gaul, T. M. Orlando, C. L. Liotta, and M. A. Pasek. “Nucleoside phosphorylation by the mineral schreibersite”. In: *Sci Rep* 5 (2015), p. 17198 (cit. on pp. 6, 58, 68, 106).
- [27] A. Beck, R. Lohrmann, and L. E. Orgel. “Phosphorylation with inorganic phosphates at moderate temperatures”. In: *Science* 157 (1967), p. 952 (cit. on p. 6).
- [28] R. Lohrmann and L. E. Orgel. “Prebiotic Synthesis: Phosphorylation in Aqueous Solution”. In: *Science* 161 (1968-07), pp. 64–66. DOI: 10.1126/science.161.3836.64 (cit. on p. 6).
- [29] J. Rabinowitz, S. Chang, and C. Ponnampereuma. “Phosphorylation on the Primitive Earth: Phosphorylation by way of Inorganic Phosphate as a Potential Prebiotic Process”. In: *Nature* 218 (1968-05), pp. 442–443. DOI: 10.1038/218442a0 (cit. on p. 6).
- [30] R. Lohrmann and L. E. Orgel. “Urea-Inorganic Phosphate Mixtures as Prebiotic Phosphorylating Agents”. In: *Science* 171 (1971-02), pp. 490–494. DOI: 10.1126/science.171.3970.490 (cit. on p. 6).
- [31] R. Österberg, L. E. Orgel, and R. Lohrmann. “Further Studies of Urea-Catalyzed Phosphorylation Reactions”. In: *J Mol Evol* 2 (1973), pp. 231–234 (cit. on p. 6).
- [32] R. Reimann and G. Zubay. “Nucleoside Phosphorylation: A Feasible Step in the Prebiotic Pathway to RNA”. In: *Orig Life Evol Biosph* 29 (1999-05), pp. 229–247 (cit. on p. 6).

- [33] C. Chyba and C. Sagan. “Endogenous production, exogenous delivery and impact-shock synthesis of organic molecules: an inventory for the origins of life”. In: *Nature* 355 (1992-01), pp. 125–132. DOI: 10.1038/355125a0 (cit. on pp. 6, 7, 12–14, 36, 58, 61, 88).
- [34] D. Trail, E. B. Watson, and N. D. Tailby. “The oxidation state of Hadean magmas and implications for early Earth’s atmosphere”. In: *Nature* 480 (2011), pp. 79–82 (cit. on pp. 7, 9, 58, 108, 145).
- [35] D. C. Catling. “Planetary Atmospheres”. In: *Physics of Terrestrial Planets and Moons*. Ed. by G. Schubert. Treatise on Geophysics, 2nd Ed. Oxford: Elsevier, 2015, pp. 429–472 (cit. on p. 7).
- [36] B. K. D. Pearce and R. E. Pudritz. “Seeding the Pregenetic Earth: Meteoritic Abundances of Nucleobases and Potential Reaction Pathways”. In: *Astrophys J* 807 (2015-07), p. 85 (cit. on pp. 7, 8, 10–12, 15, 36, 59, 61, 88, 108).
- [37] D. P. Zaleski, N. A. Seifert, A. L. Steber, M. T. Muckle, R. A. Loomis, J. F. Corby, O. Martinez Jr., K. N. Crabtree, P. R. Jewell, J. M. Hollis, F. J. Lovas, D. Vasquez, J. Nyiramahirwe, N. Sciortino, K. Johnson, M. C. McCarthy, A. J. Remijan, and B. H. Pate. “Detection of E-Cyanomethanimine toward Sagittarius B2(N) in the Green Bank Telescope PRIMOS Survey”. In: *Astrophys J Lett* 765, L10 (2013-03), p. L10. DOI: 10.1088/2041-8205/765/1/L10 (cit. on p. 7).
- [38] G. R. Adande, N. J. Woolf, and L. M. Ziurys. “Observations of Interstellar Formamide: Availability of a Prebiotic Precursor in the Galactic Habitable Zone”. In: *Astrobiology* 13 (2013-05), pp. 439–453. DOI: 10.1089/ast.2012.0912 (cit. on p. 7).
- [39] W. Martin, J. Baross, D. Kelley, and M. J. Russell. “Hydrothermal vents and the origin of life”. In: *Nat Rev Microbiol* 6 (2008), pp. 805–814 (cit. on pp. 8, 108).
- [40] L. E. Mayhew, E. T. Ellison, T. M. McCollom, T. P. Trainor, and A. S. Templeton. “Hydrogen generation from low-temperature water-rock reactions”. In: *Nature Geosci* 6 (2013-06), pp. 478–484. DOI: 10.1038/ngeo1825 (cit. on pp. 8, 108, 145).

- [41] C. Konn, J. L. Charlou, N. G. Holm, and O. Mousis. “The Production of Methane, Hydrogen, and Organic Compounds in Ultramafic-Hosted Hydrothermal Vents of the Mid-Atlantic Ridge”. In: *Astrobiology* 15 (2015-05), pp. 381–399. DOI: 10.1089/ast.2014.1198 (cit. on pp. 8, 108, 145, 146).
- [42] B. K. D. Pearce and R. E. Pudritz. “Meteorites and the RNA World: A Thermodynamic Model of Nucleobase Synthesis within Planetesimals”. In: *Astrobiology* 16 (2016-11), pp. 853–872 (cit. on pp. 8, 11–13, 59, 91, 99, 107, 145, 146).
- [43] GNS Science, Te Pu Ao. *Hydrothermal Vents*. 2017-06. URL: <https://www.gns.cri.nz/Home/Learning/Science-Topics/Ocean-Floor/Undersea-New-Zealand/Hydrothermal-Vents> (cit. on p. 8).
- [44] M. A. A. Schoonen and Y. Xu. “Nitrogen Reduction Under Hydrothermal Vent Conditions: Implications for the Prebiotic Synthesis of C-H-O-N Compounds”. In: *Astrobiology* 1 (2001-06), pp. 133–142. DOI: 10.1089/153110701753198909 (cit. on pp. 9, 59, 108).
- [45] T. M. McCollom. “Miller-Urey and Beyond: What Have We Learned About Prebiotic Organic Synthesis Reactions in the Past 60 Years?” In: *Annu Rev Earth Planet Sci* 41 (2013), pp. 207–229 (cit. on pp. 9, 10).
- [46] S. L. Miller. “Current Status of the Prebiotic Synthesis of Small Molecules”. In: *Chem Scr* 26B (1986), pp. 5–11 (cit. on p. 9).
- [47] M. Ferus, F. Pietrucci, A. M. Saitta, A. Knižek, P. Kubelík, O. Ivanek, V. Shestivska, and S. Civiš. “The evolutionary consequences of erroneous protein synthesis”. In: *Nat Rev Genet* 10 (2009), pp. 715–724 (cit. on p. 9).
- [48] S. Miyakawa, K.-I. Murasawa, K. Kobayashi, and A. B. Sawaoka. “Abiotic Synthesis of Guanine with High-Temperature Plasma”. In: *Orig Life Evol Biosph* 30 (2000-12), pp. 557–566 (cit. on p. 9).
- [49] S. Miyakawa, K. Murasawa, K. Kobayashi, and A. B. Sawaoka. “Cytosine and Uracil Synthesis by Quenching with High-Temperature Plasma”. In: *J Am Chem Soc* 121 (1999), pp. 8144–8145 (cit. on p. 9).
- [50] S. Yuasa, D. Flory, B. Basile, and J. Oró. “Abiotic Synthesis of Purines and Other Heterocyclic Compounds by the Action of Electrical Discharges”. In: *J Mol Evol* 21 (1984-02), pp. 76–80 (cit. on p. 9).

- [51] S. Rugheimer, A. Segura, L. Kaltenegger, and D. Sasselov. “UV Surface Environment of Earth-like Planets Orbiting FGKM Stars through Geological Evolution”. In: *Astrophys J* 806, 137 (2015-06), p. 137. DOI: 10.1088/0004-637X/806/1/137 (cit. on pp. 9, 55, 64, 85, 108, 145).
- [52] C. S. Cockell, D. C. Catling, W. L. Davis, K. Snook, R. L. Kepner, P. Lee, and C. P. McKay. “The Ultraviolet Environment of Mars: Biological Implications Past, Present, and Future”. In: *Icarus* 146 (2000-08), pp. 343–359. DOI: 10.1006/icar.2000.6393 (cit. on p. 9).
- [53] C. E. Boyd. “Pond Evaporation”. In: *Trans Am Fish Soc* 114 (1985), pp. 299–303 (cit. on pp. 10, 61, 72, 81).
- [54] C. E. Boyd. “Hydrology of Small Experimental Fish Ponds at Auburn, Alabama”. In: *Trans Am Fish Soc* 111 (1982), pp. 638–644 (cit. on pp. 10, 14, 61, 64, 68, 81).
- [55] N. H. Sleep. “The Hadean-Archaean environment”. In: *Cold Spring Harbor Perspect. Biol.* 2 (2010-05), a002527 (cit. on pp. 10, 14, 33, 63, 70).
- [56] C. S. Cockell. *Astrobiology: Understanding Life in the Universe*. New Jersey: Wiley-Blackwell, 2015, p. 187 (cit. on pp. 10, 63, 83).
- [57] W. R. Berghuijs and R. A. Woods. “A simple framework to quantitatively describe monthly precipitation and temperature climatology”. In: *Int J Climatol* 36 (2016), pp. 3161–3174 (cit. on pp. 10, 61, 63, 66, 82).
- [58] S. Rajamani, A. Vlassov, S. Benner, A. Coombs, F. Olasagasti, and D. Deamer. “Lipid-assisted Synthesis of RNA-like Polymers from Mononucleotides”. In: *Orig Life Evol Biosph* 38 (2008-02), pp. 57–74. DOI: 10.1007/s11084-007-9113-2 (cit. on pp. 10, 108).
- [59] V. DeGuzman, W. Vercoutere, H. Shenasa, and D. Deamer. “Generation of Oligonucleotides Under Hydrothermal Conditions by Non-enzymatic Polymerization”. In: *J Mol Evol* 78 (2014), pp. 251–262 (cit. on pp. 10, 108).
- [60] L. Da Silva, M.-C. Maurel, and D. Deamer. “Salt-Promoted Synthesis of RNA-like Molecules in Simulated Hydrothermal Conditions”. In: *J Mol Evol* 80 (2015), pp. 86–97 (cit. on pp. 10, 13, 58, 59, 69, 106, 108).

- [61] P. A. Bland, T. B. Smith, A. J. T. Jull, F. J. Berry, A. W. R. Bevan, S. Cloudt, and C. T. Pillinger. “The flux of meteorites to the Earth over the last 50,000 years”. In: *Mon Not R Astron Soc* 283 (1996-12), p. 551. DOI: 10.1093/mnras/283.2.551 (cit. on pp. 11, 58).
- [62] Y. Furukawa, H. Nakazawa, T. Sekine, T. Kobayashi, and T. Kakegawa. “Nucleobase and amino acid formation through impacts of meteorites on the early ocean”. In: *Earth Planet Sci Lett* 429 (2015-11), pp. 216–222. DOI: 10.1016/j.epsl.2015.07.049 (cit. on p. 11).
- [63] D. Catling and J. F. Kasting. “Planetary atmospheres and life”. In: *Planets and life - the emerging science of astrobiology*. Ed. by W. T. Sullivan, III and J. A. Baross. Cambridge: Cambridge University Press, 2007, pp. 91–116 (cit. on pp. 11, 108, 145, 146).
- [64] M. Ferus, D. Nesvorný, J. Šponer, P. Kubelík, R. Michalčíková, V. Shestivská, J. E. Šponer, and S. Civiš. “High-energy chemistry of formamide: A unified mechanism of nucleobase formation”. In: *Proc Nat Acad Sci* 112 (2015-01), pp. 657–662. DOI: 10.1073/pnas.1412072111 (cit. on p. 11).
- [65] K. Righter and D. P. O’Brien. “Cosmochemistry Special Feature: Terrestrial planet formation”. In: *Proceedings of the National Academy of Science* 108 (2011-11), pp. 19165–19170. DOI: 10.1073/pnas.1013480108 (cit. on pp. 11, 19, 27).
- [66] J. G. Hills and M. P. Goda. “The fragmentation of small asteroids in the atmosphere”. In: *Astron J* 105 (1993-03), pp. 1114–1144. DOI: 10.1086/116499 (cit. on pp. 11, 63, 72, 90).
- [67] T. Kenkmann, N. A. Artemieva, K. Wünnemann, M. H. Poelchau, D. Elbehausen, and H. Núñez Del Prado. “The Carancas meteorite impact crater, Peru: Geologic surveying and modeling of crater formation and atmospheric passage”. In: *Meteoritics* 44 (2009-08), pp. 985–1000. DOI: 10.1111/j.1945-5100.2009.tb00783.x (cit. on pp. 12, 72).
- [68] A. K. Cobb and R. E. Pudritz. “Nature’s Starships. I. Observed Abundances and Relative Frequencies of Amino Acids in Meteorites”. In: *Astrophys J* 783, 140 (2014-03), p. 140. DOI: 10.1088/0004-637X/783/2/140 (cit. on pp. 12, 36).

- [69] D. P. Glavin, M. P. Callahan, J. P. Dworkin, and J. E. Elsila. “The effects of parent body processes on amino acids in carbonaceous chondrites”. In: *Meteorit Planet Sci* 45 (2010-12), pp. 1948–1972. DOI: 10.1111/j.1945-5100.2010.01132.x (cit. on p. 12).
- [70] M. P. Callahan, K. E. Smith, H. J. Cleaves, J. Ruzicka, J. C. Stern, D. P. Glavin, C. H. House, and J. P. Dworkin. “Carbonaceous meteorites contain a wide range of extraterrestrial nucleobases”. In: *Proc Natl Acad Sci USA* 108 (2011-08), pp. 13995–13998. DOI: 10.1073/pnas.1106493108 (cit. on pp. 12, 15, 36, 59, 64).
- [71] S. Pizzarello, D. L. Schrader, A. A. Monroe, and D. S. Lauretta. “Large enantiomeric excesses in primitive meteorites and the diverse effects of water in cosmochemical evolution”. In: *Proc Nat Acad Sci* 109 (2012-07), pp. 11949–11954. DOI: 10.1073/pnas.1204865109 (cit. on pp. 12, 36, 109).
- [72] L. M. V. Martel. *Better Know a Meteorite Collection: Natural History Museum, London, United Kingdom*. 2009-07. URL: <http://www.psrh.hawaii.edu/July09/Meteorites.London.Museum.html> (cit. on p. 12).
- [73] M. Richmond. *The Interstellar Medium: Dust*. 2017-06. URL: [http://www.star.ucl.ac.uk/~msw/teaching/PHAS2521/ism\\_dust\\_files/ism\\_dust.html](http://www.star.ucl.ac.uk/~msw/teaching/PHAS2521/ism_dust_files/ism_dust.html) (cit. on p. 12).
- [74] S. Messenger. “Opportunities for the stratospheric collection of dust from short-period comets”. In: *Meteorit Planet Sci* 37 (2002-11), pp. 1491–1506. DOI: 10.1111/j.1945-5100.2002.tb00806.x (cit. on p. 12).
- [75] G. Matrajt, D. Brownlee, M. Sadilek, and L. Kruse. “Survival of organic phases in porous IDPs during atmospheric entry: A pulse-heating study”. In: *Meteoritics* 41 (2006-06), pp. 903–911. DOI: 10.1111/j.1945-5100.2006.tb00494.x (cit. on pp. 12, 85, 88).
- [76] M. Nuevo, C. K. Materese, and S. A. Sandford. “The Photochemistry of Pyrimidine in Realistic Astrophysical Ices and the Production of Nucleobases”. In: *Astrophys J* 793, 125 (2014-10), p. 125. DOI: 10.1088/0004-637X/793/2/125 (cit. on pp. 13, 59, 85, 89).

- [77] G. M. Muñoz Caro, U. J. Meierhenrich, W. A. Schutte, B. Barbier, A. Arcones Segovia, H. Rosenbauer, W. H.-P. Thiemann, A. Brack, and J. M. Greenberg. “Amino acids from ultraviolet irradiation of interstellar ice analogues”. In: *Nature* 416 (2002-03), pp. 403–406. DOI: 10.1038/416403a (cit. on p. 13).
- [78] V. N. Salinas, M. R. Hogerheijde, E. A. Bergin, L. I. Cleaves, C. Brinch, G. A. Blake, D. C. Lis, G. J. Melnick, O. Panić, J. C. Pearson, L. Kristensen, U. A. Yıldız, and E. F. van Dishoeck. “First detection of gas-phase ammonia in a planet-forming disk.  $\text{NH}_3$ ,  $\text{N}_2\text{H}^+$ , and  $\text{H}_2\text{O}$  in the disk around TW Hydrae”. In: *Astron Astrophys* 591, A122 (2016-06), A122. DOI: 10.1051/0004-6361/201628172 (cit. on pp. 13, 59).
- [79] J. F. Gómez, J. Trapero, S. Pascual, N. Patel, C. Morales, and J. M. Torrelles. “Ammonia observations of the nearby molecular cloud MBM 12”. In: *Mon Not R Astron Soc* 314 (2000-06), pp. 743–746. DOI: 10.1046/j.1365-8711.2000.03346.x. eprint: astro-ph/0001175 (cit. on p. 13).
- [80] L. E. Snyder and D. Buhl. “Observations of Radio Emission from Interstellar Hydrogen Cyanide”. In: *Astrophys J Lett* 163 (1971-01), p. L47. DOI: 10.1086/180664 (cit. on p. 13).
- [81] C. Walsh, H. Nomura, T. J. Millar, and Y. Aikawa. “Chemical Processes in Protoplanetary Disks. II. On the Importance of Photochemistry and X-Ray Ionization”. In: *Astrophys J* 747, 114 (2012-03), p. 114. DOI: 10.1088/0004-637X/747/2/114 (cit. on p. 13).
- [82] K. R. Schwarz and E. A. Bergin. “The Effects of Initial Abundances on Nitrogen in Protoplanetary Disks”. In: *Astrophys J* 797, 113 (2014-12), p. 113. DOI: 10.1088/0004-637X/797/2/113 (cit. on p. 13).
- [83] I. Pascucci, D. Apai, K. Luhman, T. Henning, J. Bouwman, M. R. Meyer, F. Lahuis, and A. Natta. “The Different Evolution of Gas and Dust in Disks around Sun-Like and Cool Stars”. In: *Astrophys J* 696 (2009-05), pp. 143–159. DOI: 10.1088/0004-637X/696/1/143 (cit. on pp. 13, 59).
- [84] J. Castillo-Rogez, T. V. Johnson, M. H. Lee, N. J. Turner, D. L. Matson, and J. Lunine. “ $^{26}\text{Al}$  decay: Heat production and a revised age for Iapetus”. In: *Icarus* 204 (2009-12), pp. 658–662. DOI: 10.1016/j.icarus.2009.07.025 (cit. on p. 13).

- [85] T. Lichtenberg, G. J. Golabek, T. V. Gerya, and M. R. Meyer. “The effects of short-lived radionuclides and porosity on the early thermo-mechanical evolution of planetesimals”. In: *Icarus* 274 (2016-08), pp. 350–365 (cit. on p. 13).
- [86] B. J. Travis and G. Schubert. “Hydrothermal convection in carbonaceous chondrite parent bodies”. In: *Earth Planet Sci Lett* 240 (2005-12), pp. 234–250. DOI: 10.1016/j.epsl.2005.09.008 (cit. on p. 13).
- [87] P. Higgs. “The Effect of Limited Diffusion and Wet-Dry Cycling on Reversible Polymerization Reactions: Implications for Prebiotic Synthesis of Nucleic Acids”. In: *Life* 6 (2016), p. 24 (cit. on p. 13).
- [88] M. Skilandat and R. K. O. Sigel. “Ribozymes”. In: *Brenner’s Encyclopedia of Genetics*. Ed. by S. Maloy and K. Hughes. 2nd. Amsterdam: Elsevier, 2013, pp. 254–258 (cit. on p. 13).
- [89] B. T. Burcar, L. M. Barge, D. Trail, E. B. Watson, M. J. Russell, and L. B. McGown. “RNA Oligomerization in Laboratory Analogues of Alkaline Hydrothermal Vent Systems”. In: *Astrobiology* 15 (2015-07), pp. 509–522. DOI: 10.1089/ast.2014.1280 (cit. on pp. 13, 59, 108).
- [90] M. Levy and S. L. Miller. “The stability of the RNA bases: Implications for the origin of life”. In: *Proc Natl Acad Sci USA* 93 (1998-07), pp. 7933–7938 (cit. on pp. 14, 61, 64, 83).
- [91] O. Poch, M. Jaber, F. Stalport, S. Nowak, T. Georgelin, J.-F. Lambert, C. Szopa, and P. Coll. “Effect of Nontronite Smectite Clay on the Chemical Evolution of Several Organic Molecules under Simulated Martian Surface Ultraviolet Radiation Conditions”. In: *Astrobiology* 15 (2015-03), pp. 221–237. DOI: 10.1089/ast.2014.1230 (cit. on pp. 14, 61, 64, 69, 83).
- [92] A. Tugrul. “Change in pore size distribution due to weathering of basalts and its engineering significance”. In: *Engineering Geology and the Environment*. Ed. by P. G. Marinos, G. C. Koukis, G. C. Tsiambaos, and G. C. Stournaras. Vol. 1. Proceedings International Symposium on Engineering Geology and the Environment. Rotterdam: Balkema, 1997, pp. 71–90 (cit. on pp. 14, 68).
- [93] J. R. Nimmo. “Porosity and Pore Size Distribution”. In: *Encyclopedia of Soils in the Environment, Vol. 3*. Ed. by D. Hillel. London: Elsevier, 2004, pp. 295–303 (cit. on p. 14).

- [94] S. Horikoshi, N. Serpone, S. Yoshizawa, J. Knowland, and H. Hidaka. “Photocatalyzed degradation of polymers in aqueous semiconductor suspensions. IV Theoretical and experimental examination of the photooxidative mineralization of constituent bases in nucleic acids at titania/water interfaces”. In: *J Photochem Photobiol A Chem* 120 (1999), pp. 63–74 (cit. on p. 15).
- [95] E. D. Khan. *DNA Damage*. 2014-10. URL: <https://biotechkhan.wordpress.com/2014/10/14/dna-damage/> (cit. on p. 15).
- [96] J. D. Roberts and M. C. Caserio. “Photochemistry”. In: *Basic Principles of Organic Chemistry, 2nd Ed.* Menlo Park: W. A. Benjamin, Inc., 1977, pp. 1371–1418 (cit. on pp. 15–17).
- [97] Planetary Habitability Laboratory. *Habitable Exoplanets Catalog*. 2017-04. URL: <http://phl.upr.edu/projects/habitable-exoplanets-catalog> (cit. on pp. 17, 18, 107).
- [98] M. Alessi, R. E. Pudritz, and A. J. Cridland. “On the formation and chemical composition of super Earths”. In: *Mon Not R Astron Soc* 464 (2017-01), pp. 428–452. DOI: 10.1093/mnras/stw2360 (cit. on p. 17).
- [99] L. M. Weiss and G. W. Marcy. “The Mass-Radius Relation for 65 Exoplanets Smaller than 4 Earth Radii”. In: *Astrophys J Lett* 783, L6 (2014-03), p. L6. DOI: 10.1088/2041-8205/783/1/L6 (cit. on p. 18).
- [100] L. A. Rogers. “Most 1.6 Earth-radius Planets are Not Rocky”. In: *Astrophys J* 801, 41 (2015-03), p. 41. DOI: 10.1088/0004-637X/801/1/41 (cit. on p. 18).
- [101] K. J. Zahnle. “Earth’s Earliest Atmosphere”. In: *Elements* 2 (2006), pp. 217–222 (cit. on p. 18).
- [102] M. T. Rosing. “<sup>13</sup>C-Depleted Carbon Microparticles in >3700-Ma Sea-Floor Sedimentary Rocks from West Greenland”. In: *Science* 283 (1999-01), p. 674. DOI: 10.1126/science.283.5402.674 (cit. on pp. 18, 25, 46, 48, 50, 53).
- [103] Y. Ohtomo, T. Kakegawa, A. Ishida, T. Nagase, and M. T. Rosing. “Evidence for biogenic graphite in early Archaean Isua metasedimentary rocks”. In: *Nature Geosci* 7 (2014), pp. 25–28 (cit. on pp. 18, 25, 48, 50, 55, 58, 70).

- [104] A. P. Nutman, V. C. Bennett, C. R. L. Friend, M. J. Van Kranendonk, and A. R. Chivas. “Rapid emergence of life shown by discovery of 3,700-million-year-old microbial structures”. In: *Nature* 537 (2016-09), pp. 535–538 (cit. on pp. 18, 25, 41–43, 55, 58, 70).
- [105] L. D. Deming and S. Seager. “Illusion and reality in the atmospheres of exoplanets”. In: *J Geophys Res Planets* 122 (2017-01), pp. 53–75. DOI: 10.1002/2016JE005155 (cit. on p. 18).
- [106] A. Tsiaras, M. Rocchetto, I. P. Waldmann, O. Venot, R. Varley, G. Morello, M. Damiano, G. Tinetti, E. J. Barton, S. N. Yurchenko, and J. Tennyson. “Detection of an Atmosphere Around the Super-Earth 55 Cancri e”. In: *Astrophys J* 820, 99 (2016-04), p. 99. DOI: 10.3847/0004-637X/820/2/99 (cit. on p. 18).
- [107] J. Southworth, L. Mancini, N. Madhusudhan, P. Mollière, S. Ciceri, and T. Henning. “Detection of the Atmosphere of the 1.6  $M_{\oplus}$  Exoplanet GJ 1132 b”. In: *Astron J* 153, 191 (2017-04), p. 191. DOI: 10.3847/1538-3881/aa6477 (cit. on p. 18).
- [108] N. B. Cowan, T. Greene, D. Angerhausen, N. E. Batalha, M. Clampin, K. Colón, I. J. M. Crossfield, J. J. Fortney, B. S. Gaudi, J. Harrington, N. Iro, C. F. Lillie, J. L. Linsky, M. Lopez-Morales, A. M. Mandell, and K. B. Stevenson. “Characterizing Transiting Planet Atmospheres through 2025”. In: *Publ Astron Soc Pac* 127 (2015-03), p. 311. DOI: 10.1086/680855 (cit. on p. 18).
- [109] A. Dutrey, D. Semenov, E. Chapillon, U. Gorti, S. Guilloteau, F. Hersant, M. Hogerheijde, M. Hughes, G. Meeus, H. Nomura, V. Piétu, C. Qi, and V. Wakelam. “Physical and Chemical Structure of Planet-Forming Disks Probed by Millimeter Observations and Modeling”. In: *Protostars and Planets VI*. Ed. by H. Beuther, R. S. Klessen, C. P. Dullemond, and T. Henning. Tucson: University of Arizona Press, 2014, pp. 317–338 (cit. on pp. 19, 26).
- [110] E. W. Schwieterman, N. Y. Kiang, M. N. Parenteau, C. E. Harman, S. DasSarma, T. M. Fisher, G. N. Arney, H. E. Hartnett, C. T. Reinhard, S. L. Olson, V. S. Meadows, C. S. Cockell, S. I. Walker, J. L. Grenfell, S. Hegde, S. Rugheimer, R. Hu, and T. W. Lyons. “Exoplanet Biosignatures: A Review of Remotely Detectable Signs of Life”. In: *ArXiv e-prints* (2017-05). arXiv: 1705.05791 [astro-ph.EP] (cit. on p. 19).

- [111] D. S. Spiegel, J. J. Fortney, and C. Sotin. “Structure of exoplanets”. In: *Proc Nat Acad Sci* 111 (2014-09), pp. 12622–12627. DOI: 10.1073/pnas.1304206111 (cit. on p. 19).
- [112] J. W. Schopf. “The first billion years: when did life emerge?” In: *Elements 2* (2006), pp. 229–233 (cit. on p. 23).
- [113] R. Buick. “The earliest records of life on Earth”. In: *Planets and Life*. Ed. by W. T. Sullivan and J. A. Baross. Cambridge: Cambridge University Press, 2007, pp. 237–264 (cit. on p. 23).
- [114] K. Zahnle, N. Arndt, C. Cockell, A. Halliday, E. Nisbet, F. Selsis, and N. H. Sleep. “Emergence of a Habitable Planet”. In: *Space Sci Rev* 129 (2007-03), pp. 35–78. DOI: 10.1007/s11214-007-9225-z (cit. on pp. 23, 25, 28–33, 35–37, 63, 69, 70, 73, 79).
- [115] M. Gargaud, H. Martin, P. López-García, T. Montmerle, and R. Pascal. *Young Sun, Early Earth and the Origins of Life*. Berlin: Springer-Verlag, 2012 (cit. on p. 23).
- [116] G. F. Joyce. “The antiquity of RNA-based evolution”. In: *Nature* 418 (2002-07), pp. 214–221. DOI: 10.1038/418214a (cit. on p. 23).
- [117] A. Bouvier and M. Wadhwa. “The age of the Solar System redefined by the oldest Pb-Pb age of a meteoritic inclusion”. In: *Nature Geosci* 3 (2010-09), pp. 637–641. DOI: 10.1038/ngeo941 (cit. on pp. 25, 27).
- [118] Q. Yin, S. B. Jacobsen, K. Yamashita, J. Blichert-Toft, P. Télouk, and F. Albarède. “A short timescale for terrestrial planet formation from Hf-W chronometry of meteorites”. In: *Nature* 418 (2002-08), pp. 949–952. DOI: 10.1038/nature00995 (cit. on pp. 25, 28).
- [119] M. Touboul, T. Kleine, B. Bourdon, H. Palme, and R. Wieler. “Late formation and prolonged differentiation of the Moon inferred from W isotopes in lunar metals”. In: *Nature* 450 (2007-12), pp. 1206–1209. DOI: 10.1038/nature06428 (cit. on pp. 25, 28, 29).
- [120] A. N. Halliday. “A young Moon-forming giant impact at 70-110 million years accompanied by late-stage mixing, core formation and degassing of the Earth”. In: *Philos Trans R Soc Lond A* 366 (2008), pp. 4163–4181 (cit. on pp. 25, 28, 29).

- [121] M. Barboni, P. Boehnke, B. Keller, I. E. Kohl, B. Schoene, E. D. Young, and K. D. McKeegan. “Early formation of the Moon 4.51 billion years ago”. In: *Sci Adv* 3 (2017), e1602365 (cit. on pp. 25, 28, 29).
- [122] S. A. Jacobson, A. Morbidelli, S. N. Raymond, D. P. O’Brien, K. J. Walsh, and D. C. Rubie. “Highly siderophile elements in Earth’s mantle as a clock for the Moon-forming impact”. In: *Nature* 508 (2014-04), pp. 84–87. DOI: 10.1038/nature13172 (cit. on pp. 25, 28, 29, 55).
- [123] J. Monteux, D. Andraut, and H. Samuel. “On the cooling of a deep terrestrial magma ocean”. In: *Earth Planet Sci Lett* 448 (2016-08), pp. 140–149. DOI: 10.1016/j.epsl.2016.05.010 (cit. on pp. 25, 30–32).
- [124] T. Lebrun, H. Massol, E. Chassefière, A. Davaille, E. Marcq, P. Sarda, F. Leblanc, and G. Brandeis. “Thermal evolution of an early magma ocean in interaction with the atmosphere”. In: *J Geophys Res Planets* 118 (2013-06), pp. 1155–1176. DOI: 10.1002/jgre.20068 (cit. on pp. 25, 30–32).
- [125] T. M. Harrison, J. Blichert-Toft, W. Müller, F. Albarede, P. Holden, and S. J. Mojzsis. “Heterogeneous Hadean Hafnium: Evidence of Continental Crust at 4.4 to 4.5 Ga”. In: *Science* 310 (2005), pp. 1947–1950 (cit. on pp. 25, 31, 32).
- [126] A. J. Cavosie, J. W. Valley, and S. A. Wilde. “Magmatic  $\delta^{18}\text{O}$  in 4400-3900 Ma detrital zircons: A record of the alteration and recycling of crust in the Early Archean [rapid communication]”. In: *Earth Planet Sci Lett* 235 (2005-07), pp. 663–681. DOI: 10.1016/j.epsl.2005.04.028 (cit. on pp. 25, 34).
- [127] G. Ryder, C. Koeberl, and S. J. Mojzsis. “Heavy Bombardment on the Earth at  $\sim 3.85$  Ga: The Search for Petrographic and Geochemical Evidence”. In: *Origin of the Earth and Moon*. Ed. by R. M. Canup, K. Righter, and et al. Tucson: University of Arizona Press, 2000, pp. 475–492 (cit. on pp. 25, 35).
- [128] B. A. Cohen, T. D. Swindle, and D. A. Kring. “Support for the Lunar Cataclysm Hypothesis from Lunar Meteorite Impact Melt Ages”. In: *Science* 290 (2000-12), pp. 1754–1756. DOI: 10.1126/science.290.5497.1754 (cit. on pp. 25, 35).
- [129] A. Morbidelli, H. F. Levison, K. Tsiganis, and R. Gomes. “Chaotic capture of Jupiter’s Trojan asteroids in the early Solar System”. In: *Nature* 435 (2005-05), pp. 462–465. DOI: 10.1038/nature03540 (cit. on pp. 25, 36).

- [130] P. Boehnke and T. M. Harrison. “Illusory Late Heavy Bombardments”. In: *Proc Nat Acad Sci* 113 (2016-09), pp. 10802–10806. DOI: 10.1073/pnas.1611535113 (cit. on pp. 25, 35).
- [131] D. Wacey, M. R. Kilburn, M. Saunders, J. Cliff, and M. D. Brasier. “Microfossils of sulphur-metabolizing cells in 3.4-billion-year-old rocks of Western Australia”. In: *Nat Geosci* 4 (2011), pp. 698–702 (cit. on pp. 25, 38–41).
- [132] N. J. Planavsky, D. Asael, A. Hofmann, C. T. Reinhard, S. V. Lalonde, A. Knudsen, X. Wang, F. O. Ossa, E. Pecoits, A. J. B. Smith, N. J. Beukes, A. B. Bekker, T. M. Johnson, K. O. Konhauser, T. W. Lyons, and O. J. Rouxel. “Evidence for oxygenic photosynthesis half a billion years before the Great Oxidation Event”. In: *Nat Geo* 7 (2014), p. 283 (cit. on pp. 25, 44, 45, 55).
- [133] A. L. Sessions, D. M. Doughty, P. V. Welander, R. E. Summons, and D. K. Newman. “The Continuing Puzzle of the Great Oxidation Event”. In: *Curr Bio* 19 (2009), p. 567 (cit. on pp. 25, 44, 45).
- [134] S. M. Andrews, D. J. Wilner, T. Birnstiel, J. M. Carpenter, L. M. Pérez, X.-N. Bai, K. I. Öberg, A. M. Hughes, A. Isella, and L Ricci. “Ringed Substructure and a Gap at 1 AU in the Nearest Protoplanetary Disk”. In: *Astrophys J Lett* 820 (2016), p. L40 (cit. on p. 26).
- [135] S. M. Andrews, D. J. Wilner, A. M. Hughes, C. Qi, and C. P. Dullemond. “Protoplanetary Disk Structures in Ophiuchus. II. Extension to Fainter Sources”. In: *Astrophys J* 723 (2010), pp. 1241–1254 (cit. on p. 26).
- [136] M. Krumholz. “From Massive Cores to Massive Stars”. In: *Pathways Through an Eclectic Universe*. Ed. by J. H. Knapen, T. J. Mahoney, and A. Vazdekis. Vol. 390. Astronomical Society of the Pacific Conference Series. San Francisco: Astronomical Society of the Pacific, 2008-06, pp. 16–25 (cit. on p. 27).
- [137] C. F. McKee and E. C. Ostriker. “Theory of Star Formation”. In: *Annu Rev Astron Astrophys* 45 (2007-09), pp. 565–687. DOI: 10.1146/annurev.astro.45.051806.110602 (cit. on p. 27).
- [138] G. J. MacPherson, S. B. Simon, A. M. Davis, L. Grossman, and A. N. Krot. “Calcium-Aluminum-rich Inclusions: Major Unanswered Questions”. In: *Chondrites and the Protoplanetary Disk*. Ed. by A. N. Krot, E. R. D. Scott, and B. Reipurth. Vol. 341. Astronomical Society of the Pacific Conference Series.

- San Francisco: Astronomical Society of the Pacific, 2005-12, p. 225 (cit. on p. 27).
- [139] B. J. Wood, M. J. Walter, and J. Wade. “Accretion of the Earth and segregation of its core”. In: *Nature* 441 (2006-06), pp. 825–833. DOI: 10.1038/nature04763 (cit. on p. 28).
- [140] E. D. Young, I. E. Kohl, P. H. Warren, D. C. Rubie, S. A. Jacobson, and A. Morbidelli. “Oxygen isotopic evidence for vigorous mixing during the Moon-forming giant impact”. In: *Science* 351 (2016), pp. 493–496 (cit. on p. 28).
- [141] M. Čuk and S. T. Stewart. “Making the Moon from a Fast-Spinning Earth: A Giant Impact Followed by Resonant Despinning”. In: *Science* 338 (2012-11), p. 1047. DOI: 10.1126/science.1225542 (cit. on p. 28).
- [142] R. M. Canup. “Forming a Moon with an Earth-like Composition via a Giant Impact”. In: *Science* 338 (2012-11), p. 1052. DOI: 10.1126/science.1226073 (cit. on p. 28).
- [143] A. Reufer, M. M. M. Meier, W. Benz, and R. Wieler. “A hit-and-run giant impact scenario”. In: *Icarus* 221 (2012-09), pp. 296–299. DOI: 10.1016/j.icarus.2012.07.021 (cit. on p. 28).
- [144] M. Touboul, T. Kleine, B. Bourdon, H. Palme, and R. Wieler. “Tungsten isotopes in ferroan anorthosites: Implications for the age of the Moon and lifetime of its magma ocean”. In: *Icarus* 199 (2009-02), pp. 245–249. DOI: 10.1016/j.icarus.2008.11.018 (cit. on pp. 28, 29).
- [145] R. M. Canup. “Simulations of a late lunar-forming impact”. In: *Icarus* 168 (2004-04), pp. 433–456. DOI: 10.1016/j.icarus.2003.09.028 (cit. on p. 29).
- [146] J. F. Kasting. “Runaway and moist greenhouse atmospheres and the evolution of earth and Venus”. In: *Icarus* 74 (1988-06), pp. 472–494. DOI: 10.1016/0019-1035(88)90116-9 (cit. on p. 30).
- [147] M. Čuk, D. P. Hamilton, S. J. Lock, and S. T. Stewart. “Tidal evolution of the Moon from a high-obliquity, high-angular-momentum Earth”. In: *Nature* 539 (2016), pp. 402–406 (cit. on p. 30).
- [148] R. Lathe. “Fast tidal cycling and the origin of life”. In: *Icarus* 168 (2004-03), pp. 18–22. DOI: 10.1016/j.icarus.2003.10.018 (cit. on p. 30).

- [149] S. A. Wilde, J. W. Valley, W. H. Peck, and C. M. Graham. “Evidence from detrital zircons for the existence of continental crust and oceans on the Earth 4.4Gyr ago”. In: *Nature* 409 (2001-01), pp. 175–178 (cit. on pp. 31, 34).
- [150] Y. Amelin, D.-C. Lee, A. N. Halliday, and R. T. Pidgeon. “Nature of the Earth’s earliest crust from hafnium isotopes in single detrital zircons”. In: *Nature* 399 (1999-05), pp. 252–255. DOI: 10.1038/20426 (cit. on pp. 31, 32).
- [151] N. H. Sleep and K. Zahnle. “Carbon dioxide cycling and implications for climate on ancient Earth”. In: *J Geophys Res* 106 (2001-01), pp. 1373–1400. DOI: 10.1029/2000JE001247 (cit. on pp. 32, 36).
- [152] S. Maruyama, M. Santosh, and S. Azuma. “Initiation of plate tectonics in the Hadean: Eclogitization triggered by the ABEL Bombardment”. In: *Geosci Front, in press* () (cit. on p. 32).
- [153] W. G. Ernst, N. H. Sleep, and T. Tsujimori. “Plate-tectonic evolution of the Earth: bottom-up and top-down mantle circulation”. In: *Can J Earth Sci* 53 (2016), pp. 1103–1120 (cit. on p. 32).
- [154] S. B. Shirey, B. S. Kamber, M. J. Whitehouse, P. A. Mueller, and A. R. Basu. “A Review of the Isotopic and Trace Element Evidence for Mantle and Crustal Processes in the Hadean and Archean: Implications for the Onset of Plate Tectonic Subduction”. In: *When Did Plate Tectonics Begin on Planet Earth?* Ed. by K. C. Condie and V. Pease. Special Papers, 440. Boulder, CO: The Geological Society of America, Inc., 2008, pp. 1–29 (cit. on p. 32).
- [155] C. Sagan and G. Mullen. “Earth and Mars: Evolution of Atmospheres and Surface Temperatures”. In: *Science* 177 (1972-07), pp. 52–56. DOI: 10.1126/science.177.4043.52 (cit. on p. 33).
- [156] G. Feulner. “The faint young Sun problem”. In: *Rev Geophys* 50 (2012), RG2006 (cit. on p. 33).
- [157] P. G. Higgs and N. Lehman. “The RNA World: molecular cooperation at the origins of life”. In: *Nat Rev Genet* 16 (2015), pp. 7–17 (cit. on p. 33).
- [158] E. V. Quintana, T. Barclay, W. J. Borucki, J. F. Rowe, and J. E. Chambers. “The Frequency of Giant Impacts on Earth-like Worlds”. In: *Astrophys J* 821, 126 (2016-04), p. 126. DOI: 10.3847/0004-637X/821/2/126 (cit. on p. 33).

- [159] E. B. Watson and T. M. Harrison. “Zircon Thermometer Reveals Minimum Melting Conditions on Earliest Earth”. In: *Science* 308 (2005), pp. 841–844 (cit. on pp. 34, 49).
- [160] S. J. Mojzsis, T. M. Harrison, and R. T. Pidgeon. “Oxygen-isotope evidence from ancient zircons for liquid water at the Earth’s surface 4,300Myr ago”. In: *Nature* 409 (2001-01), pp. 178–181 (cit. on p. 34).
- [161] W. H. Peck, J. W. Valley, S. A. Wilde, and C. M. Graham. “Oxygen isotope ratios and rare earth elements in 3.3 to 4.4 Ga zircons: Ion microprobe evidence for high  $\delta^{18}\text{O}$  continental crust and oceans in the Early Archean”. In: *Geochim Cosmochim Acta* 65 (2001-11), pp. 4215–4229. DOI: 10.1016/S0016-7037(01)00711-6 (cit. on p. 34).
- [162] J. W. Valley, W. H. Peck, E. M. King, and S. A. Wilde. “A cool early Earth”. In: *Geology* 30 (2002), pp. 351–354 (cit. on p. 34).
- [163] J. W. Valley, J. S. Lackey, A. J. Cavosie, C. C. Clechenko, M. J. Spicuzza, M. A. S. Basei, I. N. Bindeman, V. P. Ferreira, A. N. Sial, E. M. King, W. H. Peck, A. K. Sinha, and C. S. Wei. “4.4 billion years of crustal maturation: oxygen isotope ratios of magmatic zircon”. In: *Contrib Mineral Petrol* 150 (2005), pp. 361–580 (cit. on p. 34).
- [164] I. Bindeman. “Oxygen Isotopes in Mantle and Crustal Magmas as Revealed by Single Crystal Analysis”. In: *Rev Mineral Geochem* 9 (2008), pp. 445–478 (cit. on p. 34).
- [165] D. E. Wilhelms, J. F. McCauley, and N. J. Trask. *The Geologic History of the Moon*. United States Geological Survey Professional Paper 1348. 1987 (cit. on p. 35).
- [166] P. D. Spudis, D. E. Wilhelms, and M. S. Robinson. “The Sculptured Hills of the Taurus Highlands: Implications for the relative age of Serenitatis, basin chronologies and the cratering history of the Moon”. In: *J Geophys Res Planets* 116, E00H03 (2011-12), E00H03. DOI: 10.1029/2011JE003903 (cit. on p. 35).
- [167] N. E. B. Zellner and J. W. Delano. “ $^{40}\text{Ar}/^{39}\text{Ar}$  ages of lunar impact glasses: Relationships among Ar diffusivity, chemical composition, shape, and size”. In: *Geochim Cosmochim Acta* 161 (2015-07), pp. 203–218. DOI: 10.1016/j.gca.2015.04.013 (cit. on pp. 35, 55).

- [168] K. Tsiganis, R. Gomes, A. Morbidelli, and H. F. Levison. “Origin of the orbital architecture of the giant planets of the Solar System”. In: *Nature* 435 (2005-05), pp. 459–461. DOI: 10.1038/nature03539 (cit. on p. 36).
- [169] R. Gomes, H. F. Levison, K. Tsiganis, and A. Morbidelli. “Origin of the cataclysmic Late Heavy Bombardment period of the terrestrial planets”. In: *Nature* 435 (2005-05), pp. 466–469. DOI: 10.1038/nature03676 (cit. on p. 36).
- [170] W. F. Bottke, D. Vokrouhlický, D. Minton, D. Nesvorný, A. Morbidelli, R. Brasser, B. Simonson, and H. F. Levison. “An Archaean heavy bombardment from a destabilized extension of the asteroid belt”. In: *Nature* 485 (2012-05), pp. 78–81. DOI: 10.1038/nature10967 (cit. on p. 36).
- [171] A. Morbidelli, K. Tsiganis, A. Crida, H. F. Levison, and R. Gomes. “Dynamics of the Giant Planets of the Solar System in the Gaseous Protoplanetary Disk and Their Relationship to the Current Orbital Architecture”. In: *Astron J* 134 (2007-11), pp. 1790–1798. DOI: 10.1086/521705 (cit. on p. 36).
- [172] B. Charnay, G. Le Hir, F. Fluteau, F. Forget, and D. Catling. “A warm or a cold early Earth? New insights from a 3-D climate-carbon model”. In: *Earth Planet Sci Lett, in press* () (cit. on p. 36).
- [173] A. S. Burton, J. E. Elsila, M. P. Callahan, M. G. Martin, D. P. Glavin, N. M. Johnson, and J. P. Dworkin. “A propensity for n- $\omega$ -amino acids in thermally altered Antarctic meteorites”. In: *Meteorit Planet Sci* 47 (2012), pp. 374–386 (cit. on p. 36).
- [174] Z. Martins, M. C. Price, N. Goldman, M. A. Sephton, and M. J. Burchell. “Shock synthesis of amino acids from impacting cometary and icy planet surface analogues”. In: *Nat Geosci* 6 (2013-12), pp. 1045–1049. DOI: 10.1038/ngeo1930 (cit. on p. 36).
- [175] N. E. B. Zellner. “Cataclysm No More: New Views on the Timing and Delivery of Lunar Impactors”. In: *Orig Life Evol Biosph, in press* () (cit. on p. 36).
- [176] O. Abramov, D. A. Kring, and S. J. Mojzsis. “The impact environment of the Hadean Earth”. In: *Chemie der Erde / Geochemistry* 73 (2013-10), pp. 227–248. DOI: 10.1016/j.chemer.2013.08.004 (cit. on pp. 36, 37).
- [177] S. Moorbath. “Palaeobiology: Dating earliest life”. In: *Nature* 434 (2005), p. 155 (cit. on p. 38).

- [178] M. D. Brasier, J. Antcliffe, M. Saunders, and D. Wacey. “Changing the picture of Earth’s earliest fossils (3.5-1.9 Ga) with new approaches and new discoveries”. In: *Proc Nat Acad Sci* 112 (2015-04), pp. 4859–4864. DOI: 10.1073/pnas.1405338111 (cit. on pp. 38, 41, 55).
- [179] J. W. Schopf, A. B. Kudryavtsev, A. D. Czaja, and A. B. Tripathi. “Evidence of Archean life: Stromatolites and microfossils”. In: *Precambrian Res* 158 (2007), pp. 141–155 (cit. on p. 38).
- [180] M. Igisu, Y. Ueno, M. Shimojima, S. Nakashima, S. M. Awramik, H. Ohta, and S. Maruyama. “Micro-FTIR spectroscopic signatures of Bacterial lipids in Proterozoic microfossils”. In: *Precambrian Res* 173 (2009), pp. 19–26 (cit. on p. 38).
- [181] J. W. Schopf and A. B. Kudryavtsev. “Biogenicity of Earth’s earliest fossils: A resolution of the controversy”. In: *Gondwana Res* 22 (2012), p. 761 (cit. on p. 38).
- [182] J. W. Schopf, A. B. Kudryavtsev, K. Sugitani, and M. R. Walter. “Precambrian microbe-like pseudofossils: A promising solution to the problem”. In: *Precambrian Res* 179 (2010), pp. 191–205 (cit. on p. 38).
- [183] D. Wacey. *Early Life on Earth: A Practical Guide*. Netherlands: Springer, 2009 (cit. on p. 38).
- [184] J. W. Schopf and B. M. Packer. “Early Archean (3.3-Billion to 3.5-Billion-Year-Old) Microfossils from Warrawoona Group, Australia”. In: *Science* 237 (1987), pp. 70–73 (cit. on pp. 38, 39).
- [185] J. W. Schopf. “Microfossils of the Early Archean Apex Chert: New Evidence of the Antiquity of Life”. In: *Science* 260 (1993), pp. 640–646 (cit. on pp. 38, 39).
- [186] B. Rasmussen. “Filamentous microfossils in a 3,235-million-year-old volcanogenic massive sulphide deposit”. In: *Nature* 405 (2000), pp. 676–679 (cit. on p. 38).
- [187] Y. Ueno, Y. Isozaki, H. Yurimoto, and S. Maruyama. “Carbon Isotopic Signatures of Individual Archean Microfossils(?) from Western Australia”. In: *Int Geol Rev* 43 (2001), p. 196 (cit. on p. 38).

- [188] S. Kiyokawa, T. Ito, M. Ikehara, and F. Kitajima. “Middle Archean volcano-hydrothermal sequence: Bacterial microfossil bearing 3.2 Ga Dixon Island Formation, coastal Pilbara terrane, Australia”. In: *Geol Soc Am Bull* 118 (2006), pp. 3–22 (cit. on p. 38).
- [189] F. Westall, C. E. J. de Ronde, G. Southam, N. Grassineau, M. Colas, C. Cockell, and H. Lammer. “Implications of a 3.472–3.333 Gyr-old subaerial microbial mat from the Barber ton greenstone belt, South Africa for the UV environmental conditions on the early Earth”. In: *Phil Tran R Soc B* 361 (2006), pp. 1857–1875 (cit. on p. 38).
- [190] M. Glikson, L. J. Duck, S. D. Golding, A. Hofmann, R. Bolhar, R. Webb, J. C. F. Baiano, and L. I. Sly. “Microbial remains in some earliest Earth rocks: Comparison with a potential modern analogue”. In: *Precambrian Res* 164 (2008), pp. 187–200 (cit. on p. 38).
- [191] K. Sugitani, K. Mimura, T. Nagaoka, K. Lepot, and M. Takeuchi. “Microfossil assemblage from the 3400 Ma Strelley Pool Formation in the Pilbara Craton, Western Australia: Results form a new locality”. In: *Precambrian Res* 226 (2013), pp. 59–74 (cit. on pp. 38, 55).
- [192] K. Hickman-Lewis, R. J. Garwood, M. D. Brasier, T. Goral, H. Jiang, N. McLoughlin, and D. Wacey. “Carbonaceous microstructures from sedimentary laminated chert within the 3.46 Ga Apex Basalt, Chinaman Creek locality, Pilbara, Western Australia”. In: *Precambrian Res* 278 (2016), pp. 161–178 (cit. on pp. 38, 55).
- [193] M. S. Dodd, D. Papineau, T. Grenne, J. F. Slack, M. Rittner, F. Pirajno, J. O’Neil, and C. T. S. Little. “Evidence for early life in Earth’s oldest hydrothermal vent precipitates”. In: *Nature* 543 (2017), pp. 60–64 (cit. on pp. 38, 41, 55, 107).
- [194] A. H. Knoll and E. S. Barghoorn. “Archean microfossils showing cell division from the Swaziland system of South Africa”. In: *Science* 198 (1977), pp. 396–398 (cit. on p. 38).
- [195] M. M. Walsh and D. R. Lowe. “Filamentous microfossils from the 3,500-Myr-old Onverwacht Group, Barberton Mountain Land, South Africa”. In: *Nature* 314 (1985), pp. 530–532 (cit. on p. 38).

- [196] M. M. Walsh. “Microfossils and possible microfossils from the Early Archean Onverwacht Group, Barberton Mountain Land, South Africa”. In: *Precambrian Res* 54 (1992), pp. 271–293 (cit. on p. 38).
- [197] F. Westall, M. J. de Wit, J. Dann, S. van der Gaast, C. E. J. de Ronde, and D. Gerneke. “Early Archean fossil bacteria and biofilms in hydrothermally-influenced sediments from the Barberton greenstone belt, South Africa”. In: *Precambrian Res* 106 (2001), pp. 93–116 (cit. on p. 38).
- [198] H. Furnes, N. R. Banerjee, K. Muehlenbachs, H. Staudigel, and M. de Wit. “Early Life Recorded in Archean Pillow Lavas”. In: *Science* 304 (2004), pp. 578–581 (cit. on p. 38).
- [199] F. Westall, S. T. de Vries, W. Nijman, V. Rouchon, B. Orberger, V. Pearson, J. Watson, A. Verchovsky, I. Wright, J.-N. Rouzand, D. Marchesini, and A. Severine. “The 3.466 Ga “Kitty’s Gap Chert,” an early Archean microbial ecosystem”. In: *Geol Soc Am* 405 (2006), pp. 105–131 (cit. on p. 38).
- [200] E. J. Javaux, C. P. Marshall, and A. Bekker. “Organic-walled microfossils in 3.2-billion-year-old shallow-marine siliciclastic deposits”. In: *Nature* 463 (2010), pp. 934–938 (cit. on pp. 38, 39).
- [201] B. E. Schirrmeister, P. Sanchez-Baracaldo, and D. Wacey. “Cyanobacterial evolution during the Precambrian”. In: *Int J Astrobiology* 15 (2016), pp. 187–204 (cit. on pp. 38, 46, 47).
- [202] French, J. E. and D. F. Blake. “Discovery of Naturally Etched Fission Tracks and Alpha-Recoil Tracks in Submarine Glasses: Reevaluation of a Putative Biosignature for Earth and Mars”. In: *Geophys J Int* 2016 (2016), p. 2410573 (cit. on pp. 38, 39).
- [203] K. Sugitani, K. Grey, A. Allwood, T. Nagaoka, K. Mimura, M. Minami, C. P. Marshall, M. J. Van Kranendonk, and M. R. Walter. “Diverse microstructures from Archaean chert from the Mount Goldsworthy–Mount Grant area, Pilbara Craton, Western Australia: Microfossils, dubiofossils, or pseudofossils?” In: *Precambrian Res* 158 (2007), pp. 228–262 (cit. on p. 38).

- [204] J. M. García-Ruiz, S. T. Hyde, A. M. Carnerup, A. G. Christy, M. J. Van Kranendonk, and N. J. Welham. “Self-Assembled Silica-Carbonate Structures and Detection of Ancient Microfossils”. In: *Science* 302 (2003), pp. 1194–1197 (cit. on pp. 38, 39).
- [205] M. D. Brasier, O. R. Green, A. P. Jephcoat, A. K. Kleppe, M. J. Van Kranendonk, J. F. Lindsay, A. Steele, and N. V. Grassineau. “Questioning the evidence for Earth’s oldest fossils”. In: *Nature* 416 (2002-03), pp. 76–81. DOI: 10.1038/416076a (cit. on pp. 38, 39).
- [206] J. M. García-Ruiz. “Carbonate precipitation into alkaline silica-rich environments”. In: *Geology* 26 (1998), p. 843 (cit. on p. 39).
- [207] B. T. De Gregorio, T. G. Sharp, G. J. Flynn, S. Wirick, and R. L. Hervig. “Biogenic origin for Earth’s oldest putative microfossils”. In: *Geology* 37 (2009), pp. 631–634 (cit. on p. 39).
- [208] K. J. McNamara and S. M. Awramik. “Stromatolites: a key to understanding the early evolution of life”. In: *Sci Prog* 76 (1992), pp. 345–364 (cit. on p. 41).
- [209] W. Altermann, J. Kazmierczak, A. Oren, and D. T. Wright. “Cyanobacterial calcification and its rock-building potential during 3.5 billion years of Earth history”. In: *Geobiology* 4 (2006), pp. 147–166 (cit. on p. 41).
- [210] A. C. Allwood, M. R. Walter, B. S. Kamber, C. P. Marshall, and I. W. Burch. “Stromatolite reef from the Early Archaean era of Australia”. In: *Nature* 441 (2006-06), pp. 714–718. DOI: 10.1038/nature04764 (cit. on pp. 41, 42).
- [211] H. J. Hoffman. “Origin of 3.45 Ga coniform stromatolites in Warrawoona Group, Western Australia”. In: *Geol Soc Am Bull* 111 (1999), p. 1256 (cit. on p. 42).
- [212] N. Noffke, D. Christian, D. Wacey, and R. M. Hazen. “Microbially Induced Sedimentary Structures Recording an Ancient Ecosystem in the ca. 3.48 Billion-Year-Old Dresser Formation, Pilbara, Western Australia”. In: *Astrobiology* 13 (2013-12), pp. 1103–1124. DOI: 10.1089/ast.2013.1030 (cit. on pp. 42, 55).
- [213] T. Djokic, M. J. Van Kranendonk, K. A. Campbell, M. R. Walter, and C. R. Ward. “Earliest signs of life on land preserved in ca. 3.5 Ga hot spring deposits”. In: *Nat Commun* 8 (2017), p. 15263 (cit. on pp. 42, 55).

- [214] J. P. Grotzinger and D. H. Rothman. “An abiotic model for stromatolite morphogenesis”. In: *Nature* 383 (1996), pp. 423–425 (cit. on p. 42).
- [215] M. J. Van Kranendonk. “Morphology as an Indicator of Biogenicity for 3.5–3.2 Ga Fossil Stromatolites from the Pilbara Craton, Western Australia”. In: *Advances in Stromatolite Geobiology*. Ed. by J. Reitner, M. H. Trauth, K. Stüwe, and D. A. Yuen. Lecture Notes in Earth Sciences 13. Berlin: Springer, 2011, pp. 537–554 (cit. on p. 42).
- [216] O. Peterffy, M. Calner, and V. Vajda. “Early Jurassic microbial mats—A potential response to reduced biotic activity in the aftermath of the end-Triassic mass extinction event”. In: *Palaeogeogr Palaeoclimatol Palaeoecol* 464 (2016), pp. 76–85 (cit. on p. 42).
- [217] J. W. Grula. “Rethinking the Paleoproterozoic Great Oxidation Event: A Biological Perspective”. In: *Astrobiology Science Conference 2010: Evolution and Life: Surviving Catastrophes and Extremes on Earth and Beyond*. LPI Contributions, Vol. 1538. 2010, p. 5071 (cit. on p. 44).
- [218] R. Buick. “When did oxygenic photosynthesis evolve?” In: *Phil Trans R Soc B* 363 (2008), p. 2731 (cit. on p. 44).
- [219] T. H. van Andel. *New Views on an Old Planet*. Cambridge: Cambridge University Press, 1994 (cit. on p. 44).
- [220] Z. Lu, Y. C. Chang, Q.-Z. Yin, C. Y. Ng, and W. M. Jackson. “Evidence for direct molecular oxygen production in CO<sub>2</sub> photodissociation”. In: *Science* 346 (2014), pp. 61–64 (cit. on p. 44).
- [221] A. J. Kaufmann, F. A. Corsetti, and M. A. Varni. “The effect of rising atmospheric oxygen on carbon and sulfur isotope anomalies in the Neoproterozoic Johnnie Formation, Death Valley, USA”. In: *Chem Geo* 237 (2007), p. 47 (cit. on pp. 44, 45).
- [222] A. D. Anbar, Y. Duan, T. W. Lyons, G. L. Arnold, B. Kendall, R. A. Creaser, A. J. Kaufman, G. W. Gordon, C. Scott, J. Garvin, and R. Buick. “A Whiff of Oxygen Before the Great Oxidation Event?” In: *Science* 317 (2007-09), p. 1903. DOI: 10.1126/science.1140325 (cit. on pp. 44, 45).
- [223] J. Farquhar, H. Bao, and M. Thiemens. “Atmospheric Influence of Earth’s Earliest Sulfur Cycle”. In: *Science* 289 (2000), pp. 756–758 (cit. on p. 44).

- [224] A. A. Pavlov and J. F. Kasting. “Mass-Independent Fractionation of Sulfur Isotopes in Archean Sediments: Strong Evidence for an Anoxic Archean Atmosphere”. In: *Astrobiology* 2 (2002-03), pp. 27–41. DOI: 10.1089/153110702753621321 (cit. on p. 44).
- [225] P. K. Pufahl and E. E. Hiatt. “Oxygenation of the Earth’s atmosphere-ocean system: A review of physical and chemical sedimentologic responses”. In: *Mar Pet Geol* 32 (2012), p. 1 (cit. on p. 44).
- [226] A. O. Nier and E. A. Gulbransen. “Variations in the Relative Abundance of the Carbon Isotopes”. In: *J Am Chem Soc* 61 (1939), p. 697 (cit. on p. 46).
- [227] B. F. Murphey and A. O. Nier. “Variations in the relative abundance of the carbon isotopes”. In: *Phys Rev* 59 (1941), p. 771 (cit. on p. 46).
- [228] D. M. White and R. L. Irvine. “Analysis of Bioremediation in Organic Soils”. In: *Bioremediation: Principles and Practice, Fundamentals and Applications*. Ed. by K. Sikdar and R. L. Irvine. Vol. 1. Lancaster, PA: Technomic Publishing Co, 1998, pp. 185–220 (cit. on p. 46).
- [229] G. V. Subbarao and C. Johansen. “Transpiration Efficiency: Avenues for Genetic Enhancement”. In: *Handbook of Plant and Crop Physiology*. Ed. by M. Pessarakli. New York: Marcel Dekker, 2001, pp. 835–856 (cit. on p. 46).
- [230] M. J. DeNiro and S. Epstein. “Mechanism of carbon isotope fractionation associated with lipid synthesis”. In: *Nature* 197 (1977), pp. 261–263 (cit. on p. 46).
- [231] M. Schidlowski. “A 3,800-million-year isotopic record of life from carbon in sedimentary rocks”. In: *Nature* 333 (1988), pp. 313–318 (cit. on pp. 46, 48, 49).
- [232] F. J. Luque, J.-M. Huizenga, E. Crespo-Feo, H. Wada, L. Ortega, and J. F. Barrenechea. “Vein graphite deposits: geological settings, origin, and economic significance”. In: *Miner Deposita* 49 (2014), p. 261 (cit. on p. 47).
- [233] M. A. van Zuilen, A. Lepland, and G. Arrhenius. “Reassessing the evidence for the earliest traces of life”. In: *Nature* 418 (2002), pp. 627–630 (cit. on pp. 47, 48).
- [234] C. M. Fedo and M. J. Whitehouse. “Metasomatic Origin of Quartz-Pyroxene Rock, Akilia, Greenland, and Implications for Earth’s Earliest Life”. In: *Science* 296 (2002), pp. 1448–1452 (cit. on pp. 47, 48, 55).

- [235] T. M. McCollom and J. S. Seewald. “Abiotic Synthesis of Organic Compounds in Deep-Sea Hydrothermal Environments”. In: *Chem Rev* 107 (2007), pp. 382–401 (cit. on p. 47).
- [236] T. Mueller, E. B. Watson, D. Trail, M. Wiedenbeck, J. Van Orman, and E. H. Hauri. “Diffusive fractionation of carbon isotopes in  $\gamma$ -Fe: Experiment, models and implications for early solar system processes”. In: *Geochim Cosmochim Acta* 127 (2014), pp. 57–66 (cit. on p. 47).
- [237] S. Shilobreeva, I. Martinez, V. Busigny, P. Agrinier, and C. Laverne. “Insights into C and H storage in the altered oceanic crust: Results from ODP/IODP Hole 1256D”. In: *Geochim Cosmochim Acta* 75 (2011), pp. 2237–2255 (cit. on p. 47).
- [238] N. V. Grassineau, P. Abell, P. W. U. Appel, D. Lowry, and E. G. Nisbet. “Early life signatures in sulfur and carbon isotopes from Isua, Barberton, Wabigoon (Steep Rock), and Belingwe Greenstone Belts (3.8 to 2.7 Ga)”. In: *Evolution of Early Earth’s Atmosphere, Hydrosphere, and Biosphere—Constraints from Ore Deposits*. Ed. by S. E. Kesler and H. Ohmoto. GSA Memoirs 198. Boulder, CO: The Geological Society of America, Inc., 2006, pp. 32–52 (cit. on pp. 48, 50).
- [239] S. J. Mojzsis, G. Arrhenius, K. D. McKeegan, T. M. Harrison, A. P. Nutman, and C. R. L. Friend. “Evidence for life on Earth before 3,800 million years ago”. In: *Nature* 384 (1996-11), pp. 55–59. DOI: 10.1038/384055a0 (cit. on pp. 48, 49, 53).
- [240] A. M. Mloszewska, E. Pecoits, and K. O. Konhauser. “Banded Iron Formation”. In: *Encyclopedia of Astrobiology*. Ed. by M. Gargaud, R. Amils, J. Cernicharo Quintanilla, H. J. Cleaves, W. M. Irvine, D. Pinti, and M. Viso. Berlin: Springer, 2011, pp. 140–143 (cit. on p. 48).
- [241] A. M. Mloszewska, S. J. Mojzsis, E. Pecoits, D. Papineau, N. Dauphas, and K. O. Konhauser. “Chemical sedimentary protoliths in the  $> 3.75$  Ga Nuvvuagittuq Supracrustal Belt (Québec, Canada)”. In: *Gondwana Res* 23 (2013), pp. 574–594 (cit. on pp. 48, 49).
- [242] A. J. B. Smith. “The life and times of banded iron formations”. In: *Geology* 43 (2015), pp. 1111–1112 (cit. on p. 48).

- [243] D. Papineau, B. T. De Gregorio, G. D. Cody, J. O’Neil, A. Steele, R. M. Stroud, and M. L. Fogel. “Young poorly crystalline graphite in the >3.8-Gyr-old Nuvvuagittuq banded iron formation”. In: *Nat Geosci* 4 (2011), pp. 376–379 (cit. on p. 49).
- [244] E. A. Bell, P. Boehnke, T. M. Harrison, and W. L. Mao. “Potentially biogenic carbon preserved in a 4.1 billion-year-old zircon”. In: *Proc Natl Acad Sci USA* 112 (2015), pp. 14518–14521 (cit. on pp. 49, 107).
- [245] A. A. Nemchin, M. J. Whitehouse, M. Menneken, T. Geisler, R. T. Pidgeon, and S. A. Wilde. “A light carbon reservoir recorded in zircon-hosted diamond from the Jack Hills”. In: *Nature* 454 (2008), pp. 92–95 (cit. on pp. 49, 107).
- [246] C. R. Woese and G. E. Fox. “Phylogenetic structure of the prokaryotic domain: the primary kingdoms”. In: *Proc Nat Acad Sci USA* 74 (1977), pp. 5088–5090 (cit. on p. 50).
- [247] J. P. Gogarten, H. Kibak, L. Taiz, E. J. Bowman, M. F. Manolson, R. J. Poole, T. Date, and T. Oshima. “Evolution of the vacuolar H<sup>+</sup>-ATPase: implications for the origin of eukaryotes”. In: *Proc Nat Acad Sci USA* 86 (1989), pp. 6661–6665 (cit. on pp. 50, 51).
- [248] N. Iwabe, K. Kuma, M. Hasegawa, S. Osawa, and T. Miyata. “Evolutionary relationship of archaeobacteria, eubacteria, and eukaryotes inferred from phylogenetic trees of duplicated genes”. In: *Proc Natl Acad Sci USA* 86 (1989), pp. 9355–9359 (cit. on pp. 50, 51).
- [249] L. Margulis. *Origin of Eukaryotic Cells*. New Haven, CT: Yale University Press, 1970 (cit. on p. 50).
- [250] K. S. Merezhkovsky. “The theory of two plasms as foundation of symbiogenesis, a new doctrine on the origins of organisms”. In: *Proceedings of Studies of the Imperial Kazan University* 12 (1909), pp. 1–102 (cit. on p. 50).
- [251] P. Lopez-Garcia and D. Moreira. “Open questions on the origin of eukaryotes”. In: *Trends Ecol Evol* 30 (2015), pp. 697–708 (cit. on p. 50).
- [252] E. V. Koonin and N. Yutin. “The dispersed archaeal eukaryome and the complex archaeal ancestor of eukaryotes”. In: *Cold Spring Harb Perspect Biol* 6 (2014), a016188 (cit. on p. 50).

- [253] T. A. Williams, P. G. Foster, C. J. Cox, and T. M. Embley. “An archaeal origin of eukaryotes supports only two primary domains of life”. In: *Nature* 504 (2013), pp. 231–236 (cit. on p. 51).
- [254] R. Furukawa, M. Nakagawa, T. Kuroyanagi, S. Yokobori, and A. Yamagishi. “Quest for ancestors of eukaryal cells based on phylogenetic analyses of aminoacyl-tRNA synthetases”. In: *J Mol Evol* 84 (2017), pp. 51–66 (cit. on p. 51).
- [255] P. P. Sheridan, K. H. Freeman, and J. E. Brenchley. “Estimated minimal divergence times of the major bacterial and archaeal phyla”. In: *Geomicrobiol J* 20 (2003), pp. 1–14 (cit. on pp. 51, 52).
- [256] R. E. Summons, L. L. Jahnke, J. M. Hope, and G. A. Logan. “2-methylhopanoids as biomarkers for cyanobacterial oxygenic photosynthesis”. In: *Nature* 400 (1999), pp. 554–557 (cit. on p. 51).
- [257] A. Rambaut and L. Bromham. “Estimating divergence dates from molecular sequences”. In: *Mol Biol Evol* 15 (1998), pp. 442–448 (cit. on p. 51).
- [258] Drummond A. J., S. Y. W. Ho, M. J. Phillips, and A. Rambaut. “Relaxed phylogenetics and dating with confidence”. In: *PLoS Biol* 4 (2006), e88 (cit. on p. 51).
- [259] G. I. McFadden. “Origin and evolution of plastids and photosynthesis in euharyotes”. In: *Cold Spring Harb Perspect Biol* 6 (2014), a016105 (cit. on p. 52).
- [260] Gupta R. S. “Molecular markers for photosynthetic bacteria and insights into the origin and spread of photosynthesis”. In: *Genome Evolution of Photosynthetic Bacteria, Vol. 66, 1st Ed.* Ed. by J. T. Beatty. Cambridge: Academic Press, 2013, pp. 37–66 (cit. on p. 52).
- [261] M. M. Tice and D. R. Lowe. “Hydrogen-based carbon fixation in the earliest known photosynthetic organisms”. In: *Geology* 34 (2006), pp. 37–40 (cit. on p. 52).
- [262] J. M. Olson. “Photosynthesis in the Archean Era”. In: *Photosynthesis Res* 88 (2006), pp. 109–117 (cit. on p. 52).
- [263] L. A. David and E. J. Alm. “Rapid evolutionary innovation during an Archaean genetic expansion”. In: *Nature* 469 (2011), pp. 93–96 (cit. on p. 52).

- [264] Goldblatt, C., T. D. Robinson, K. J. Zahnle, and D. Crisp. “Low simulated radiation limit for runaway greenhouse climates”. In: *Nat Geo* 6 (2013), p. 661 (cit. on p. 54).
- [265] S. N. Raymond and A. Morbidelli. “The Grand Tack model: a critical review”. In: *Complex Planetary Systems, Proceedings of the International Astronomical Union*. Ed. by Z. Knežević and A. Lemaître. Vol. 310. IAU Symposium. Cambridge: Cambridge University Press, 2014-07, pp. 194–203. DOI: 10.1017/S1743921314008254 (cit. on p. 55).
- [266] P. Mollière, R. van Boekel, C. Dullemond, T. Henning, and C. Mordasini. “Model Atmospheres of Irradiated Exoplanets: The Influence of Stellar Parameters, Metallicity, and the C/O Ratio”. In: *Astrophys J* 813, 47 (2015-11), p. 47. DOI: 10.1088/0004-637X/813/1/47 (cit. on p. 55).
- [267] R. Hu and S. Seager. “Photochemistry in Terrestrial Exoplanet Atmospheres. III. Photochemistry and Thermochemistry in Thick Atmospheres on Super Earths and Mini Neptunes”. In: *Astrophys J* 784 (2014), p. 63 (cit. on p. 55).
- [268] L. Kaltenegger, D. Sasselov, and S. Rugheimer. “Water-planets in the Habitable Zone: Atmospheric Chemistry, Observable Features, and the Case of Kepler-62e and -62f”. In: *Astrophys J Lett* 775, L47 (2013-10), p. L47. DOI: 10.1088/2041-8205/775/2/L47 (cit. on p. 55).
- [269] C. F. Chyba. “Impact delivery and erosion of planetary oceans in the early inner solar system”. In: *Nature* 343 (1990-01), pp. 129–133. DOI: 10.1038/343129a0 (cit. on pp. 58, 60, 61, 63, 73, 74, 78).
- [270] L. E. Orgel. “Prebiotic chemistry and the origin of the RNA world”. In: *Crit Rev Biochem Mol Biol* 39 (2004-04), pp. 99–123 (cit. on p. 58).
- [271] O. Abramov and S. J. Mojzsis. “Microbial habitability of the Hadean Earth during the late heavy bombardment”. In: *Nature* 459 (2009-05), pp. 419–422. DOI: 10.1038/nature08015 (cit. on pp. 60, 61, 63, 73, 74, 78).
- [272] M. T. McCulloch and V. C. Bennett. “Evolution of the early Earth: Constraints from  $^{143}\text{Nd}$ - $^{142}\text{Nd}$  isotopic systematics”. In: *Lithos* 30 (1993), pp. 237–255 (cit. on pp. 60, 61, 70, 79).

- [273] J. A. Downing, Y. T. Prairie, J. J. Cole, C. M. Duarte, L. J. Tranvik, R. G. Striegl, W. H. McDowell, P. Kortelainen, N. F. Caraco, J. M. Melack, and J. J. Middelburg. “The global abundance and size distribution of lakes, ponds, and impoundments”. In: *Limnol Oceanogr* 51 (2006), pp. 2388–2397 (cit. on pp. 60, 61, 71).
- [274] T. H. Burbine, T. J. McCoy, A. Meibom, B. Gladman, and K. Keil. “Meteoritic Parent Bodies: Their Number and Identification”. In: *Asteroids III*. Ed. by W. F. Bottke Jr., A. Cellino, P. Paolicchi, and R. P. Binzel. Tucson: University of Arizona Press, 2002-03, pp. 653–667 (cit. on pp. 60, 61, 88, 99).
- [275] J. P. Ferris, A. R. Hill, R. Liu, and L. E. Orgel. “Synthesis of long prebiotic oligomers on mineral surfaces”. In: *Nature* 381 (1996-05), pp. 59–61. DOI: 10.1038/381059a0 (cit. on p. 59).
- [276] C. F. Chyba. “Terrestrial mantle siderophiles and the lunar impact record”. In: *Icarus* 92 (1991-08), pp. 217–233. DOI: 10.1016/0019-1035(91)90047-W (cit. on pp. 63, 72).
- [277] B. Wozniak and J. Dera. “Light Absorption by Water Molecules and Inorganic Substances Dissolved in Sea Water”. In: *Light Absorption in Sea Water*. Atmospheric and Oceanographic Sciences Library. New York: Springer-Verlag, 2007, pp. 11–81 (cit. on pp. 64, 80).
- [278] B. L. Carrier, L. W. Beegle, R. Bhartia, and W. J. Abbey. “Attenuation of UV Radiation in Rocks and Minerals: Implications for Biosignature Preservation and Detection on Mars”. In: *Lunar and Planetary Science Conference*. Vol. 48. Lunar and Planetary Science Conference. 2017-03, p. 2678 (cit. on pp. 64, 107).
- [279] G. J. Handschuh, R. Lohrmann, and L. E. Orgel. “The Effect of  $Mg^{2+}$  and  $Ca^{2+}$  on Urea-Catalyzed Phosphorylation Reactions”. In: *J Mol Evol* 2 (1973), pp. 251–262 (cit. on pp. 64, 69).
- [280] H. R. Hulett. “Non-enzymatic Hydrolysis of Adenosine Phosphates”. In: *Nature* 225 (1970-03), pp. 1248–1249 (cit. on p. 64).
- [281] R. H. Reichle, R. D. Koster, G. J. M. De Lannoy, B. A. Forman, Q. Liu, S. P. P. Mahanama, and A. Touré. “Assessment and Enhancement of MERRA Land Surface Hydrology Estimates”. In: *J Clim* 24 (2011), pp. 6322–6338 (cit. on p. 66).

- [282] Y. Furukawa, M. Horiuchi, and T. Kakegawa. “Selective Stabilization of Ribose by Borate”. In: *Orig Life Evol Biosph* 43 (2013), pp. 353–361 (cit. on p. 68).
- [283] H. Pech, A. Henry, C. S. Khachikian, T. M. Salmassi, G. Hanrahan, and K. L. Foster. “Detection of Geothermal Phosphite Using High-Performance Liquid Chromatography”. In: *Environ Sci Technol* 43 (2009), pp. 7671–7675 (cit. on p. 68).
- [284] B. Damer and D. W. Deamer. “Coupled Phases and Combinatorial Selection in Fluctuating Hydrothermal Pools: A Scenario to Guide Experimental Approaches to the Origin of Cellular Life”. In: *Life* 5 (2015-03), pp. 872–887 (cit. on pp. 69, 70, 107, 109).
- [285] K. Zahnle and N. H. Sleep. “Impacts and the Early Evolution of Life”. In: *Comets and the Origin and Evolution of Life*. Ed. by P. J. Thomas, R. D. Hicks, C. F. Chyba, and C. P. McKay. Berlin: Springer-Verlag, 2006, p. 207. DOI: 10.1007/3-540-33088-7\_7 (cit. on p. 69).
- [286] N. Ya. Dodonova, M. N. Kiseleva, L. A. Remisova, and N. M. Tsyrganenko. “The Vacuum Ultraviolet Photochemistry of Nucleotides”. In: *Photochemistry and Photobiology* 35 (1982-01), pp. 129–132 (cit. on p. 69).
- [287] W. Kladwang, J. Hum, and R. Das. “Ultraviolet Shadowing of RNA Can Cause Significant Chemical Damage in Seconds”. In: *Sci Rep* 2, 517 (2012-07), p. 517. DOI: 10.1038/srep00517 (cit. on p. 69).
- [288] M. J. Van Kranendonk. “Two types of Archean continental crust: plume and plate tectonics on early Earth”. In: *Am J Sci* 310 (2010-12), pp. 1187–1209 (cit. on p. 70).
- [289] R. S. Clarke Jr., E. Jarosewich, B. Mason, J. Nelen, M. Gomez, and J. R. Hyde. “The Allende, Mexico, Meteorite Shower”. In: *Smithson Contrib Earth Sci* 5 (1971-02), pp. 1–53 (cit. on p. 72).
- [290] R. G. Strom, R. Malhotra, T. Ito, F. Yoshida, and D. A. Kring. “The Origin of Planetary Impactors in the Inner Solar System”. In: *Science* 309 (2005-09), pp. 1847–1850. DOI: 10.1126/science.1113544. eprint: astro-ph/0510200 (cit. on pp. 73, 74).

- [291] W. F. Bottke, D. D. Durda, D. Nesvorný, R. Jedicke, A. Morbidelli, D. Vokrouhlický, and H. Levison. “The fossilized size distribution of the main asteroid belt”. In: *Icarus* 175 (2005-05), pp. 111–140. DOI: 10.1016/j.icarus.2004.10.026 (cit. on p. 74).
- [292] P. Ehrenfreund, D. P. Glavin, O. Botta, G. Cooper, and J. L. Bada. “Special Feature: Extraterrestrial amino acids in Orgueil and Ivuna: Tracing the parent body of CI type carbonaceous chondrites”. In: *Proc Natl Acad Sci USA* 98 (2001-02), pp. 2138–2141. DOI: 10.1073/pnas.051502898 (cit. on p. 75).
- [293] E. W. Weisstein. *CRC Concise Encyclopedia of Mathematics, Second Edition*. Boca Raton: CRC Press, 2002. ISBN: 9781420035223. URL: <https://books.google.de/books?id=aFDWuZZs1UUC> (cit. on p. 76).
- [294] B. Lang and M. Kowalski. “On the Possible Number of Mass Fragments From Pultusk Meteorite Shower, 1868”. In: *Meteoritics* 6 (1971-09) (cit. on p. 79).
- [295] G. J. Consolmagno, R. J. Macke, P. Rochette, D. T. Britt, and J. Gattacceca. “Density, magnetic susceptibility, and the characterization of ordinary chondrite falls and showers”. In: *Meteoritics* 41 (2006-03), pp. 331–342. DOI: 10.1111/j.1945-5100.2006.tb00466.x (cit. on p. 79).
- [296] C. Bounama, S. Franck, and W. von Bloh. “The fate of Earth’s ocean”. In: *Hydrol Earth Syst Sci* 5 (2001-12), pp. 569–575 (cit. on p. 79).
- [297] N. L. Evans, C. J. Bennett, S. Ullrich, and R. I. Kaiser. “On the Interaction of Adenine with Ionizing Radiation: Mechanistical Studies and Astrobiological Implications”. In: *Astrophys J* 730, 69 (2011-04), p. 69. DOI: 10.1088/0004-637X/730/2/69 (cit. on p. 80).
- [298] J. Kua and J. L. Bada. “Primordial Ocean Chemistry and its Compatibility with the RNA World”. In: *Orig Life Evol Biosph* 41 (2011-12), pp. 553–558. DOI: 10.1007/s11084-011-9250-5 (cit. on p. 83).
- [299] C. S. Cockell. “The ultraviolet radiation environment of Earth and Mars: past and present”. In: *Astrobiology. The Quest for the Conditions of Life*. Ed. by G. Horneck and C. Baumstark-Khan. Berlin: Springer, 2002, pp. 219–232 (cit. on p. 85).

- [300] C. M. Corrigan, M. E. Zolensky, J. Dahl, M. Long, J. Weir, C. Sapp, and P. J. Burkett. “The porosity and permeability of chondritic meteorites and interplanetary dust particles”. In: *Meteoritics* 32 (1997-07). DOI: 10.1111/j.1945-5100.1997.tb01296.x (cit. on pp. 85, 100).
- [301] P. A. Bland, M. D. Jackson, R. F. Coker, B. A. Cohen, J. B. W. Webber, M. R. Lee, C. M. Duffy, R. J. Chater, M. G. Ardakani, D. S. McPhail, D. W. McComb, and G. K. Benedix. “Why aqueous alteration in asteroids was isochemical: High porosity  $\neq$  high permeability”. In: *Earth Planet Sci Lett* 287 (2009-10), pp. 559–568. DOI: 10.1016/j.epsl.2009.09.004 (cit. on pp. 85, 100).
- [302] J. Palguta, G. Schubert, and B. J. Travis. “Fluid flow and chemical alteration in carbonaceous chondrite parent bodies”. In: *Earth Planet Sci Lett* 296 (2010-08), pp. 235–243. DOI: 10.1016/j.epsl.2010.05.003 (cit. on p. 99).
- [303] K. P. Saripalli, R. J. Serne, P. D. Meyer, and B. P. McGrail. “Prediction of Diffusion Coefficients in Porous Media Using Tortuosity Factors Based on Interfacial Areas”. In: *Ground Water* 40 (2002), pp. 346–352 (cit. on pp. 99, 100).
- [304] J. van Brakel and P. M. Heertjes. “Analysis of Diffusion in Macroporous Media in Terms of a Porosity, a Tortuosity and a Constrictivity Factor”. In: *Int J Heat Mass Transfer* 17 (1974), pp. 1093–1103 (cit. on pp. 99, 100).
- [305] S Caré. “Influence of aggregates on chloride diffusion coefficient into mortar”. In: *Cem Conc Res* 33 (2003), pp. 1021–1028 (cit. on pp. 99, 100).
- [306] T. B. Boving and P. Grathwohl. “Tracer diffusion coefficients in sedimentary rocks: correlation to porosity and hydraulic conductivity”. In: *J Contam Hydrol* 53 (2001), pp. 85–100 (cit. on pp. 99, 100).
- [307] P. Baaske, F. M. Weinert, S. Duhr, K. H. Lemke, M. J. Russell, and D. Braun. “Extreme accumulation of nucleotides in simulated hydrothermal pore systems”. In: *Proc Natl Acad Sci USA* 104 (2007-05), pp. 9346–9351 (cit. on pp. 100, 101).
- [308] R. J. Macke, G. J. Consolmagno, and D. T. Britt. “Density, porosity, and magnetic susceptibility of carbonaceous chondrites”. In: *Meteoritics* 46 (2011-12), pp. 1842–1862. DOI: 10.1111/j.1945-5100.2011.01298.x (cit. on pp. 99, 100).

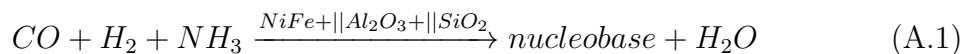
- [309] D. El Abassi, A. Ibhi, B. Faiz, and I. Aboudaoud. “A simple method for the determination of the porosity and tortuosity of meteorites with ultrasound”. In: *J Geophys Eng* 10.5, 055003 (2013-10), p. 055003. DOI: 10.1088/1742-2132/10/5/055003 (cit. on p. 100).
- [310] P. A. Domenico and V. V. Palciauskas. “Theoretical Analysis of Forced Convective Heat Transfer in Regional Ground-Water Flow”. In: *Geol Soc Am Bull* 84 (1973-12), pp. 3803–3814 (cit. on p. 101).
- [311] M. A. Sheremet. “Mathematical Simulation of Nonstationary Regimes of Natural Convection in a Cubical Enclosure with Finite-Thickness Heat-Conducting Walls”. In: *J Eng Thermophys* 22 (2013), pp. 298–308 (cit. on p. 101).
- [312] L. Otero, A. D. Molina-García, and P. D. Sans. “Some Interrelated Thermophysical Properties of Liquid Water and Ice. I. A User-Friendly Modeling Review for Food High-Pressure Processing”. In: *Crit Rev Food Sci Nutr* 42 (2002), pp. 339–352 (cit. on p. 101).
- [313] A. F. G. Jacobs, B. G. Heusinkveld, A. Kraai, and K. P. Paaijmans. “Diurnal temperature fluctuations in an artificial small shallow water body”. In: *Int J Biometeorol* 52 (2008), pp. 271–280 (cit. on p. 101).
- [314] H. Mutschler, A. Wochner, and P. Holliger. “Freeze-thaw cycles as drivers of complex ribozyme assembly”. In: *Nature Chem* 7 (2015-06), pp. 502–508 (cit. on p. 107).
- [315] H. Naraoka, A. Shimoyama, and K. Harada. “Molecular Distribution of Monocarboxylic Acids in Asuka Carbonaceous Chondrites from Antarctica”. In: *Orig Life Evol Biosph* 29 (1999-03), pp. 187–201 (cit. on p. 109).
- [316] R. W. Hilts, C. D. K. Herd, D. N. Simkus, and G. F. Slater. “Soluble organic compounds in the Tagish Lake meteorite”. In: *Meteoritics and Planetary Science* 49 (2014-04), pp. 526–549. DOI: 10.1111/maps.12272 (cit. on p. 109).

# Appendix A

## Nucleobase Synthesis in WLPs

There are three reactions that potentially produced nucleobases in WLPs on the early Earth. These are, FTT reactions, HCN-based reactions, and formamide reactions.

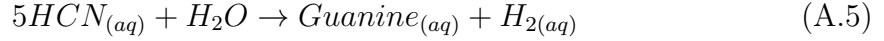
Similarly to hydrothermal systems, FTT reactions (Equation A.1 below) could theoretically produce nucleobases in WLPs near volcanically active areas; where serpentinization of igneous rocks can provide a constant source of  $H_2$  [40]. WLPs would also contain dissolved  $CO_2$  from equilibrium with the early atmosphere [34, 51], which can react with  $H_2$  to provide a source of  $CO$  [41]. Finally,  $NH_3$  could be available in WLPs from a multi-step reaction pathway that begins with the oxidation of  $N_2$  in the atmosphere by lightning, and ends with the reduction of  $NO_2^-$  by dissolved ferrous iron [63]. The initial oxidation reaction likely fixed  $3 \times 10^9$ – $3 \times 10^{11}$  g of nitrogen per year in the early Earth atmosphere, however the concentrations of  $NH_3$  produced in bodies of water from this series of reactions is not quantified.



Catalysts are shown above the reaction arrow, with ‘+||’ symbolizing ‘and/or.’

HCN-based aqueous reactions could also potentially produce nucleobases in WLPs. Below are 4 thermodynamically favourable reaction pathways which our past simulations have shown likely produced a fraction of the nucleobases formed in meteorite parent bodies [42].





HCN could have entered WLPs from the atmosphere where it is produced when the products of methane photodissociation ( $CH_3$ ,  $CH_2$ ) react with nitrogen [63]. The main abiotic source of atmospheric methane is from mid-ocean ridges, driven by a FTT reaction ( $3H_2 + CO \rightarrow CH_4 + H_2O$ ) and the Sabatier reaction ( $4H_2 + CO_2 \rightarrow CH_4 + 2H_2O$ ) [41, 63]. However, it is estimated that only  $\sim 5 \times 10^8$  mol HCN/yr would be produced in the early Earth atmosphere from such a methane source [63]. To put this HCN abundance into context, if  $\sim 5 \times 10^8$  mol of HCN was dissolved in all of Earth's surface water uniformly, the concentration of HCN in ponds would be  $\sim 20$  pptr. Formaldehyde ( $CH_2O$ ), which is required for the theoretical uracil and cytosine reactions above, was also likely produced in the weakly reducing early Earth atmosphere via photochemical reactions [8, 63].

The final possible reaction to produce 3 of the 4 RNA nucleobases in WLPs is the reaction of neat formamide ( $CH_3NO$ ) in the presence of titania, alumina, or silica metals (see reaction equation below). This reaction can produce all nucleobases except guanine.



Catalysts are shown above the reaction arrow, with '||' symbolizing 'or.'

Formamide forms when HCN dissolves in water [8]. However, formamide reactions are thermodynamically unfavourable [42], and thus nucleobases are unlikely to concentrate from such reactions over time.